ASYMMETRIC INLET FLOWS THROUGH AXIAL COMPRESSORS

by

C. S. Tan

GT&PDL Report No. 151 January, 1980

GAS TURBINE & PLASMA DYNAMICS LABORATORY
MASSACHUSETTS INSTITUTE OF TECHNOLOGY
CAMBRIDGE, MASSACHUSETTS

ASYMMETRIC INLET FLOWS THROUGH AXIAL COMPRESSORS

by

C. S. Tan

GT&PDL Report No. 151 January, 1980

This work, carried out in the Gas Turbine and Plasma Dynamics Laboratory, was supported by AFOSR Contract F49620-78-C-0084.

PART I - "THREE-DIMENSIONAL VORTICITY-INDUCED FLOW EFFECTS IN HIGHLY-LOADED AXIAL COMPRESSORS"
GT&PDL REPORT NUMBER 141

PART II - "ASYMMETRIC INLET FLOWS THROUGH AXIAL COMPRESSORS"
GT&PDL REPORT NUMBER 151

ABSTRACT

A new analytical method is proposed for the study of flow through highly-loaded turbomachine stages. The technique is used in the present study in order to: (i) analyze the three-dimensional induced effects of the viscous blade wakes in an isolated rotor; and (ii) to study the effects of the passage of distorted flow through an axial compressor rotor or stator. In Part I (GT&PDL Report Number 141), it is found, in contrast with the more familiar situation behind aircraft wings, that the induced effects of the vorticity in the (viscous) wakes are important in practical axial turbomachinery; for example, the flow angles through highly-loaded rotors are modified to a significant extent by such wake effects. The induced disturbances grow in strength within a certain distance downstream of the blade row before beginning to decay inversely with such axial distance. In agreement with earlier predictions, pressure disturbances and vorticity disturbances cannot be decoupled in swirling flow. Similarly, in part II (GT&PDL Report Number 151), it is found that major differences arise on comparing two-dimensional with three-dimensional analyses, both for rectilinear and for annular configurations. Further, only the last of these three-dimensional analyses can adequately describe the true flow phenomena in highly-loaded turbomachines. This is because such a description properly includes both centrifugal effects together with two important distinct types of vorticity: the trailing vorticity and the vorticity associated with any stagnation pressure gradients present. Such an analysis predicts, a strongly persisting downstream pressure field which in many cases increases before again beginning to decay inversely with the axial distance downstream, both for free-vortex stators and rotors. By contrast, three-dimensional wheel flow analysis predicts indefinitely persisting downstream disturbances. Further, a purely two-dimensional theory indicates for a stator, the downstream static pressure to be uniform, while even a three-dimensional rectilinear cascade theory would predict only an exponentially decaying pressure field. The amplitude of the above persistent downstream disturbances decreases for free-vortex downstream flow as the number of significant circumferential harmonics of the inlet distortion increases. These analytical results agree well with available experimental data recently obtained in annular cascades.

ACKNOWLEDGEMENTS

It has been very fortunate and a great privilege for the author to have had the opportunity to carry out the research described in this thesis under Professor James E. McCune, the Chairman of the author's Doctoral Committee, and Professor Sir William R. Hawthorne, Master of Churchill College, Cambridge University, whose stimulating questions have helped the author to further understand flows in turbomachinery. Hardly any paragraph in this thesis can the author claim to be entirely his; any valuable idea in this thesis is a result of the constant discussion with them and their critical comments. In addition, their advice, their constant encouragement, and personal warmth have made the author's association with them over the past two years a very special and memorable one.

Further he would also like to express his sincere gratitude to:

Professor Sir William R. Hawthorne for making arrangements for the author to be at Cambridge University on three occasions, and for making it possible for the author to have fruitful and useful discussions on distorted inlet flows with Mr. N. A. Mitchell of Cambridge University.

Professor James E. McCune, among other things, for editing the major portion of the thesis with patience and meticulosity.

Professor Jack L. Kerrebrock for his thoughtful and critical comments and for the valuable discussions with him.

Professor E. M. Greitzer for making available the experimental data on distorted flow through annular cascades, and for the elucidating discussions on flow through turbomachines.

Professor M. Finston for the useful discussions.

Professor T. H. Dupree for being on the author's Doctoral Committee.

Gayle Ivey for her constant availability and help when needed.

Holly Rathbun for accepting the tedious task of typing this thesis.

Mr. W. K. Cheng for permitting me to use the subroutines he developed for generating Bessel Functions of high orders.

Throughout his Doctoral Study, the author is supported by a Research Assistanship made available through the Gas Turbine and Plasma Dynamics Laboratory which, besides providing competent scientific and technical education, has an internationally cosmopolitan atmosphere. Undoubtedly, in the course of pursuing scientific and technical knowledge, students from many lands, besides interacting academically, have also interacted culturally; this in itself is an invaluable education.

Finally, the author dedicates this thesis to his beloved Father and his late beloved Mother who, in spite of their illiteracy, insisted on his acquiring a higher education.

TABLE OF CONTENTS

TABLE OF CONTENTS (CONTINUED)

TABLE OF CONTENTS (CONTINUED)

TABLE OF CONTENTS (CONTINUED)

OVERALL SUMMARY

An analytical technique, based in part on the Clebsch-Hawthorne formulation, is proposed for use in the predictions of the nature of steady flows through axial turbomachines. Essentially, the method describes the internal aerodynamics of the flow in such machines in terms of any vorticity field present or, as in the case of non-homentropic flow, the reduced vorticity field. The usefulness and simplicity of this approach emerges especially clearly in the particular case of three-dimensional flows, although two-dimensional flows can be similarly analyzed. The basic formulation is exact, but realistic simplifying assumptions are made to keep the problem tractable as well as practical. For example, three-dimensional aspects of the flow resulting from the finite number of blades or inlet maldistribution are treated as perturbations about the mean streamlines derived exactly from the available (non-linear) axisymmetric throughflow-treatments.

In Part I, the proposed method is used to analyze the three-dimensional induced effects of the viscous wakes flowing downstream from the blades on an isolated rotor (or stator) producing free-vortex mean downstream flows encased in an infinite cylindrical annulus. This swirling downstream flow field is then pictured as being threaded with vortex filaments representing the blade-wakes. Because the vorticity field can be related to the variation of the thermodynamical properties of the fluid, the presence of such viscous wakes necessarily implies a variation of entropy from streamline to streamline, or, in the incompressible limit, a corresponding variation of stagnation pressure. Linearization of the analysis is achieved by expanding about an axisymmetric throughflow;

free-vortex mean flow is assumed in the example in Part I. In contrast to external aerodynamics about wings, the blade wakes so described modify the flow angles through highly-loaded rotors significantly. This is in agreement with earlier predictions that pressure disturbances, vorticity disturbances, and entropy disturbances cannot be decoupled in compressible swirling flows.

In Part II, this technique is further applied to analyze the passage of distorted flow through an axial compressor rotor or stator. In this portion of the work, the actuator-disc limit is taken; this concept is introduced in order to suppress the individual identity of the blades. Thus the description of the flow can be taken as steady in absolute coordinates. The flow field is again pictured as being threaded with vortex filaments; in this case the vorticity is either introduced far upstream or can be considered to spring from the solid surfaces of the blades represented by the disc. The resulting linearized analysis yields an overall description of the blade row performance in the presence of inlet flow distortions. It is found that major differences arise on comparing two-dimensional with three-dimensional analyses, both for rectilinear and for annular configurations. In fact, only the last analysis can adequately describe the flow phenomena in highly-loaded turbomachines, because it includes the centrifugal effects together with two important distinct types of vorticity. One of these is the trailing vorticity associated with any spanwise variation of blade loading which may result; the other is associated directly with the inlet distortion. The latter vorticity develops a streamwise component as it swirls downstream, becoming superimposed on any shed circulation already present. This

produces important three-dimensional effects for practical loading. The result again demonstrates that pressure disturbances and vorticity disturbances are not separable in swirling flow. The results are compared successfully not only with earlier three-dimensional analyses but also with recent experimental data.

INTRODUCTION

Axial-flow compressors are the principal type of compressor used in aircraft gas-turbine power plants, primarily because of their unique match with many of the basic requirements of aircraft power-plants. For example, such requirements include high efficiency, high-air-flow rate per unit frontal area and high pressure ratio per stage. In addition, an aircraft engine must be as compact as possible. Engineers in this field attempt to design compressors which meet as many of these basic requirements as possible. In the process, the designer hopes to use a scheme which is accurate enough so that the cost and time involved in the development of the device can be minimized. In any case, the design of an axial-flow compressor ultimately requires the most accurate available calculation of the flow through such compressor blade-rows.

Flow through the blading of an axial-compressor is extremely complex, beginning with the fact that it is inherently three-dimensional in nature. Moreover, not only does the flow have gradients in the axial, radial and circumferential directions, it is time dependent as well. In addition, viscous effects must be taken into consideration in practical compressor studies. Thus, the complete governing equations of fluid flow through turbomachines have not yet been solved. In particular, strictly numerical efforts to represent the flow through the flow passages formed by the blades, the hub, and the casing (especially in the full three-dimensional case) are still in a rapidly developing stage. One thus sees that the fluid mechanical problem in axial compressors continues to present an extremely challenging problem in the field of applied fluid mechanics,

both theoretically and experimentally.

In an effort to provide an increasingly effective basis for designing and understanding axial compressors, research in this field has been quite extensive. Even so, there remains a formidable gap between the information predictable on purely theoretical grounds and that required for the actual production of an efficient, practical machine of this type. In an attempt to close this gap, various empirical techniques have been devised that combine comparatively simplified theories with available experimental data. Even the use of these empirical techniques, however, often requires a considerable investment of time and effort. Often, for developmental purposes, whole series of costly tests requiring continued trial and error become necessary. Consequently, there remains strong motivation for the search for increasingly efficient and accurate ways of predicting the fluid behavior within a "turbomachine"*. In the process continued experimental studies are crucial in establishing improved understanding of the fluid behavior within a turbomachine.

As a comparison, workers studying the air flow past an isolated wing are often faced with a somewhat easier task compared with those involved in the analysis of internal flows of the type just described. Even though the primary problem of both can be described in terms of the determination of the velocity arising at an arbitrary point on an airfoil surface by the overall flow fields (pressure, vorticity, ...) associated with all other confining surfaces present, the geometrical complexity in turbomachines is frequently more difficult. Further, unlike incoming flow over an isolated

* In the following, "turbomachine" will be used to refer to the axial type, unless stated otherwise.

wing, the flow in many regions of a turbomachine is necessarily swirling in nature. As already mentioned, an important consequence is that the behavior of the working fluid can be modified considerably. Furthermore, the actual flow through a rotor is always unsteady with respect to uniform flow in a stator, and vice versa. That is, for example, circumferential variations (for instance, those brought about by rotor blade wakes), even though time-independent with respect to the rotor, will inevitably give rise to unsteady flow in the preceding and succeeding stators. Because of the arrangement of blade rows, a stator or a rotor almost always encounters a stream of wakes which have left their generating surfaces only a short distance ahead. An analogous situation is not usually the case for an isolated aircraft wing flying through the free air. In addition to the above complexities, inlet distortions involving variations in both the stagnation pressure and stagnation temperature arise; frequently the phenomena of rotating stall and surge occur as well in axial compressors under certain operating conditions.

The drive towards a compact and light weight design of an engine for aircraft application has resulted in an increase of stage pressure ratio and high mass flow rate per unit frontal area. This certainly requires that each element of the turbomachine be operating near its aerodynamic limit. Therefore, the compressor blades must tolerate large relative Mach numbers so that high mass flow rate and high relative speeds can be achieved. Investigations on free-vortex rotors have indicated the feasibility of obtaining high efficiency from rotors in which the Mach numbers at the tips are as high as 1.35, while those near the hub remain subsonic (transonic rotors). Because the flow is supersonic relative to the rotor

near the tip, the complexity of the flow has further been increased by the presence of shock waves (which lead to shock-wave boundary-layer interaction) in the blade passage. In the transonic regime, the working fluid has to be considered as compressible. This implies, from a mathematical point of view, that the aerodynamic and the thermodynamic equations which govern the fluid flow are strongly coupled and highly non-linear. Very often, no known exact non-trivial solution exists and a linearized perturbation technique is used to obtain solutions.

The work described in Part I deals only with one aspect of the fluid flow through a blade row encased in an infinite cylindrical annulus; namely, the three-dimensional behavior of the viscous blade wakes in the downstream swirling flow and their effect on the performance of the blade row. It is hoped that this work can in someway aid in the eventual closing of the "gap" mentioned earlier.

In Part II, an analytical investigation regarding the three-dimensional aspects of asymmetric inlet flows on the performance of turbomachines is presented; its results are compared with those of two-dimensional theory and three-dimensional theory neglecting the centrifugal effects (i.e., distorted flows through rectilinear cascades) to show the important differences. The theoretical predictions are compared with a set of available experimental data. The performance of axial compressors operating under distorted inlet flows has been widely studied because of the effect of inlet flow distortion on compressor stall, mechanical reliability and efficiency.

The theoretical work is considered entirely from the point of view of the fluid flow through the blade row. Both the incompressible flow

and the compressible flow (except for the inlet distortion problem) are considered but the working fluid is assumed to be inviscid outside the blading. The equations of motion for the flow of a real fluid in an axial flow compressor are nonlinear three-dimensioned equations. Accordingly, realistic simplifying assumptions are made so that fruitful and tractable analysis is possible. For instance, linearizing approximations are introduced to keep the mathematical problems tractable. Such procedures are necessarily conditional upon obtaining physically valid flow descriptions even though the problem may remain very complex. Since solutions of aerothermodynamic equations for the flow with small deviation from free-vortex motion often provide a useful basis for turbomachine design (even though compressors have for some time been designed on other bases), attention is focused here on obtaining solutions for nearly free-vortex motion. Extension to more general mean flows is feasible and underway in a separate study.

PART II

ASYMMETRIC INLET FLOWS THROUGH AXIAL COMPRESSORS

CHAPTER 1 - SOURCES OF INLET DISTORTION AND ITS CONSEQUENCES

A persistent problem in the development of air-breathing propulsion systems for modern aircraft consists in the difficulty of predicting various harmful effects of non-uniform inlet flow on engine performance. The design of a compressor is normally based upon the assumption that the engine will receive a uniform, smooth flow at its inlet. Often, however, for real flight conditions where complex inlet flow distortions frequently occurs. Such a simplification can be misleading in terms of actual engine performance. In general, inlet distortions may either be represented by a stagnation pressure defect, a stagnation temperature non-uniformity or a combination of both. Each of the distortion types may be either radial, circumferential or a combination of both.

Stagnation pressure distortion may result, for example, from separation from the inlet tip due to aircraft operation at high angles of attack and/or yaw, for example, as caused by wind gusts, or by wakes from the nearby spides and struts, or even neighboring aircrafts. Interference between the boundary layers and shock waves, leading to localized flow separation can, also provide sources of stagnation pressure distortion.

Similarly, temperature distortions can result, from armament firing from the injection of hot exhaust gases from thrust reverses, or from exhaust plumes of the nearby aircrafts and so on. Recirculation of exhaust gases from the nozzle of the engines in STOL-VTOL applications constitutes a further source of stagnation temperature non-uniformity in gas turbine engines.

Moreover, stagnation temperature distortions (or combined stagnation pressure and temperature maldistribution) may enter intermediate or aft compressor stages in the modern multi-spool compressor systems as a consequence of inlet stagnation pressure distortions in preceeding stages. Similarly, following a high pressure ratio fan in a present day by-pass engine, stagnation pressure maldistribution upstream of the fan can create significant temperature distortion in the core compressor inlet.

This frequent occurrence of asymmetric inlet flows, which can have a severe effect on compressor stall margins and performance has resulted in the devotion of a considerable amount of study of such flows in turbo-machines. The work to be described in this portion of the present study will be concerned with asymmetric inlet flow possessing significant pressure distortion; incompressibility will be assumed to a simplicity, and our primary focus will be on effects not predictable in two-dimensional models, some of which are analogous with effects found in Part I of this work.

Early treatments of distorted flows were based on the so-called parallel compressor[42-44] model which assumes that: (1) for distorted inlet flow, the compressor can be considered to be segmented into a series of "sub-compressors", each operating independently of one another and each having the same performance characteristics on the corresponding compressor in undistorted flow; (2) the exit static pressures of each sub-compressor are the same; and (3) there are no circumferential cross flows occurring within the given compressor stage. This type of analytical model is concerned with the gross effects of the inlet distortion on the performance of the axial compressor as a whole; and because of the assumptions made, it

has certain significant limitations.

More detailed studies of inlet distortion were carried out with the development of theories of two-dimensional non-uniform flow through actuator disc[45-49] such as those of F. Ehrich, W. D. Rannie and F. E. Marble, Whitehead, Yeh and others. In the latter works, the assumption is made that the flow non-uniformities are small (relative to the azimuthal mean) so that a linearized perturbation analysis about axisymmetric flow is possible. Because of the assumption of two-dimensionality, the vorticity disturbances associated with the flow non-uniformities are purely convected in those models; the static pressure perturbations are consequently at most potential disturbances satisfying Laplace's equation and, as a result, this pressure and vorticity cannot interact. In addition, the flow is assumed to be steady in a given frame of reference, and various assumptions are made to incorporate the characteristics of the blades (for instance, the effect of blade incidence on the flow outlet angle behine the blade row) into those various theories. Extension of this type of approach to three-dimensions was attempted by Yeh,[50] Kryzwoblocki[51] and Dixon.[52]

Dunham[53-56] developed a more general three-dimensional theory for the small disturbance of a free vortex flow in an annular duct and applied his model to the flow through an actuator disc just downstream from a stationary or rotating gauze. The flow upstream of the disc and gauze was assumed irrotational and the stagnation pressure perturbation introduced at the disc was prescribed. Numerical results for the axial velocity perturbation at the disc were obtained. Dunham clearly emphasized the importance of both the axial and tangential components of vorticity

(see also Part I of the research), and as Dunham pointed out, their presence constitutes a major difference between two and three-dimensional analysis. As an approximation, Yeh, Dunham, and others, also introduced a rectangular duct model of the annular case, thereby omitting centrifugal effects. Dunham showed, as one might expect, that such a model is a reasonable approximation for flows only with moderate to small swirl.

Recently, Greitzer[57] developed a quasi-three-dimensional theory which includes, in an approximate but very useful way, some of the more important of the three-dimensional phenomena noted by Dunham. In the regions for which they were intended, Greitzer's theoretical predictions are in good agreement with experimental measurements carried out in an annular swirl rig by Strand.

Here, in order to describe three-dimensional distorted flows through a blade row, we will make further use of the Clebsch-Hawthorne formulation for treating rotational flows; we have already found this approach to be successful (Part I) in describing the induced effects of viscous blade wakes behind turbomachine rotor. In the present case, a circumferentially, radially, varying velocity profile (taken to be purely axial in absolute coordinate far upstream), together with a prescribed free vortex mean downstream flow will be assumed. For stator, of course, such a flow may be considered steady in the absolute frame of reference. But similar flow through a rotor is inherently unsteady because there will be necessary an abrupt change of aerodynamic loading on the rotor as each of its blades moves in and out of the above prescribed inlet distortion.

In this study, we assume that the (averages or dominant)

circumferential wave legth of the distortion is sufficiently large compared to the blade spacing to allow the neglect of the effects of individual (discrete) blades flow. That is, the effects of any abrupt changes in the aerodynamic loading on the blades is assumed negligible in the following. Under these assumptions the flow can be considered (at least) to be quasi-steady, which also implies a slow variation with time of local inlet conditions at any particular blade channel. We further neglect, in consequence, any structure induced by the individual blades on the original inlet distortion pattern. Finally, we use this assumption of quasi-steadiness (again in the absolute frame) to justify treating each individual blade row as an actuator disc. [The analytical model developed in the present discussion is further taken to be inviscid in the sense that the blade loss characteristics are not taken into consideration (see, however, Part I)].

In general, because of the geometry of turbomachines, the introduction of an inlet distortion in the axial velocity profile will result in a spanwise variation of loading on the blades. Consequently, trailing vortices will spring from the solid surfaces of the blades represented by the disc (we may note, as Dunham also pointed out, that these vortices are absent in two-dimensional theory). In addition, in analogy with certain phenomena discussed in Part I, those vortex filaments resulting from the upstream non-uniform flow itself will be transported by the mean flow, and these two types of vorticity will superpose themselves upon one another as the flow swirls downstream. The "secondary vorticity" (of Part I), which develops as the flow proceeds, and induces a corresponding secondary flow.The two effects together give rise to important three-dimensional

phenomena unaccounted for by earlier two-dimensional theories. We shall see, for practical devices, that such three-dimensional effects can be of a sufficient magnitude so as to significantly effect the rotor performance. It is well known that axial compressors can be stalled, and the engine instability or surge initiated, as a result of distorted flow. When a compressor stage stalls, the flow of air through the compressor can be significantly blocked. The occurrence of surge consists of a stall-recovery-stall cycle.

Fig. II.1 shows diagramatically the characteristics of a typical compressor. We note that the size of the region of stall free operation decreases rapidly as the design pressure ratio is increased. Thus, one sees that an attainment of adequate stall margins may require a reduction in the work done per stage of the compressor, which implies increasing the engine weight and size. Therefore, it is important to develop a knowledge when and why a compressor will stall and what changes in compressor design might enable the compressor to be more tolerant to a distorted flow. The development of this knowledge requires both theoretical and experimental studies of fundamental nature.

As mentioned earlier, exact solutions to equations corresponding to an exact formulation of fluid flow phenomena with specified boundary conditions are usually not attainable; approximate techniques are almost always used to obtain useful and understandable solutions. In this connection, it is important to note that blades in axial flow compressors are frequently highly loaded, operating near stalling. In consequence, relatively small perturbations in the flow field, which might otherwise be of little consequence may trigger blade stall. This fact justifies the

development of a linearized perturbation theory as one approach to a useful, approximate solution, especially when a small perturbation is taken with respect to highly loaded reference operating condition.

In what follows, we first use the Clebsch-Hawthorne formulation in terms of a classical two dimensional approach in order to illustrate the simplicity and usefullness of the scheme. The two-dimensionality assumption can then be relaxed first allowing for variations in the spanwise direction while neglecting centrifugal effects. Finally, this is followed by the development of a more complete three-dimensional (actuator disc theory) for distorted flow through an annular cascade. The distorted flow through a single blade row is treated first; it is then shown how the present theory can be extended to multiple blade rows, consisting of rotors, stators, rotors, etc. Results from each step of the developing theory are compared to show the significant differences. Specifically, numerical results are obtained for stator to compare with the results of Greitzer and Strand,[57] and for a rotor to compare with Rizvi's data.[59,60]

CHAPTER 2 - ANALYTICAL DESCRIPTION OF DISTORTED FLOW THROUGH TURBOMACHINES

2.1 The Clebsch-Hawthorne Formulation

We will use the technique of Clebsch-Hawthorne Formulation of general rotational flow for the description of distorted flow through turbomachines. This formulation has been described in some detail in Chapter 2 of Part I for inviscid and incompressible fluid but in its exact form so that exact solutions are usually unattainable. Here, appropriate approximations will be introduced to keep the analysis tractable.

The asymmetric inlet flow will be assumed to be a small shear superimposed upon a known mean flow so that

$$\frac{\Delta P_t^u}{\frac{1}{2}\rho\bar{V}^2} \sim \frac{\tilde{V}^u}{\bar{V}} \sim \varepsilon << 1. \tag{2.1}$$

It will also be assumed that the flow outlet angles from the blades are independent of the incidence; i.e., we exclude the consideration of the blade characteristics, the inclusion of which may make a difference.

We note from Eq. (2.1) that the change in stagnation pressure is small and therefore the vorticity associated with it is small too. In consequence, the flow may be separated into a mean potential flow of zeroth order, $\underset{\sim}{\bar{V}}$, and a perturbation flow of $O(\varepsilon)$, $\underset{\sim}{\tilde{V}}$. To order ε, Eq. (2.14) in Part I becomes

$$\underset{\sim}{\bar{V}} \times \underset{\sim}{\Omega} = \nabla \frac{P_t}{\rho}. \tag{2.2}$$

The vorticity is given by

$$\underset{\sim}{\Omega} = \nabla \times \underset{\sim}{\tilde{V}} \tag{2.3}$$

The approximation leading to Eq. (2.2) also results in

$$\underset{\sim}{\bar{V}} \cdot \nabla \frac{P_t}{\rho} = 0 \,, \tag{2.4}$$

implying that the stagnation pressure remains constant on streamlines of the mean potential flow.

We have shown in Chapter 2 of Part I that one can separate the vorticity into two components: one ($\underset{\sim}{\Omega}\tau$) being associated with the gradient in stagnation pressure, and the other ($\lambda\bar{V}$) lies on the mean streamlines of the mean flow, in consistence with the approximation here. The latter is usually the trailing vorticity that has sprung from solid surfaces of the blades forming the actuator disc. We write quite generally,

$$\underset{\sim}{\Omega} = \nabla \times \underset{\sim}{\tilde{V}} = \underset{\sim}{\Omega}\tau + \lambda \underset{\sim}{\bar{V}} \,, \tag{2.5}$$

with the portion, $\underset{\sim}{\Omega}\tau$, satisfying

$$\underset{\sim}{\bar{V}} \times \underset{\sim}{\Omega}\tau = \nabla \frac{P_t}{\rho} \tag{2.6}$$

Thus, with the approximations here, Eqs. (2.24) and (2.28) become

$$\lambda \bar{V} = \nabla S \times \nabla \Gamma \,, \tag{2.7}$$

and

$$\underset{\sim}{\Omega}\tau = \nabla \frac{P_t}{\rho} \times \nabla \bar{\tau} \,, \tag{2.8}$$

where we have used the drift function $\bar{\tau}$ of the mean flow by virtue of (2.1)

This drift function $\bar{\tau}$ is given by

$$\bar{\tau} = \int^{S} \frac{ds}{\bar{V}} \tag{2.9}$$

Note that both the equations (2.7) and (2.8), guarantee that the vectors, $\lambda \underset{\sim}{\bar{V}}$ and $\underset{\sim}{\Omega}\tau$ (hence $\underset{\sim}{\Omega}$), are solenoidal.

The continuity condition

$$\nabla \cdot \underset{\sim}{V} = 0 \tag{2.10}$$

applies to $\underset{\sim}{\bar{V}}$ as well as to $\underset{\sim}{\tilde{V}}$ so that we can write

$$\underset{\sim}{V} = \underset{\sim}{\bar{V}} + \underset{\sim}{\tilde{V}} = \nabla\alpha \times \nabla\beta \qquad \text{[Eq. (2.22) in Part I]}, \tag{2.11}$$

and

$$\underset{\sim}{\bar{V}} = \nabla\alpha \times \nabla\psi \tag{2.12}$$

where we have written

$$\beta = \psi + \delta\beta \tag{2.13}$$

with

$$\left|\frac{\delta\beta}{\psi}\right| \sim \varepsilon. \tag{2.14}$$

Because of the continuity condition on $\underset{\sim}{\bar{V}}$ and the solenoidality of the vector $\lambda \underset{\sim}{\bar{V}}$ we can write

$$\underset{\sim}{\bar{V}} \cdot \nabla\lambda = 0 \tag{2.15}$$

so that

$$\lambda = \lambda(\alpha, \psi), \tag{2.16}$$

by virtue of Eq. (2.12). Similarly, Eqs. (2.4) and (2.12) allow us to write

$$P_t = P_t(\alpha, \psi) \tag{2.17}$$

Note that $\bar{P}_t = \bar{P}_t(\psi)$ only.

With reference to Chapter 2 in Part I, we can write, in general,

$$\underset{\sim}{\tilde{V}} = \nabla\phi + \underset{\sim}{A} \ , \tag{2.18}$$

where it then follows, using Eqs. (2.5), (2.7), and (2.8), that

$$\underset{\sim}{A} = \left(\frac{P_t - \bar{P}_t}{\rho}\right)\nabla\bar{\tau} + S\nabla\Gamma \ . \tag{2.19}$$

We note that by substituting for λ from Eq. (2.16) and for $\underset{\sim}{\bar{V}}$ from Eq. (2.12) in the LHS of Eq. (2.7), the functions S and Γ (and hence $S\nabla\Gamma$) can only depend on α and ψ only.

Upstream of the blade row, the shear disturbance has associated with it a stagnation pressure gradient only so that $\underset{\sim}{\Omega}\tau$ is non-zero while the Beltrami component of vorticity is absent. Thus,

$$\underset{\sim}{\tilde{V}}^u = \nabla\phi^u + \left(\frac{P_t^u - \bar{P}_t^u}{\rho}\right)\nabla\bar{\tau}^u \ . \tag{2.20}$$

The upstream maldistribution in stagnation pressure will modulate the upstream flow angles, thus leading to a variation in spanwise blade loading in general, and hence to trailing vorticity (Beltrami flow). In consequence, both types of vorticity, $\underset{\sim}{\Omega}\tau$ and $\lambda\underset{\sim}{\bar{V}}$, are present in the downstream flow field. Thus

$$\underset{\sim}{V}^d = \nabla\phi^d + \left(\frac{P_t^d - \bar{P}_t^d}{\rho}\right)\nabla\bar{\tau}^d + S\nabla\Gamma \ , \tag{2.21}$$

where $S\nabla\Gamma$ is a result of any Beltrami component of vorticity arising in the flow.

Application of the continuity condition to Eqs. (2.20) and (2.21) leads to

$$\nabla^2\phi^u = -\nabla\left(\frac{P_t^u - \bar{P}_t^u}{\rho}\right)\cdot\nabla\bar{\tau}^u - \left(\frac{P_t^u - \bar{P}_t^u}{\rho}\right)\nabla^2\bar{\tau}^u \ , \tag{2.22}$$

and

$$\nabla^2\phi^d = -\nabla\left(\frac{P_t^d - \bar{P}_t^d}{\rho}\right)\cdot\nabla\bar{\tau}^d - \left(\frac{P_t^d - \bar{P}_t^d}{\rho}\right)\nabla^2\bar{\tau}^d \ , \tag{2.23}$$

which form the governing equations for the upstream and the downstream perturbation potential ϕ^u and ϕ^d respectively. The solutions for ϕ^u and ϕ^d are obtainable from Eqs. (2.22) and (2.23) with an appropriate set of physical boundary conditions.

We shall solve Eqs. (2.22) and (2.23) consistently for the following cases: (i) A distorted inlet flow through a two-dimensional cascade; and (ii) A distorted inlet flow through a three-dimensional rectilinear cascade, in the next two sections.

The case of an inlet distortion through an annular cascade will be analyzed similarly in Chapter 3.

2.2 Two-Dimensional Theory

Description of the Flow Field.

Consider the two dimensional flow through an isolated cascade. The

two-dimensional flow field is obtained by "unwrapping" an isolated annular cascade in an infinite annular duct at some radius R. Because of the assumption of two-dimensionality, radial flow would be negligible so that Cartesian coordinates may be used. The cascade will be placed at the origin of the x-axis (which is along the annular duct) and extends from $-\pi R$ to πR along the y-axis (which coincides with the circumferential direction). Hence, the y-coordinate is periodic with a period of $2\pi R$. Furthermore, the cascade is represented by an actuator line to suppress the effects of individual blades. The flow field is shown schematically in Fig. II.2. A y-varying and purely axial velocity profile, $(\bar{V}_x{}^u + \tilde{V}_x{}^u{}_{-\infty}(y), 0)$, far upstream and a mean downstream flow, $(\bar{V}_x{}^d, \bar{V}_y{}^d)$, inclining at an angle of $\tan^{-1}(\bar{V}y^d/\bar{V}_x{}^d)$ to the x-axis are specified.

The assumption of two-dimensionality implies that there is no variation of fluid properties in the spanwise direction, consequently the Beltrami component of vorticity resulting from spanwise variation of blade loading is absent. Hence, $\lambda = 0$, and so is $S\nabla\Gamma$ in Eq. (2.19).

Eq. (4) implies that in the upstream region,

$$\frac{\partial}{\partial x}(P_t^u) = 0, \tag{2.24}$$

so that

$$P_t^u - \bar{P}_t^u = P_t^u(y) \; ; \tag{2.25}$$

while in the downstream region, we would have

$$\left(\bar{V}_x^d \frac{\partial}{\partial x} + \bar{V}_y^d \frac{\partial}{\partial y}\right)\frac{P_t^d}{\rho} = 0 \; , \tag{2.26}$$

the integration of which along the mean streamlines give

$$P_t^d - \bar{P}_t^d = P_t^d\left(y - x\frac{\bar{V}_y^d}{\bar{V}_x^d}\right) . \tag{2.27}$$

Because of the periodicity in y, it is convenient to represent functions by Fourier series. We therefore write

$$\frac{P_t^u - \bar{P}_t^u}{\rho \bar{V}_x^u} = \sum_{n=1}^{\infty} C_n e^{iny} , \tag{2.28}$$

and

$$\frac{P_t^d - \bar{P}_t^d}{\rho \bar{V}_x^d} = \sum_{n=1}^{\infty} P_n e^{in(y - x\tan\bar{\alpha}_2)} , \tag{2.29}$$

where we have used

$$\bar{\alpha}_2 = \tan^{-1}\left(\bar{V}_y^d / \bar{V}_x^d\right) . \tag{2.30}$$

The drift function, $\bar{\tau}^u$, of the upstream flow is given by

$$\bar{\tau}^u = \int^x \frac{dx}{\bar{V}_x^u} = \frac{x}{\bar{V}_x^u} , \tag{2.31}$$

while that of the downstream mean flow is given by

$$\bar{\tau}^d = \int^x \frac{dx}{\bar{V}_x^d} = \frac{x}{\bar{V}_x^d} , \tag{2.32}$$

or

$$\bar{\tau}^d = \int^y \frac{dy}{\bar{V}_y^d} = \frac{y}{\bar{V}_y^d} , \tag{2.33}$$

where, in each case, we have dropped an unneeded constant of integration. We shall learn in the next section that the drift function $\bar{\tau}^d$ given in

Eq. (2.32) will describe the downstream vorticity field.

Collecting these results for both the upstream and the downstream flow region, we obtain expressions for the perturbation velocities using Eqs. (2.20) and (2.21)

$$\tilde{\underset{\sim}{V}}^{u} = \nabla\phi^{u} + \sum_{n=1}^{\infty} C_n e^{iny}\hat{e}_x \tag{2.34}$$

and

$$\tilde{\underset{\sim}{V}}^{d} = \nabla\phi^{d} + \sum_{n=1}^{\infty} P_n e^{in(y-x\tan\bar{\alpha}_2)}\hat{e}_x . \tag{2.35}$$

Substituting the results obtained above in Eqs. (2.22) and (2.23), we obtain

$$\frac{\partial^2\phi^{u}}{\partial x^2} + \frac{\partial^2\phi^{u}}{\partial y^2} = 0 , \tag{2.36}$$

and

$$\frac{\partial^2\phi^{d}}{\partial x^2} + \frac{\partial^2\phi^{d}}{\partial y^2} = \sum_{n=1}^{\infty} inP_n\tan\bar{\alpha}_2 e^{in(y-x\tan\bar{\alpha}_2)} , \tag{2.37}$$

the solutions of which are given by

$$\phi^{u} = \sum_{n=1}^{\infty} A_n^{u} e^{iny}e^{nx} , \tag{2.38}$$

and

$$\phi^{d} = \sum_{n=1}^{\infty} A_n^{d} e^{iny}e^{-nx} - \sum_{n=1}^{\infty} \frac{iP_n\tan\bar{\alpha}_2}{n\sec^2\bar{\alpha}_2} e^{in(y-x\tan\bar{\alpha}_2)} . \tag{2.39}$$

The unknowns, A_n^{u}, A_n^{d} and P_n are to be determined from the three physical boundary condtions at the blade row.

Matching Conditions at the Blade Row

(i) An Isolated Rotor Blade Row:

The three matching conditions at the blade row will be found from the continuity equation, a relation for the leaving angle from the cascade and the Bernoulli equation (or the specification of stagnation pressure change across the blade-row).

The continuity condition gives

$$\bar{V}_x^u = \bar{V}_x^d = \bar{V}_x \quad . \tag{2.40}$$

for the mean flow. Application of the continuity condition to the perturbed flow gives

$$\tilde{V}_x^u = \tilde{V}_x^d \tag{2.41}$$

or for each harmonic n,

$$nA_n^u + C_n = -nA_n^d - P_n \sin^2\bar{\alpha}_2 + P_n \tag{2.42}$$

The outlet angle from the cascade will be taken as constant; i.e., it is independent of the incidence. Under these circumstances,

$$\frac{U - \bar{V}_y^d - \tilde{V}_y^d}{\bar{V}_x^d + \tilde{V}_x^d} = \frac{U - \bar{V}_y^d}{\bar{V}_x^d} = \text{constant} \tag{2.43}$$

where U is the rotating speed of the rotor. Consistent with the approximation here, Eq. (2.41) becomes,

$$\tilde{V}_y^d = -\frac{(U - \bar{V}_y^d)}{\bar{V}_x^d}\tilde{V}_x^d \quad , \tag{2.44}$$

or for each harmonic n,

$$in A_n^d + \frac{P_n \tan\bar{\alpha}_2}{\sec^2\bar{\alpha}_2} = -\frac{(U-\bar{V}_y^d)}{\bar{V}_x^d}(nA_n^u + C_n) \,, \tag{2.45}$$

where we have used Eq. (2.41).

The Bernoulli equation for the flow through a rotor is

$$P^u + \frac{1}{2}\rho[V_x^{u2} + (V_y^u - U)^2] = P^d + \frac{1}{2}\rho[V_x^{d2} + (V_y^d - U)^2] \tag{2.46}$$

where the assumption of quasi-steady flow is implied. Keeping terms of order ε, Eq. (2.46) can be rewritten as

$$\frac{P_t^u}{\rho} - \frac{\bar{P}_t^u}{\rho} - U\tilde{V}_y^u = \frac{P_t^d}{\rho} - \frac{\bar{P}_t^d}{\rho} - U\tilde{V}_y^d \,, \tag{2.47}$$

or for each harmonic n, we have

$$C_n - \frac{U}{\bar{V}_x} in(A_n^u + C_n) = P_n - \frac{U}{\bar{V}_x}\left(inA_n^d + \frac{P_n \tan\bar{\alpha}_2}{\sec^2\bar{\alpha}_2}\right) \tag{2.48}$$

Simultaneous solution of Eqs. (2.42), (2.45) and (2.48) gives the three unknowns A_n^u, A_n^d, and P_n as

$$P_n = \frac{C_n\left\{2 - \frac{\tan\bar{\alpha}_2}{U} + i\left(U - \tan\bar{\alpha}_2 - \frac{1}{U}\right)\right\}}{\left\{2 - \frac{1}{2}U\sin 2\bar{\alpha}_2 - \frac{\tan\bar{\alpha}_2}{U}\right\} + i\left\{-\frac{1}{U} - U\cos^2\bar{\alpha}_2\right\}} \,, \tag{2.49}$$

$$A_n^d = iU\cos^2\bar{\alpha}_2 P_n / n\left\{1 + i(U - \tan\bar{\alpha}_2)\right\} \tag{2.50}$$

and

$$A_n^u = -A_n^d - C_n/n + \cos^2\bar{\alpha}_2 P_n/n \,. \tag{2.51}$$

Eq. (2.49) shows that the stagnation pressure distortion passes through the rotor with a simple change of amplitude and phase.

The velocity components of perturbed flow are:

for the upstream region,

$$V_x^u = \bar{V}_x + \sum_{n=1}^{\infty} n A_n^u e^{iny} e^{nx} + \sum_{n=1}^{\infty} C_n e^{iny} \,, \tag{2.52}$$

$$V_y^u = \sum_{n=1}^{\infty} in A_n^u e^{iny} e^{nx} \,.$$

for the downstream region,

$$V_x^d = \bar{V}_x - \sum_{n=1}^{\infty} n A_n^d e^{iny} e^{-nx} - \sum_{n=1}^{\infty} P_n \sin^2\bar{\alpha}_2 e^{in(y-x\tan\bar{\alpha}_2)} + \sum_{n=1}^{\infty} P_n e^{in(y-x\tan\bar{\alpha}_2)} \,, \tag{2.53}$$

$$V_y^d = \bar{V}_y^d + \sum_{n=1}^{\infty} in A_n^d e^{iny} e^{-nx} + \sum_{n=1}^{\infty} \frac{P_n \tan\bar{\alpha}_2}{\sec^2\bar{\alpha}_2} e^{in(y-x\tan\bar{\alpha}_2)} \,.$$

(ii) An Isolated Stator Blade Row:

The matching conditions across a stator are just a special case of the matching conditions across a rotor. The equality of the axial velocity is the same for a rotor as well as a stator. The remaining two equations for a stator may be obtained from the rotor matching conditions by letting U=0.

The results are:

$$P_n = C_n \,, \tag{2.54}$$

$$A_n^d = 0 \,, \tag{2.55}$$

$$A_n^u = \frac{\cos^2\bar{\alpha}_2}{n} C_n - \frac{C_n}{n} \,. \tag{2.56}$$

The velocity components of the perturbed flow are:

for the upstream region,

$$V_x^u = \bar{V}_x + \sum_{n=1}^{\infty} n A_n^u e^{iny} e^{nx} + \sum_{n=1}^{\infty} C_n e^{iny}, \tag{2.57}$$

$$V_y^u = \sum_{n=1}^{\infty} in A_n^u e^{iny} e^{nx}.$$

for the downstream region,

$$V_x^d = \bar{V}_x - \sum_{n=1}^{\infty} C_n \sin^2\bar{\alpha}_2 e^{in(y-x\tan\bar{\alpha}_2)} + \sum_{n=1}^{\infty} P_n e^{in(y-x\tan\bar{\alpha}_2)}, \tag{2.58}$$

$$V_y^d = \bar{V}_y^d + \sum_{n=1}^{\infty} \frac{C_n \tan\bar{\alpha}_2}{\sec^2\bar{\alpha}_2} e^{in(y-x\tan\bar{\alpha}_2)}.$$

The Vorticity Field

The vorticity components of the flow field are given by

$$\underset{\sim}{\Omega}^u = -\sum_{n=1}^{\infty} in C_n e^{iny} \hat{e}_z, \tag{2.59}$$

$$\underset{\sim}{\Omega}^d = -\sum_{n=1}^{\infty} in P_n e^{in(y-x\tan\bar{\alpha}_2)} \hat{e}_z, \tag{2.60}$$

for the case of an isolated rotor. By replacing P_n in Eq. (2.60) with C_n, we obtain the corresponding result for the case of an isolated stator.

We thus see that the vorticity component lies on planes perpendicular to the x-y plane are always in the z-direction only; this is expected from the two-dimensionality assumption. These vortex filaments are simply convected by the upstream mean flow and the downstream mean flow. It is also noted that the vortex filaments pass through a stator without any change in magnitude. However, this is not the case for the rotor, for the

vortex filaments pass through the rotor with a change in magnitude given by the difference in P_n and C_n. This is because the individual blades of the rotor are moving relative to the fixed circulation distribution, and hence are unsteady;[58] they therefore shed vortices at their trailing edges. We shall show later that the strength of these shed vortices are exactly given by the difference in P_n and C_n.

The Downstream Pressure Field:

From the linearized Bernoulli equation for the flow, we find that the downstream perturbation static pressure is given by

$$\frac{\delta P}{\rho \bar{V}_x} = \frac{P-\bar{P}}{\rho \bar{V}_x} = \frac{P_t-\bar{P}_t}{\rho \bar{V}_x} - \bar{\underset{\sim}{V}} \cdot \tilde{\underset{\sim}{V}} \frac{1}{\bar{V}_x} , \tag{2.61}$$

For the rotor case,

$$\frac{\delta P^d}{\rho \bar{V}_x} = \sum_{n=1}^{\infty} n A_n^d e^{iny} e^{-nx} - \tan\bar{\alpha}_2 \sum_{n=1}^{\infty} in A_n^d e^{iny} e^{-nx} , \tag{2.62}$$

showing that the downstream static pressure field is totally due to the irrotational disturbances, and therefore decays exponentially with distance from the blade row. The introduction of rotational disturbances do not induce any static pressure field simply because these rotational disturbances are purely convected by the mean flow.

For the stator case,

$$\frac{\delta P^d}{\rho \bar{V}_x} = 0 , \tag{2.63}$$

so that the downstream static pressure field is uniform and all the streamlines are parallel. This is because all the irrotational disturbances take place upstream of the stator and the rotational disturbances are purely

convected by the mean flow.

2.3 Three-Dimensional Rectilinear Cascade Theory

Description of the Flow Field (Fig. II.3)

We will relax the assumption of two-dimensionality by allowing properties of the fluid to vary in the spanwise direction. A purely axial velocity profile $[(\bar{V}_x^u + \tilde{V}^u_{x-\infty}(y,z),0,0)]$ far upstream but varying in the y- and z-direction is assumed. We will also assume that the cascade is designed to give almost constant turning of the flow so that the downstream mean flow, $(\bar{V}_x^d, \bar{V}_y^d, 0)$, is inclined at a constant angle of $\tan^{-1}(\bar{V}_y^d/\bar{V}_x^d)$ to the x-axis. We thus have, by virtue of this relaxation,

$$\frac{P_t^u - \bar{P}_t^u}{\rho \bar{V}_x^u} = \sum_{n=1}^{\infty} C_n(z)\, e^{iny} , \tag{2.64}$$

and

$$\frac{P_t^d - \bar{P}_t^d}{\rho \bar{V}_x^d} = \sum_{n=1}^{\infty} P_n(z)\, e^{in(y - x\tan\bar{\alpha}_2)} , \tag{2.65}$$

where we have used Eq. (2.30). The drift function of the flow are as given in Eqs. (2.31), (2.32), and (2.33).

We will now show that the drift function $\bar{\tau}^d$ of the downstream mean flow as given by Eq. (2.32) describes the vorticity field consistently. The upstream vorticity is

$$\underset{\sim}{\Omega}^u = \sum_{n=1}^{\infty} \frac{dC_n}{dz}\, e^{iny}\, \hat{e}_y - \sum_{n=1}^{\infty} in C_n(z)\, e^{iny}\, \hat{e}_z , \tag{2.66}$$

indicating that the upstream vortex filaments lie on planes of constant x, and they are purely convected by the upstream mean flow.

Because of the relaxation of two-dimensionality here, blade loading can vary in the spanwise direction so that Beltrami component of vorticity is present in the downstream flow region resulting from flow angle variation introduced by the inlet distortion. This vorticity component springs from the solid surfaces of the blades, being different from that resulting from a gradient in stagnation pressure; therefore we will leave it for later consideration for the time being. The downstream vorticity arising from a gradient in stagnation pressure is

$$\underset{\sim}{\Omega}^{d}_{P_t} = +\sum_{n=1}^{\infty} \frac{dP_n}{dz} e^{in(y-x\tan\bar{\alpha}_2)} \hat{e}_y - \sum_{n=1}^{\infty} inP_n(z) e^{in(y-x\tan\bar{\alpha}_2)} \hat{e}_z . \tag{2.67}$$

on using $\bar{\tau}^d$ in Eq. (2.32); however, it would be

$$\underset{\sim}{\Omega}^{d}_{P_t} = -\sum_{n=1}^{\infty} \frac{dP_n}{dz} e^{in(y-x\tan\bar{\alpha}_2)} \hat{e}_x - \sum_{n=1}^{\infty} in\tan\bar{\alpha}_2 P_n(z) e^{in(y-x\tan\bar{\alpha}_2)} \hat{e}_z . \tag{2.68}$$

if we have used $\bar{\tau}^d$ in Eq. (2.33).

The vorticity given in Eq. (2.67) lies on plane of constant x and at the exit plane of the cascade (i.e., at x = 0), it is

$$\underset{\sim}{\Omega}^{d}_{P_t} = \sum_{n=1}^{\infty} \frac{dP_n}{dz} e^{iny} \hat{e}_y - \sum_{n=1}^{\infty} inP_n(z) e^{iny} \hat{e}_z . \tag{2.69}$$

However, the vorticity given in Eq. (2.68) does not lie on planes of constant x, but rather on planes of constant y and its value at the exit plane of the cascade (i.e., at x = 0) is

$$\cdot \underset{\sim}{\Omega}^{d}_{P_t} = -\sum_{n=1}^{\infty} \frac{dP_n(z)}{dz} e^{iny}\, \hat{e}_x - \sum_{n=1}^{\infty} in \tan\bar{\alpha}_2\, P_n(z)\, e^{iny}\, \hat{e}_z . \tag{2.70}$$

These vortex filaments should remain on planes of constant x as they approach and emerge from the cascade. However, the use of the drift function $\bar{\tau}^d$ in Eq. (2.33) to describe the downstream vorticity field does not fit this picture, for the vorticity so described does not lie on x = 0 plane, and has a component in the x-direction. This violates Kelvin's Law. Hence, we conclude that the drift function $\bar{\tau}^d$ given in Eq. (2.32) describes the downstream vorticity field correctly.

The Beltrami component of vorticity, as given in Eq. (2.7), implies that it lies at the intersection of surfaces of constant S and constant Γ. Eq. (2.15) implies that

$$\bar{V}_x^d \frac{\partial \lambda}{\partial x} + \bar{V}_y^d \frac{\partial \lambda}{\partial y} = 0, \tag{2.71}$$

so that its integration along the mean streamlines yields

$$\lambda = \lambda(z, y - x \tan\bar{\alpha}_2). \tag{2.72}$$

By taking

$$S = S(y - x \tan\bar{\alpha}_2), \tag{2.73}$$

Eq. (2.7) ensures that the Beltrami vorticity will coicide with the mean streamlines. Substitution of Eq. (2.73) in

$$\bar{\underline{V}} \times (\nabla S \times \nabla \Gamma) = 0$$

simply yields

$$\bar{\underline{V}} \cdot \nabla \Gamma = 0 \,, \tag{2.74a}$$

or

$$\bar{V}_x \frac{\partial \Gamma}{\partial x} + \bar{V}_y^d \frac{\partial \Gamma}{\partial y} = 0 \,. \tag{2.74b}$$

Without loss of generality, we can simply choose

$$\Gamma = \Gamma(z) \tag{2.75}$$

as indicated by Eq. (2.74). (Γ is related to the blade circulation.)

Because of the periodicity in the y-coordinate, we write

$$S \nabla \Gamma = \sum_{n=1}^{\infty} G_n(z) e^{in(y - x \tan \bar{\alpha}_2)} \hat{e}_z \,. \tag{2.76}$$

Collecting these results we obtain

$$\tilde{\underline{V}}^u = \nabla \phi^u + \sum_{n=1}^{\infty} C_n(z) e^{iny} \hat{e}_x \tag{2.77}$$

for the upstream flow region; and

$$\tilde{\underline{V}}^d = \nabla \phi^d + \sum_{n=1}^{\infty} P_n(z) e^{in(y - x \tan \bar{\alpha}_2)} \hat{e}_x + \sum_{n=1}^{\infty} G_n(z) e^{in(y - x \tan \bar{\alpha}_2)} \hat{e}_z \,. \tag{2.78}$$

for the downstream flow region.

Substitution of the above results in Eqs. (2.22) and (2.23) yields

$$\frac{\partial^2 \phi^u}{\partial x^2} + \frac{\partial^2 \phi^u}{\partial y^2} + \frac{\partial^2 \phi^u}{\partial z^2} = 0 \,, \tag{2.79}$$

and

$$\frac{\partial^2\phi^d}{\partial x^2}+\frac{\partial^2\phi^d}{\partial y^2}+\frac{\partial^2\phi^d}{\partial z^2}=\sum_{n=1}^{\infty} in\tan\bar{\alpha}_2 P_n(z)\, e^{in(y-x\tan\bar{\alpha}_2)} - \sum_{n=1}^{\infty}\frac{dG_n}{dz}e^{in(y-x\tan\bar{\alpha}_2)} \quad ; \tag{2.80}$$

the solutions of which give

$$\phi^u=\sum_{n=1}^{\infty}\sum_{p=0}^{\infty}A^u_{np}\, e^{\lambda_{np}x}e^{iny}\cos\left(\frac{p\pi}{l}z\right), \tag{2.81}$$

and

$$\phi^d=\sum_{n=1}^{\infty}\sum_{p=0}^{\infty}A^d_{np}e^{-\lambda_{np}x}e^{iny}\cos\left(\frac{p\pi}{l}z\right)+\sum_{n=1}^{\infty}\sum_{p=0}^{\infty}X_{np}(x)\, e^{iny}\cos\left(\frac{p\pi}{l}z\right) \tag{2.82}$$

with

$$X_{np}(x)=-\frac{2e^{-inx\tan\bar{\alpha}_2}}{l(\lambda_{np}^2+n^2\tan^2\bar{\alpha}_2)}\left\{in\tan\bar{\alpha}_2\int_0^l P_n(z)\cos\frac{p\pi}{l}z\,dz-\frac{p\pi}{l}\int_0^l G_n(z)\sin\frac{p\pi}{l}z\,dz\right\} \tag{2.83}$$

(Appendix II.A)

where we have used the boundary conditions that

$$V_z=0 \qquad z=0,\,l \tag{2.84}$$

and

$$G_n(z)=0 \qquad z=0,\,l \tag{2.85}$$

The axial eigenvalues λ_{np} are given by

$$\lambda_{np}^2 = \left(n^2 + \frac{p^2\pi^2}{l^2}\right) ; \tag{2.86}$$

l being the height of the duct in which the cascade is encased.

Inspection of Eqs. (2.81) and (2.82) shows that the remaining unknowns are A_{np}^{u}, $P_n(z)$, and $G_n(z)$; they will be determined in the following.

Matching Conditions at the Blade Row:

(i) An Isolated Rotor Blade Row:

We require four matching conditions at the blade row for the determination of the four unknowns; namely, A_{np}^{u}, $P_n(z)$, and $G_n(z)$. Three of them are provided by those stated in the previous section: the continuity condition, a relation for the leaving angle from the cascade, and the Bernoulli equation. The additional matching condition is provided by the fact that the blade exert negligible spanwise force on the fluid so that the z-component of velocity is continuous there.

The continuity condition gives, for the mean flow, Eq. (2.40); while for the perturbed flow it gives Eq. (2.41) so that for each harmonic n,

$$\sum_{p=0}^{\infty} \lambda_{np} A_{np}^{u} \cos\frac{p\pi}{l} z + C_n(z) = -\sum_{p=0}^{\infty} \lambda_{np} A_{np}^{d} \cos\frac{p\pi}{l} z + \sum_{p=0}^{\infty} X'_{np}(0) \cos\frac{p\pi}{l} z + P_n(z) \tag{2.87}$$

The continuity of spanwise component of velocity gives

$$V_z^u = V_z^d , \tag{2.88a}$$

or

$$\sum_{p=0}^{\infty} \frac{p\pi}{l} A_{np}^{u} \sin\frac{p\pi}{l} z = -\sum_{p=0}^{\infty} \frac{p\pi}{l} A_{np}^{d} \sin\frac{p\pi}{l} z - \sum_{p=0}^{\infty} \frac{p\pi}{l} X_{np}(0) \sin\frac{p\pi}{l} z + G_n(z) \tag{2.88b}$$

for each harmonic n.

The assumption of constant outlet angle gives

$$\sum_{p=0}^{\infty} in A_{np}^{d} \cos\frac{p\pi}{l}z + \sum_{p=0}^{\infty} in X_{np}(0) \cos\frac{p\pi}{l}z = \frac{U-\bar{V}_y^{d}}{\bar{V}_x}\left(\sum_{p=0}^{\infty}\lambda_{np} A_{np}^{u}\cos\frac{p\pi}{l}z + C_n(z)\right) \tag{2.89}$$

Application of the Bernoulli equation gives

$$C_n(z) - U\sum_{p=0}^{\infty} in A_{np}^{u}\cos\frac{p\pi}{l}z = P_n(z)$$

$$-U\left[\sum_{p=0}^{\infty} in A_{np}^{d}\cos\frac{p\pi}{l}z + \sum_{p=0}^{\infty} in X_{np}(0)\cos\frac{p\pi}{l}z\right] \tag{2.90}$$

Eq. (2.88b) shows that $G_n(z)$ can be expanded into a Fourier sine series of the form

$$G_n(z) = \sum_{p=0}^{\infty} g_{np}\sin\frac{p\pi}{l}z \tag{2.91}$$

while Eqs. (2.89) and (2.90) show that both $C_n(z)$ and $P_n(z)$ can be expanded into a Fourier cosine series,

$$C_n(z) = \sum_{p=0}^{\infty} C_{np}\cos\frac{p\pi}{l}z \tag{2.92}$$

and

$$P_n(z) = C_n(z) + \sum_{p=0}^{\infty} P_{np}\cos\frac{p\pi}{l}z \tag{2.93}$$

Using Eqs. (2.91), (2.92), and (2.93) in $X_{np}(0)$ and $X'_{np}(0)$, we obtain

$$X_{np}(0) = -\frac{1}{(\lambda_{np}^2 + n^2\tan^2\bar{\alpha}_2)}\left\{in\tan\bar{\alpha}_2 (C_{np}+P_{np}) - \frac{P\pi}{l} g_{np}\right\}, \tag{2.94}$$

and

$$X'_{np}(0) = \frac{in\tan\bar{\alpha}_2}{(\lambda_{np}^2 + n^2\tan^2\bar{\alpha}_2)}\left\{in\tan\bar{\alpha}_2 (C_{np}+P_{np}) - \frac{P\pi}{l} g_{np}\right\} \tag{2.95}$$

On substituting Eqs. (2.91) to (2.95) in Eqs. (2.87) to (2.90), we obtain, by virtue of the orthogonal property of the trigonometrical functions, the following 4 by 4 matrix equation for each n and p,

$$\begin{bmatrix} \lambda_{np} & \lambda_{np}\left[\frac{n^2\tan^2\bar{\alpha}_2}{D} - 1\right] & \frac{P\pi in\tan\bar{\alpha}_2}{l\,D} \\ -\frac{P\pi}{l} & \frac{P\pi}{l} & -\frac{P\pi in\tan\bar{\alpha}_2}{l\,D} \\ \frac{U-\bar{V}_y^d}{\bar{V}_x}\lambda_{np} & in & \frac{n^2\tan^2\bar{\alpha}_2}{D} \\ -inU & inU\left[\frac{Un^2\tan^2\bar{\alpha}_2}{D} - 1\right] & \frac{P\pi inU}{l\,D} \end{bmatrix} \begin{bmatrix} A_{np}^u \\ A_{np}^d \\ P_{np} \\ g_{np} \end{bmatrix} = \begin{bmatrix} -\frac{n^2\tan^2\bar{\alpha}_2}{D} C_{np} \\ \frac{P\pi in\tan\bar{\alpha}_2}{l\,D} C_{np} \\ -\left[\frac{U-\bar{V}_y^d}{\bar{V}_x} + \frac{n^2\tan\bar{\alpha}_2}{D}\right] C_{np} \\ -\frac{Un^2\tan\bar{\alpha}_2}{D} C_{np} \end{bmatrix} \tag{2.96}$$

$$D = \lambda_{np}^2 + n^2\tan^2\bar{\alpha}_2$$

which can readily be inverted to give the unknowns A_{np}^{u}, A_{np}^{d}, P_{np} and G_{np}. With their determination, the velocity components of the perturbed flow are: for the upstream region,

$$V_x^u = \bar{V}_x + \sum_{n=1}^{\infty}\sum_{p=0}^{\infty} \lambda_{np} A_{np}^u e^{\lambda_{np} x} e^{iny} \cos\frac{p\pi}{l} z + \sum_{n=1}^{\infty} C_n(z) e^{iny}$$

$$V_y^u = -\sum_{n=1}^{\infty}\sum_{p=0}^{\infty} in A_{np}^u e^{\lambda_{np} x} e^{iny} \cos\frac{p\pi}{l} z \,, \tag{2.97}$$

$$V_z^u = -\sum_{n=1}^{\infty}\sum_{p=0}^{\infty} \frac{p\pi}{l} A_{np}^u e^{\lambda_{np} x} e^{iny} \sin\frac{p\pi}{l} z \;;$$

for the downstream flow region,

$$V_x^d = \bar{V}_x - \sum_{n=1}^{\infty}\sum_{p=0}^{\infty} \lambda_{np} A_{np}^d e^{-\lambda_{np} x} e^{iny} \cos\frac{p\pi}{l} z + \sum_{n=1}^{\infty}\sum_{p=0}^{\infty} X'_{np}(x) e^{iny} \cos\frac{p\pi}{l} z + \sum_{n=1}^{\infty} P_n(z) e^{in(y - x\tan\bar{\alpha}_2)} \,,$$

$$V_y^d = \bar{V}_y^d + \sum_{n=1}^{\infty}\sum_{p=0}^{\infty} in A_{np}^d e^{-\lambda_{np} x} e^{iny} \cos\frac{p\pi}{l} z + \sum_{n=1}^{\infty}\sum_{p=0}^{\infty} in X_{np}(x) e^{iny} \cos\frac{p\pi}{l} z \,. \tag{2.98}$$

$$V_z^d = -\sum_{n=1}^{\infty}\sum_{p=0}^{\infty} \frac{p\pi}{l} A_{np}^d e^{-\lambda_{np} x} e^{iny} \sin\frac{p\pi}{l} z - \sum_{n=1}^{\infty}\sum_{p=0}^{\infty} \frac{p\pi}{l} X_{np}(x) e^{iny} \sin\frac{p\pi}{l} z + \sum_{n=1}^{\infty} G_n(z) e^{in(y - x\tan\bar{\alpha}_2)}$$

(ii) An Isolated Stator Blade Row:

The results for a stagnation pressure distortion passing through a stator may be obtained from those of the rotor above by letting U = 0 and $P_{np} = 0$; the stagnation pressure distortion would pass through the stator without any change in magnitude or phase. With U = 0, and $P_{np} = 0$, the matrix equation (2.98) reduces to a 3 by 3 matrix equation for each n and p,

$$\begin{bmatrix} \lambda_{np} & \lambda_{np} & \frac{p\pi in\tan\bar{\alpha}_2}{lD} \\ -\frac{p\pi}{l} & \frac{p\pi}{l} & \left[\frac{p^2\pi^2}{l^2D}-1\right] \\ -\tan\bar{\alpha}_2\lambda_{np} & in & \frac{p\pi in}{lD} \end{bmatrix} \begin{bmatrix} A^u_{np} \\ A^d_{np} \\ g_{np} \end{bmatrix} = \begin{bmatrix} -\frac{n^2\tan^2\bar{\alpha}_2}{D}C_{np} \\ \frac{p\pi in\tan\bar{\alpha}_2}{lD}C_{np} \\ \left[\tan\bar{\alpha}_2-\frac{n^2\tan^2\bar{\alpha}_2}{D}\right]C_{np} \end{bmatrix} \tag{2.99}$$

$$D = \lambda_{np}^2 + n^2\tan^2\bar{\alpha}_2 .$$

which on inversion gives the unknowns A^u_{np}, A^d_{np}, and G_{np}. The perturbed velocity field is described by Eqs. (2.97) and (2.98) for the upstream and the downstream flow region, with $C_n(z)$ replacing $P_n(z)$ in Eq. (2.98).

The Vorticity Field:

The vorticity components of the flow field are given by

$$\underset{\sim}{\Omega}^u = \sum_{n=1}^{\infty}\frac{dG_n}{dz}e^{iny}\hat{e}_y - \sum_{n=1}^{\infty} in\,C_n(z)\,e^{iny}\hat{e}_z \tag{2.66}$$

$$\underset{\sim}{\Omega}^d = \sum_{n=1}^{\infty} inG_n(z)\,e^{in(y-x\tan\bar{\alpha}_2)}\hat{e}_x + \sum_{n=1}^{\infty}\left[\frac{dP_n}{dz}+in\tan\bar{\alpha}_2 G_n(z)\right]e^{in(y-x\tan\bar{\alpha}_2)}\hat{e}_y$$

$$-\sum_{n=1}^{\infty} inP_n(z)\,e^{in(y-x\tan\bar{\alpha}_2)}\hat{e}_z , \tag{2.100}$$

for the isolated rotor case. By replacing $P_n(z)$ with $C_n(z)$ in Eq. (2.100) we obtain the corresponding result for the isolated stator case.

The vortex filaments are purely convected by the mean flow. Upstream of the blade row, they lie on planes of constant x. The presence of the Beltrami component of vorticity and a radial shear in stagnation pressure gives rise to a streamwise component of vorticity in the downstream flow field; it is given by

$$-\Omega_S = \frac{\bar{V}_x}{\bar{V}} \sum_{n=1}^{\infty} in G_n(z) e^{in(y - x\tan\bar{\alpha}_2)} + \frac{\bar{V}_y}{\bar{V}} \sum_{n=1}^{\infty} \left(\frac{dP_n}{dz} + in\tan\bar{\alpha}_2 G_n(z) \right) e^{in(y - x\tan\bar{\alpha}_2)} . \quad (2.101)$$

The streamwise vorticity, which remains unchanged as it moves downstream, will induce a secondary flow, and hence spanwise velocity; in consequence, the whole flow field has to readjust itself to satisfy the continuity condition thus giving rise to three-dimensional effects.

From Eqs. (2.88) and (2.90) for a rotor, we obtain the result that

$$n U G_n(z) = i \frac{d}{dz}(P_n - C_n) . \quad (2.102)$$

If $\Gamma(z)$ is the circulation about each of the B blades on a rotor represented by the actuator disc, then

$$B\tilde{\Gamma}(z) = -BS(\tilde{V}_y^d - \tilde{V}_y^u)\big|_{x=0} , \quad (2.103)$$

(we have taken $\Gamma(2) = \Gamma_0 + \tilde{\Gamma}(2)$ with $\Gamma_0 = -s\bar{V}_y^d$)

where s is the blade spacing. But Eqs. (2.47) or (2.90) gives

$$(\tilde{V}_y^d - \tilde{V}_y^u)\big|_{x=0} = \frac{1}{U}\left(\sum_{n=1}^{\infty} P_n e^{iny} - \sum_{n=1}^{\infty} C_n e^{iny} \right) \quad (2.104)$$

so that on using Eq. (2.103) we obtain

$$\sum_{n=1}^{\infty}(P_n - C_n)e^{iny} = -U\frac{\tilde{\Pi}(z)}{S} . \tag{2.105}$$

From Eq. (2.102), we then have the result that

$$\sum_{n=1}^{\infty} in G_n e^{iny} = \frac{1}{S}\frac{d\tilde{\Pi}}{dz} = \frac{1}{S}\frac{d\Gamma}{dz} , \tag{2.106}$$

indicating that G_n is a consequence of the variation of the blade circulation, which leads to trailing vorticity behind the blade row.

We finally note that the spanwise vortex filament changes in magnitude as it passes through the rotor, as is readily seen from Eqs. (2.66), (2.100), and (2.93). This is a result of the shed vorticies from the trailing edges of the rotor since it is under the condition of unsteady flow.[58]

The Downstream Pressure Field

Using Eqs. (2.61), we find that the downstream static pressure field is given by

$$\frac{\delta p^d}{\rho \bar{V}_x} = \sum_{n=1}^{\infty}\sum_{p=0}^{\infty} \lambda_{np} A^d_{np} e^{-\lambda_{np} x} e^{iny} \cos\frac{p\pi}{l} z - \tan\bar{\alpha}_2 \sum_{n=1}^{\infty}\sum_{p=0}^{\infty} in A^d_{np} e^{-\lambda_{np} x} e^{iny} \cos\frac{p\pi}{l} z . \tag{2.107}$$

for both the case of a rotor and a stator. The static pressure field is totally due to the potential disturbances, and therefore decays exponentially with distance. The induced disturbances make no contribution since they are purely convected by the mean flow. We note that, in contrast to the two-dimensional case, there is a static pressure field behind a stator because of the presence of trailing vorticity.

CHAPTER 3 - ASYMMETRIC FLOW THROUGH ANNULAR CASCADES

3.1 Description of the Flow Field

Consider the flow through an isolated annular cascade, encased in an infinite cylindrical annulus, using the right-handed coordinate system (r,θ,z). The flow will be assumed to have a purely axial velocity profile $[(0,0,\bar{V}_z^u + \tilde{V}_{z-\infty})]$ far upstream but varying in the radial and circumferential direction, and a free vortex mean flow, $(0,\bar{V}_\theta^d,\bar{V}_z^d)$, downstream (Fig. II.4). The annular cascade will be replaced by an actuator disc, placed at the origin of the z-axis, so that the individual identity of the blades is suppressed. It should be noted that the redistribution of the radial flow is not restricted by the baldes so that it may not be quite realistic to contract the blade-row to a disc as in the two-dimensional case. Instead, the disc has to be located at an appropriate location within the blade row.

Appropriate to a free vortex mean flow (when the assumption of incompressibility is valid), we have,

$$\bar{V}_z^u = \bar{V}_z^d = \bar{V}_z = \text{constant} \tag{3.1}$$

and

$$\bar{V}_\theta^d = \frac{K_o \bar{V}_z}{r} \tag{3.2}$$

where we have used

$$K_o = \frac{\bar{V}_\theta^d r}{\bar{V}_z} \tag{3.3}$$

to indicate the strength of the mean swirl velocity.

The modulation of the flow angle by the introduction of an upstream asymmetric flow pattern results in a spanwise variation of blade-loading, consequently trailing vorticies spring from the trailing edges of the blades. Thus, the upstream flow is threaded with vortex filaments arising from a gradient in stagnation pressure, while the downstream flow is threaded with vortex filaments which arise from a gradient in stagnation pressure as a result of the passage of the distorted flow through the blade row, as well as with those which spring from the solid surfaces of the blades forming the disc. As before, the analytical technique used will be that of giving a correct and consistent prescription of the vorticity field so that the internal aerodynamics of the flow can be conveniently described.

Expanding Eq. (2.4) in cylindrical coordinates, we obtain,

$$\bar{V}_z \frac{\partial}{\partial z}\left(\frac{P_t^u}{\rho}\right) = 0, \tag{3.4}$$

so that

$$P_t^u - \bar{P}_t^u = P_t^u(r,\theta), \tag{3.5}$$

in the upstream flow region; however, in the downstream flow region, we obtain,

$$\frac{\bar{V}_\theta^d}{r}\frac{\partial}{\partial\theta}\left(\frac{P_t^d}{\rho}\right) + \bar{V}_z \frac{\partial}{\partial z}\left(\frac{P_t^d}{\rho}\right) = 0, \tag{3.6}$$

so that its integration along the mean stream trajectory gives

$$P_t^d - \bar{P}_t^d = P_t^d(r, \bar{\alpha}^d), \tag{3.7}$$

where we have used

$$\bar{\alpha}^d = \theta - z\frac{K_0}{\bar{r}^2} . \tag{3.8}$$

Because of the inherent periodicity in the circumferential direction in flow through turbomachines, it is conveneint to represent functions by Fourier series. Hence, we write,

$$\frac{P_t^u - \bar{P}_t^u}{\rho \bar{V}_z} = \sum_{n=1}^{\infty} C_n(r)\, e^{in\theta} , \tag{3.9}$$

and

$$\frac{P_t^d - \bar{P}_t^d}{\rho \bar{V}_z} = \sum_{n=1}^{\infty} P_n(r)\, e^{in\bar{\alpha}^d} , \tag{3.10}$$

where n is the circumferential harmonics.

The drift function $\bar{\tau}^u$ of the upstream mean flow is

$$\bar{\tau}^u = \frac{z}{\bar{V}_z} . \tag{3.11}$$

Guided by the analysis given in Section 2.3 or Section 3.1 of Part I, the drift function $\bar{\tau}^d$ which will give a correct and consistent description of the vorticity field resulting from a gradient in stagnation pressure is given by

$$\bar{\tau}^d = \frac{z}{\bar{V}_z} \tag{2.12}$$

We have dropped the constant of integration (which is of no importance here) in both Eqs. (3.11) and (3.12). With the knowledge of the gradient

in stagnation pressure and the drift function of the mean flow, the vorticity resulting from the stagnation pressure gradient is known.

The Beltrami component of vorticity, as described by Eq. (2.7), lies at the intersection of surfaces of constant S and Γ. But Eq. (2.15), which guarantees that the Beltrami vorticity be divergence-free, implies that

$$\frac{\bar{V}_\theta^d}{r}\frac{\partial \lambda}{\partial \theta} + \bar{V}_z \frac{\partial \lambda}{\partial z} = 0 , \tag{3.13}$$

so that

$$\lambda = \lambda(r, \bar{\alpha}^d), \tag{3.14}$$

in essentially in agreement with Eq. (2.16).

By taking

$$S = S(\bar{\alpha}^d), \tag{3.15}$$

the Beltrami vorticity will coincide with the mean streamlines since they are lines of constant $\bar{\alpha}^d$. Substitution of Eq. (3.15) in

$$\tilde{\underset{\sim}{V}} \times (\nabla S \times \nabla \Gamma) = 0$$

simply yields

$$\tilde{\underset{\sim}{V}} \cdot \nabla \Gamma = 0 , \tag{3.16}$$

or

$$\frac{\bar{V}_\theta^d}{r}\frac{\partial \Gamma}{\partial \theta} + \bar{V}_z \frac{\partial \Gamma}{\partial z} = 0 , \tag{3.17}$$

so that

$$\Gamma(=\Gamma(r,\bar{\alpha}^d)\ . \tag{3.18}$$

Because of Eq. (3.15), the dependence of Γ on $\bar{\alpha}^d$ can be discarded without any loss of generality. Thus,

$$\Gamma=\Gamma(r) \tag{3.19}$$

only. Hence, by virtue of the periodicity in the circumferential direction,

$$S(\bar{\alpha}^d)\nabla\Gamma(r)=\sum_{n=1}^{\infty}G_n(r)e^{in\bar{\alpha}^d}\hat{e}_r\ , \tag{3.20}$$

and the Beltrami vorticity is given by

$$\begin{aligned}\lambda\bar{V} &= \nabla S(\bar{\alpha}^d)\times\nabla\Gamma(r)\\ &=\sum_{n=1}^{\infty}\nabla(e^{in\bar{\alpha}^d})\times\nabla\Gamma_n(r)\\ &=\sum_{n=1}^{\infty}\nabla(e^{in\bar{\alpha}^d})\times(G_n(r)\hat{e}_r)\ .\end{aligned} \tag{3.21}$$

The $G_n(r)$ will be determined subsequently.

Collecting these results for the upstream and the downstream flow region, we arrive at an expression for the perturbation velocities there of the form

$$\tilde{\underset{\sim}{V}}^u=\nabla\phi^u+\sum_{n=1}^{\infty}C_n(r)e^{in\theta}\hat{e}_z\ , \tag{3.22}$$

and

$$\underset{\sim}{\tilde{V}}^d = \nabla\phi^d + \sum_{n=1}^{\infty} P_n(r)\, e^{in\bar{\alpha}^d}\hat{e}_z + \sum_{n=1}^{\infty} G_n(r)\, e^{in\bar{\alpha}^d}\hat{e}_r \,. \tag{3.23}$$

Substitution of the above results in Eqs. (2.22) and (2.23) (or using continuity, $\nabla \cdot \underset{\sim}{\tilde{V}} = 0$), we readily obtain equations for ϕ^u and ϕ^d, which in terms of cylindrical coordinates, are

$$\frac{\partial^2\phi^u}{\partial r^2} + \frac{1}{r}\frac{\partial\phi^u}{\partial r} + \frac{1}{r^2}\frac{\partial^2\phi^u}{\partial\theta^2} + \frac{\partial^2\phi^u}{\partial z^2} = 0 \,, \tag{3.24}$$

and

$$\frac{\partial^2\phi^d}{\partial r^2} + \frac{1}{r}\frac{\partial\phi^d}{\partial r} + \frac{1}{r^2}\frac{\partial^2\phi^d}{\partial\theta^2} + \frac{\partial^2\phi^d}{\partial z^2} = -\frac{1}{r}\frac{\partial}{\partial r}\left[r\sum_{n=1}^{\infty} G_n(r)\, e^{in\bar{\alpha}^d}\right] - \frac{\partial}{\partial z}\left[\sum_{n=1}^{\infty} P_n(r)\, e^{in\bar{\alpha}^d}\right]$$

$$= \sum_{n=1}^{\infty}\left(\frac{inK_0 P_n(r)}{r^2} - \frac{1}{r}\frac{d}{dr}rG_n(r)\right)e^{in\bar{\alpha}^d}$$

$$-z\sum_{n=1}^{\infty}\frac{2inK_0 G_n(r)}{r^3}\, e^{in\bar{\alpha}^d} \,, \tag{3.25}$$

where we note the last term on the RHS in Eq. (3.25) is secular in z.

Both Eqs. (3.24) and (3.25) are to be solved under the boundary conditions at the hub ($r = r_h$) and the tip ($r = r_t$) that the radial velocities should vanish there.

3.2 Determination of the Three-Dimensional Perturbed Flow

Before proceeding to the complete solution of Eqs. (3.24) and (3.25), we will make the variables dimensionless using the following characteristic scales: axial velocity $\bar{V}_z$, tip radius r_T, and density ρ. The pressure will be measured in units of $\rho\bar{V}_z^{\,2}$.

The solutions of Eqs. (3.24) and (3.25) can be written in the form of

$$\phi_d^u = \sum_{n=1}^{\infty}\sum_{p=1}^{\infty} A_{np}^u e^{-\lambda_{np}|z|} R_{np}(r) e^{in\theta} + \phi_I^d(r,\theta,z) H(z). \tag{3.26}$$

where H(z) is the Heaviside function defined in Eq. (3.30) in Part I.

The first double sum in Eq. (3.26) represents the exponentially decaying homogeneous solution typical of flow through an annular duct. The normalized radial eigenfunction $R_{np}(r)$ is a linear combination of the Bessel Functions of the first kind J_n and the second kind Y_n with order n and argument $(\lambda_{np} r)$; it is given by

$$R_{np}(r) = \frac{\left\{ J_n(\lambda_{np} r) - \frac{J_n'(\lambda_{np})}{Y_n'(\lambda_{np})} Y_n(\lambda_{np} r) \right\}}{\sqrt{\int_h^1 r \left\{ J_n(\lambda_{np} r) - \frac{J_n'(\lambda_{np})}{Y_n'(\lambda_{np})} Y_n(\lambda_{np} r) \right\}^2 dr}} \tag{3.27}$$

(Its orthogonal property has been described in Chapter 3 of Part I).

where the primes on J_n and Y_n denote differentiation with respect to argument, and we have also introduced $h(=r_h/r_t)$ as the hub-to-tip ratio.

It has been shown[13,14] that $G_n(r)$, the contribution of the shed circulation to the downstream velocity component $\tilde{v}_r^d$, must vanish at the hub and the tip. This is necessary so, otherwise the strength of the trailing vorticity at the tip would be finite which would in turn imply a finite

induced radial velocity there. With this in mind, the vanishing of the radial velocities at the hub and the shroud is guaranteed by taking the characteristic values of λ_{np}, to be the roots of

$$J_n'(\lambda_{np}h)Y_n'(\lambda_{np}) - J_n'(\lambda_{np})Y_n'(\lambda_{np}h) = 0, \tag{3.28}$$

and by imposing the boundary conditions

$$\left.\frac{\partial \phi_I^d}{\partial r}\right|_h = \left.\frac{\partial \phi_I^d}{\partial r}\right|_1 = 0, \tag{3.29}$$

on the solution $\phi_I^d(r,\theta,z)$.

We can construct a solution for ϕ_I^d by using the same technique as we used for finding the induced potential of the blade wakes in Chapter 3 of Part I; i.e., we express $\phi_I^d(r,\theta,z)$ as a product of three functions, each depending on r, θ, and z only,

$$\phi_I^d(r,\theta,z) = \sum_{n=1}^{\infty}\sum_{p=1}^{\infty} Z_{np}(z)\,R_{np}(r)\,e^{in\theta}. \tag{3.30}$$

Substitution of Eq. (3.30) in Eq. (3.25) and application of the hub and tip boundary conditions allows one to determine the $Z_{np}(z)$ in the form

$$Z_{np}(z) = -\int_h^1 \frac{\left[r G_n \frac{dR_{np}}{dr} + in\frac{K_0}{r^2}R_{np}P_n\right]}{\left(\lambda_{np}^2 + \frac{n^2K_0^2}{r^4}\right)} e^{-\frac{inK_0z}{r^2}}\,dr. \tag{3.31}$$

(See Appendix II.B)

Inspection of Eqs. (3.26), (3.30) and (3.31) shows that the remaining unknowns, for each n and p to be $A_{np}^{d_u}$, $P_n(r)$ and $G_n(r)$. Determination of these quantities follows from the matching at the actuator disc.

3.3 Matching at the Blade Row

For the case of an isolated blade row with upstream flow field extending to minus infinity, and the downstream flow field to plus infinity, the upstream and the downstream solutions of the perturbed flow have to be appropriately matched at the actuator disc to represent a physically valid flow. This is what we have been doing for all the previous analyses, and these matching conditions at the actuator disc are usually derivable from conditions relating to the conservation of mass, momentum and energy.

The determination of the four sets of unknowns, $\{A^{u}_{np}\}$, $\{P_n(r)\}$ and $\{G_n(r)\}$, requires four independent matching conditions. They are the same as the ones we used in Section 3 of Chapter 2.

(i) An Isolated Rotor Blade Row

The continuity condition simply requires that the axial velocity be continuous at the disc. Because of Eq. (3.1), we have

$$\left.\frac{\partial \phi^u}{\partial z}\right|_{z=0^-} + \sum_{n=1}^{\infty} C_n(r)\, e^{in\theta} = \left.\frac{\partial \phi^d}{\partial z}\right|_{z=0^+} + \sum_{n=1}^{\infty} P_n(r)\, e^{in\theta} \,. \tag{3.32}$$

Becaue the blades exert negligible radial force, the radial velocity is the same on either side of the disc; hence

$$\left.\frac{\partial \phi^u}{\partial r}\right|_{z=0^-} = \left.\frac{\partial \phi^d}{\partial r}\right|_{z=0^+} + \sum_{n=1}^{\infty} G_n(r)\, e^{in\theta} \,. \tag{3.33}$$

The energy condition, being expressed as a change of the stagnation pressure over the blade row, is determined by the work done. Since the blade-row characteristics are not being considered, we recognize that this is simply the Bernoulli equation. Hence, for a rotor, rotating at speed ω, we have,

$$\left(p_t^d - \bar{p}_t^d\right) - \left(p_t^u - \bar{p}_t^u\right) = \rho\omega r\left(\frac{1}{r}\frac{\partial\phi^d}{\partial\theta}\bigg|_{z=0^+} - \frac{1}{r}\frac{\partial\phi^u}{\partial\theta}\bigg|_{z=0^-}\right), \tag{3.34}$$

or

$$\sum_{n=1}^{\infty}(P_n - C_n)e^{in\theta} = \frac{\omega r}{\bar{V}_z}\left(\frac{1}{r}\frac{\partial\phi^d}{\partial\theta}\bigg|_{z=0^+} - \frac{1}{r}\frac{\partial\phi^u}{\partial\theta}\bigg|_{z=0^-}\right).$$

The fluid outlet angle relative to the blades is specified and assumed to be independent of the inlet angle, so that, for the rotor at z = 0:

$$\frac{\bar{V}_\theta^d + \frac{1}{r}\frac{\partial\phi^d}{\partial\theta}\Big|_{z=0^+} - \omega r}{\bar{V}_z + \frac{\partial\phi^d}{\partial z}\Big|_{z=0^+} + \sum_{n=1}^{\infty}P_n e^{in\theta}} = \frac{\bar{V}_\theta^d - \omega r}{\bar{V}_z} = \frac{K_0}{r} - \frac{\omega r}{\bar{V}_z}.$$

Thus,

$$\frac{1}{r}\frac{\partial\phi^d}{\partial\theta}\bigg|_{z=0^+} = \left(\frac{K_0}{r} - \frac{\omega r}{\bar{V}_z}\right)\left(\frac{\partial\phi^d}{\partial z}\bigg|_{z=0^+} + \sum_{n=1}^{\infty}P_n e^{in\theta}\right)$$

$$= \left(\frac{K_0}{r} - \frac{\omega r}{\bar{V}_z}\right)\left(\frac{\partial\phi^u}{\partial z}\bigg|_{z=0^-} + \sum_{n=1}^{\infty}C_n e^{in\theta}\right) \tag{3.35}$$

by virtue of Eq. (3.32). Note that since the variables are dimensionless, $\bar{V}_z$ is effectively unity.

By substitution from Eq. (3.26) and (3.30) we obtain, for each circumferential harmonic n, the following corresponding set of equations:

$$\sum_{p=1}^{\infty}A_{np}^u\lambda_{np}R_{np}(r) + C_n(r) = -\sum_{p=1}^{\infty}\lambda_{np}A_{np}^d R_{np}(r) + \sum_{p=1}^{\infty}Z'_{np}(0)\,R_{np}(r) + P_n(r), \tag{3.36}$$

$$\sum_{p=1}^{\infty} A_{np}^{u} \frac{dR_{np}}{dr} = \sum_{p=1}^{\infty} A_{np}^{d} \frac{dR_{np}}{dr} + \sum_{p=1}^{\infty} Z_{np}(0) \frac{dR_{np}}{dr} + G_n(r) , \tag{3.37}$$

$$\sum_{p=1}^{\infty} \left[in A_{np}^{d} - (K_0 - \omega r^2) \lambda_{np} A_{np}^{u} \right] R_{np}(r) = -\sum_{p=1}^{\infty} Z_{np}(0) in R_{np}(r) + (K_0 - \omega r^2) C_n(r) , \tag{3.38}$$

$$\sum_{p=1}^{\infty} in\omega (A_{np}^{d} - A_{np}^{u}) R_{np}(r) - P_n(r) = -C_n(r) - \omega \sum_{p=1}^{\infty} in Z_{np}(0) R_{np}(r) . \tag{3.39}$$

We note that

$$Z_{np}(0) = -\int_h^1 \frac{\left[r G_n \frac{dR_{np}}{dr} + in \frac{K_0}{r} R_{np}(r) P_n(r) \right]}{\left(\lambda_{np}^2 + \frac{n^2 K_0^2}{r^4} \right)} dr , \tag{3.40}$$

and

$$Z'_{np}(0) = \int_h^1 \frac{\frac{in K_0}{r^2} \left[r G_n(r) \frac{dR_{np}}{dr} + in \frac{K_0}{r} R_{np}(r) P_n(r) \right]}{\left(\lambda_{np}^2 + \frac{n^2 K_0^2}{r^4} \right)} dr . \tag{3.41}$$

Equations (3.36) and (3.37) indicate that the functions $G_n(r)$ and $P_n(r)$, can be expanded in the forms:

$$G_n(r) = \sum_{p=1}^{\infty} G_{np} \frac{dR_{np}(r)}{dr} \tag{3.42}$$

and

$$P_n(r) = C_n(r) + \sum_{p=1}^{\infty} P_{np} R_{np}(r) . \tag{3.43}$$

In fact, as will be seen later, it is convenient to do so. Also, the

expression (3.42) is conveneint in allowing for the hub and tip properties of the shed circulation mentioned above Eq. (3.28).

We note that Eqs. (3.33) or (3.37) can be integrated with respect to r, and the constant of integration may be taken to be zero without affecting the quantities of interest. This is tantamount to saying the constant of integration merely changes the perturbation potential ϕ by a constant and since we are interested in the gradient of the potential, this constant is inconsequential. This fact will be exploited in the following.

Substitution of Eqs. (3.40) to (3.43) in Eqs. (3.36) to (3.39), and on multiplying each of the equations from (3.36) to (3.39) by r R_{nq} and integrating from r = h to r = 1 we obtain, by virtue of the orthogonality of the normalized functions R_{nq}, the following corresponding set of equations,

$$\lambda_{np}A^{u}_{np}+\lambda_{np}A^{d}_{np}-in k_0\sum_{q=1}^{\infty}G_{nq}X_{3npq}-P_{np}+\eta^2K_0^2\sum_{q=1}^{\infty}P_{nq}Y_{1npq}=-\eta^2K_0^2S_{1np}\,, \tag{3.44}$$

$$A^{u}_{np}-A^{d}_{np}-G_{np}+\sum_{q=1}^{\infty}G_{nq}X_{5npq}+in k_0\sum_{q=1}^{\infty}P_{nq}Y_{3npq}=-in k_0 S_{3np}\,, \tag{3.45}$$

$$\omega A^{u}_{np}-\omega A^{d}_{np}+\omega\sum_{q=1}^{\infty}G_{nq}X_{5npq}+in k_0\omega\sum_{q=1}^{\infty}P_{nq}Y_{3npq}-i\frac{P_{np}}{\eta}=-in k_0 S_{3np}\omega\,, \tag{3.46}$$

$$\lambda_{np}K_0A^{u}_{np}-\omega\sum_{q=1}^{\infty}\lambda_{nq}A^{u}_{nq}T_{3npq}-in A^{d}_{np}+in\sum_{q=1}^{\infty}G_{nq}X_{5npq}-\eta^2K_0\sum_{q=1}^{\infty}P_{nq}Y_{3npq}$$
$$=\eta^2K_0S_{3np}-(\alpha_{np}-\beta_{np})\,. \tag{3.47}$$

where

$$X_{3npq}=\int_h^1 \frac{r^3 \frac{dR_{np}}{dr}\frac{dR_{nq}}{dr}}{(\lambda_{np}^2 r^4+n^2k_0^2)}\,, \quad X_{5npq}=\int_h^1 \frac{r^5 \frac{dR_{np}}{dr}\frac{dR_{nq}}{dr}}{(\lambda_{np}^2 r^4+n^2k_0^2)}\,dr\,,$$

$$Y_{1npq}=\int_h^1 \frac{r R_{np}R_{nq}}{(\lambda_{np}^2 r^4+n^2k_0^2)}\,dr \quad , Y_{3npq}=\int_h^1 \frac{r^3 R_{np}R_{nq}}{(\lambda_{np}^2 r^4+n^2k_0^2)}\,dr\,,$$

$$S_{1np}=\int_h^1 \frac{r C_n R_{np}}{(\lambda_{np}^2 r^4+n^2k_0^2)}\,dr \quad , S_{3np}=\int_h^1 \frac{r^3 C_n R_{np}}{(\lambda_{np}^2 r^4+n^2k_0^2)}\,dr\,,$$

$$\alpha_{np}=K_0\int_h^1 C_n r R_{np}\,dr \quad , \beta_{np}=\omega\int_h^1 C_n r^3 R_{np}\,dr\,,$$

and

$$T_{3npq}=\int_h^1 r^3 R_{np}R_{nq}\,dr.$$

It is noted that the integrals X_{3npq}, X_{5npq}, Y_{1nqp}, and Y_{3npq} are not symmetric with respect to p and q; furthermore, it is also noted that the value of these integrals peaks around the neighborhood of p = q. Whenever the difference between p and q is large, the value of these integrals is small. However, this does not apply to the integral T_{3npq}.

Before proceeding to the description of the solution of the unknowns, let us take a look at the implication of the set of equations (3.44) to (3.47). In contrast to analogous but simpler situations, in which the upstream flow is uniform, and either the Beltrami vorticity or the vorticity resulting from a gradient in stagnation pressure is assumed to dominate so

that it can be treated alone, inspection of the present equations shows that each radial harmonic, p, is coupled to all the others and can not be separated. However, the circumferential harmonics remain separable and only the radial harmonics interfere among themselves. An analogous case arises when we were studying the induced effects of the blade wakes in which the assumption of incompressibility does not hold; there we mentioned that it is the presence of the downstream swirl (hence a centrifugal force field) which modifies the downstream radial eigenfunctions (so that they are different from the upstream ones) thus leading to the interference among the radial harmonics.

In Section 3, Chapter 2 of Part II, we analyzed the case of a distorted flow through an isolated three-dimensional rectilinear cascade encased in a duct; there, even though both the Beltrami vorticity and the vorticity resulting from a gradient in stagnation pressure are present downstream of the cascade, the harmonics n and p are still separable. This is so because of the absence of the centrifugal force field there. In the annular geometry here, besides the presence of the two types of vorticity downstream of the disc, components of streamwise vorticity develop as the flow proceeds because of the downstream free vortex swirl. Thus, the interference among the radial harmonics, p, here is a result of the presence of the centrifugal force field and the simultaneous presence of the "secondary" and Beltrami vorticity components. This is expected to alter the physical flow picture radically. Such interference among the radial harmonics leads to the necessity of solving a matrix equation for the final determination of the sets of unknowns, $\{A^{u}_{d}{}_{np}\}$, $\{G_{np}\}$, $\{P_{np}\}$, and for complete satisfaction of the matching conditions at the disc.

The set of equations (3.44) to (3.47) forms a set of 4p linear equations with 4p unknowns, thus leading to a 4p by 4p complex matrix equation given on the following page. This matix equation can readily be inverted to give the unknowns A^{u}_{np}, G_{np}, and P_{np}. Once these unknowns are determined, the velocity components of the flow field are given by:

in the upstream flow region,

$$V_z^u = \bar{V}_z + \sum_{n=1}^{\infty}\sum_{p=1}^{\infty} \lambda_{np} A^u_{np} R_{np}(r)\, e^{in\theta} e^{\lambda_{np} z} + \sum_{n=1}^{\infty} C_n e^{in\theta} ,$$

$$V_\theta^u = \frac{1}{r}\sum_{n=1}^{\infty}\sum_{p=1}^{\infty} in A^u_{np} R_{np}(r)\, e^{in\theta} e^{\lambda_{np} z} , \qquad (3.48)$$

$$V_r^u = \sum_{n=1}^{\infty}\sum_{p=1}^{\infty} A^u_{np} \frac{dR_{np}}{dr} e^{in\theta} e^{\lambda_{np} z} ;$$

while in the downstream flow region,

$$V_z^d = \bar{V}_z - \sum_{n=1}^{\infty}\sum_{p=1}^{\infty} \lambda_{np} A^d_{np} R_{np}(r)\, e^{in\theta} e^{-\lambda_{np} z} + \sum_{n=1}^{\infty}\sum_{p=1}^{\infty} Z'_{np}(z) R_{np}(r)\, e^{in\theta} + \sum_{n=1}^{\infty}\sum_{p=1}^{\infty} P_{np} R_{np}(r) e^{in\bar{\alpha}^d} ,$$

$$V_\theta^d = \bar{V}_\theta^d + \frac{1}{r}\sum_{n=1}^{\infty}\sum_{p=1}^{\infty} in A^d_{np} R_{np}(r) e^{in\theta} e^{-\lambda_{np} z} + \frac{1}{r}\sum_{n=1}^{\infty}\sum_{p=1}^{\infty} in Z_{np}(z) R_{np}(r) e^{in\theta} , \qquad (3.49)$$

$$V_r^d = \sum_{n=1}^{\infty}\sum_{p=1}^{\infty} A^d_{np} \frac{dR_{np}}{dr} e^{in\theta} e^{-\lambda_{np} z} + \sum_{n=1}^{\infty}\sum_{p=1}^{\infty} Z_{np}(z) \frac{dR_{np}}{dr} e^{in\theta} + \sum_{n=1}^{\infty}\sum_{p=1}^{\infty} G_{np} \frac{dR_{np}}{dr} e^{in\bar{\alpha}^d} .$$

with the $Z_{np}(z)$ [from $Z'_{np}(z)$ may be obtained] now given by

$$
\begin{bmatrix}
[\lambda_{ni}\delta_{ij}] & [\lambda_{ni}\delta_{ij}] & [-inkX_{3nij}] & [n^2k^2Y_{1nij} - \delta_{ij}] \\
[\delta_{ij}] & [-\delta_{ij}] & [X_{5nij} - \delta_{ij}] & [inkY_{3nij}] \\
\left[\frac{\omega}{\bar{V}_z}\delta_{ij}\right] & \left[-\frac{\omega}{\bar{V}_z}\delta_{ij}\right] & \left[\frac{\omega}{\bar{V}_z}X_{5nij}\right] & \left[i\frac{\omega}{\bar{V}_z}nkY_{3nij} - i\frac{\delta_{ij}}{n}\right] \\
\left[\lambda_{ni}k\delta_{ij} - \frac{\omega}{\bar{V}_z}\lambda_{nj}T_{3nij}\right] & [-in\delta_{ij}] & [inX_{5nij}] & [-n^2kY_{3nij}]
\end{bmatrix}
\begin{bmatrix} [A^u_{ni}] \\ [A^d_{ni}] \\ [G_{ni}] \\ [P_{ni}] \end{bmatrix}
=
\begin{bmatrix} [-n^2k^2S_{1ni}] \\ [-inkS_{3ni}] \\ \left[-i\frac{\omega}{\bar{V}_z}nkS_{3ni}\right] \\ [n^2kS_{3ni} - (\alpha_{ni} - \beta_{ni})] \end{bmatrix}
$$

where $[a_{ij}]$ is a submatrix with elements a_{ij},

and $_{ij} = 1$ if $i=j$
0 if $i \neq j$

Each suffix i and j runs from 1 to p so that each submatrix is either a p by 1 matrix (i.e., a column matrix) or a p by p matrix. [For the purpose of this diagram, therefore, i and j replace p and q as the running indicies in the set of equations below.] $K = K_0$, $\omega = K_1$

$$Z_{np}(z) = -\sum_{q=1}^{\infty} G_{nq} \int_h^1 \frac{r \frac{dR_{np}}{dr}\frac{dR_{nq}}{dr}}{\left(\lambda_{np}^2 + \frac{n^2 k_0^2}{r^2}\right)} e^{-\frac{ink_0 z}{r^2}} dr - in \sum_{q=1}^{\infty} P_{nq} \int_h^1 \frac{\frac{k_0}{r} R_{nq} R_{np}}{\left(\lambda_{np}^2 + \frac{n^2 k_0^2}{r^2}\right)} e^{-\frac{ink_0 z}{r^2}} dr \,. \qquad (3.50)$$

(ii) An Isolated Stator Blade Row:

Since the matching conditions across a stator are just a special case of the matching conditions across a rotor, the results for a distorted flow through a stator may be obtained from those of a rotor by letting $\omega = 0$, and $C_n = P_n$ [or $P_{np} = 0$ in Eq. (3.43)]; because a stator does no work, the stagnation pressure distortion passes through a stator and emerges at the exit plane without any change in magnitude or phase. With $\omega = 0$, and $P_{np} = 0$, the matrix equation for the determination of the sets of unknowns, $\{A_{np}^{H}\}$ and $\{G_{np}\}$, becomes a 3p by 3p one given on the following page.

3.4 Development of the Vortex Filaments in the Flow Field

We now write out the (r,θ,z) vorticity field [in absolute coordinates, $\nabla \times \underset{\sim}{V} = \underset{\sim}{\Omega} = (\xi,\eta,\zeta)$], upstream and downstream of the disc:

	Upstream	Downstream
ξ	$\sum_{n=1}^{\infty} \frac{in}{r} C_n e^{in\theta}$	$\sum_{n=1}^{\infty} \frac{in}{r} P_n(r)\, e^{in\bar{\alpha}d}$
η	$-\sum_{n=1}^{\infty} \frac{dG_n}{dr} e^{in\theta}$	$-\sum_{n=1}^{\infty} \left\{\frac{inK_0}{r^2} G_n + \frac{2ink_0 z}{r^3} P_n + \frac{dP_n}{dr}\right\} e^{in\bar{\alpha}d}$
ζ	0	$-\sum_{n=1}^{\infty} \frac{inG_n(r)}{r} e^{in\bar{\alpha}d}$

The vortex filaments are convected by the mean flow; upstream of the blade row, they lie on planes of constant z. A portion of the vorticity

$$\left[\begin{array}{c|c|c} [\lambda_{ni}\delta_{ij}] & [\lambda_{ni}\delta_{ij}] & [-inKX_{3nij}] \\ \hline [\delta_{ij}] & [-\delta_{ij}] & [X_{5nij} - \delta_{ij}] \\ \hline [-\lambda_{ni}K\delta_{ij}] & [in\delta_{ij}] & [-inX_{5nij}] \end{array}\right] \left[\begin{array}{c} [A^u_{ni}] \\ \hline [A^d_{ni}] \\ \hline [G_{ni}] \end{array}\right] \left[\begin{array}{c} [-n^2K^2S_{1ni}] \\ \hline [-inKS_{3ni}] \\ \hline [-n^2KS_{3ni} + \alpha_{ni}] \end{array}\right]$$

Here $K = K_0$

Matrix equation for the stator case

(represented by the P_n, C_n terms) is associated with the total pressure distortion at the inlet, corresponding qualitatively with the two-dimensional actuator disc analyses. The above expressions also illustrate the fact that even if the incoming vorticity is purely radial (i.e., C_n is a constant), a (θ,z)-component of the vorticity develops as the flow swirls downstream.

From Eqs. (3.34) and (3.35) for a rotor, we find further that

$$n\omega G_n = i\frac{d}{dr}(P_n - C_n). \tag{3.51}$$

If $\Gamma(r,\theta)$ is the circulation about each of B blades on a many-bladed rotor represented by the actuator disc, then

$$B\tilde{\Gamma}(r,\theta) = -2\pi r\left(\frac{1}{r}\frac{\partial\phi^d}{\partial\theta} - \frac{1}{r}\frac{\partial\phi^u}{\partial\theta}\right)\Big|_{z=0}, \tag{3.52}$$

so that from Eq. (3.35)

$$\sum_{n=1}^{\infty}(P_n - C_n)e^{in\theta} = -\omega\frac{B\tilde{\Gamma}(r,\theta)}{2\pi}, \tag{3.53}$$

[Note that we have taken $\Gamma(r,\theta) = \Gamma_0 + \tilde{\Gamma}(r,\theta)$ with $\Gamma_0 = 2\pi r\bar{V}_\theta{}^d$ = constant]. Thus, the asymmetrical inlet flow leads to an asymmetrical circulation distribution on the disc. Eq. (3.51) then becomes

$$\sum_{n=1}^{\infty} inG_n e^{in\theta} = \frac{B}{2\pi}\frac{\partial}{\partial r}\Gamma(r,\theta), \tag{3.54}$$

(as $B \to \infty$, $B\Gamma$ remains finite in the actuator disc limit)

indicating that G_n is a consequence of the variation of the blade circulation which leads to trailing vorticity behind the blade row. Thus, as

we anticipated earlier, a Beltrami component of the downstream vorticity (represented by the G_n terms) also develops, which is a distinct feature of the three-dimensional theory. Both of the above types of vorticity swirl downstream with the mean flow.

Furthermore, as the radial vortex filaments, associated with the stagnation pressure distortion, move downstream, a component of tangential vorticity (η in the above expression) develops, thus giving rise to "secondary vorticity" which superimposes itself upon any vorticity present due to the shed circulation. However, unlike the shed circulation, this secondary vorticity changes its value as the flow proceeds. The downstream develpment of these vorticies and its influences on the induced perturbations can be explained in the same way as we have described for the case of blade wakes in Section 4, Chapter 3 of Part I. It is expected that the presence of the streamwise vorticity will lead to significant radial velocity components which will negate the basic premises of two-dimensional theory. [We also mention here that in the case of a distorted flow through a three-dimensional cascade, the vorticity resulting from the stagnation pressure distortion contributes no secondary vorticity at all as the flow proceeds. The streamwise components of vorticity there are solely due to the shed circulation.]

It is also noted the radial vortex filament changes in magnitude as it passes through a rotor forming the disc, as indicated by the expression for ξ above and Eq. (3.43). This is becuase the rotor is under the condition of unsteady flow as each of its blade is moving relative to a fixed circulation distribution on the disc;[58] in consequence, shed vorticies spring from the trailing edges of the rotor accounting for the change in

strength of the radial vortex filaments crossing the rotor.

3.5 The Downstream Static Pressure Field

From the linearized Bernoulli equation for the flow, we find that the downstream perturbation static pressure, in its dimensionless form, is given by

$$\delta P = P^d - \bar{P}^d = P_t - \bar{P}_t - \underline{\bar{V}} \cdot \underset{\sim}{\tilde{V}} . \tag{3.55}$$

Substitution of Eqs. (3.48) and (3.49) in Eq. (3.55) yields

$$\delta P^d = \sum_{n=1}^{\infty}\sum_{p=1}^{\infty} \lambda_{np} A^d_{np} R_{np}(r) e^{in\theta} e^{-\lambda_{np} z} - \frac{K_0}{r^2}\sum_{n=1}^{\infty}\sum_{p=1}^{\infty} in A^d_{np} R^d_{np}(r) e^{in\theta} e^{-\lambda_{np} z}$$

$$- \sum_{n=1}^{\infty}\sum_{p=1}^{\infty} Z'_{np}(z) R_{np}(r) e^{in\theta} - \frac{K_0}{r^2}\sum_{n=1}^{\infty}\sum_{p=1}^{\infty} in Z_{np}(z) R_{np}(r) e^{in\theta} . \tag{3.56}$$

The first two double sums, a result of the potential disturbances, decay exponentailly with distance downstream from the disc. However, the last two double sums, being caused by the induced disturbances, do not possess this exponentially decaying behavior. The fact that the induced disturbances induce a static pressure field indicates that they are not convected by the mean flow at all, in contrast to the case of a distorted flow through a two-dimensional and three-dimensional cascades where the induced disturbances are purely convected by the mean flow. This change in behavior of the induced disturbances in rectilinear cascade to that of induced disturbances in annular cascade is due to the presence of a centrifugal force field induced by the swirling flow in the latter case. It is this centrifugal effect which couples the pressure disturbances and the induced disturbances together, as has been

predicted earlier by Kerrebrock[21]. We have seen that it is the same physical mechanism which causes the blade wakes to induce a pressure field (Part I).

It will be explained in the next section that for an upstream distortion which has a low circumferential harmonic n, the resulting downstream perturbation static pressure can persist for a considerable distance downstream from the disc. For many cases, this static pressure field will have a peak value at some distance from the blade row; eventually this static pressure field, as well as other rotational disturbances, will decay inversely with the axial distance z. This behavior is closely related to the downstream development of the vorticity field as explained in the previous section, section 4 of Chapter 3, and Chapter 6 of Part I.

We have seen in the preceeding Chapter that even with distorted inlet flow, the two-dimensional theory predicts that the static pressure downstream will be everywhere uniform. In contrast, Strand's[57] experiments showed a large, systematic circumferential perturbation of the static pressure, persisting for several tip diameters downstream of a stator blade row. Even the analysis we did for a distorted flow through a three-dimensional cascade (which neglects centrifugal effects) predicts that the downstream pressure field decays exponentially with distance from the blade row, and therefore cannot explain this observed behavior of the downstream static pressure field. Thus, this behavior is only explainable in the context of the present analysis for a distorted inlet flow through an annular cascade.

3.6 Downstream Behaivor of the Rotational Disturbances and the Analytical Behavior of the Integral $Z_{np}(z)$

The analytical behavior of the type of integral, $Z_{np}(z)$ appearing in Eq. (3.31) and its physical implications have been discussed in considerable detail in Chapter 6 of Part I. Its behavior is directly related to the downstream development of the vortex filaments as explained earlier. Therefore, the discussion presented in Chapter 6 of Part I can be carried over here to explain the analytical behavior of the integral and the downstream behavior of the rotational disturbances. However, we must take note of one important point; here the argument of the exponential factor has a factor n, the circumferential harmonic, and not nB, the product of the circumferential harmonic number and the blade number, as in the case of blade wakes discussed in Chapter 6 of Part I. In consequence, the integral $Z_{np}(z)$ here would reach its asymtotical behavior in a larger axial distance as the argument in the exponential factor is less than that for the case of blade wakes by a factor of B, which is usually of the order of 40. This would imply that the rotational disturbances (and hence the downstream static pressure field) will persist for a larger distance downstream of the blade row before eventually decaying inversely with the axial distance z to a negligible level.

By following the analytical technique employed in Chapter 6 of Part I, we find that the asymptotic expansion of the integral $Z_{np}(z)$ for large value of Z is given by

$$Z_{np}(z) \sim \frac{i}{z}\left[\frac{F_{np}(h)\,h^3}{2nk_0}e^{-ink_0z/h^2} - \frac{F_{np}(1)}{2nk_0}e^{-ink_0z}\right], \tag{3.57}$$

where

$$F_{np}(r) = \left[r G_{rn}(r)\frac{dR_{np}}{dr} + \frac{ink_0}{r}R_{np}(r)P_n(r)\right] \Big/ \left(\lambda_{np}^2 + \frac{n^2k_0^2}{r^4}\right). \tag{3.58}$$

Thus, the rotational disturbances (and hence the predicted pressure field) decays as z^{-1} far downstream as indicated earlier. This will be further substantiated by actual numerical examples later.

3.7 Asymmetric Disturbances in Multiple Blade Rows

Here, we will attempt to indicate how the present analytical technique can be extended readily to the treatment of interacting blade rows. By successive applications of the results of the previous Sections in this Chapter, a general theory of a distorted inlet flow through blade rows with finite axial spacing can be developed. However, it is expected such an analysis would lead to rather complicated expressions. As before, the analysis will be restricted to a distortion with wave lengths large compared with the blade gap.

As a specific example, let us consider the case of a rotor followed by a stator far away from other blade rows (i.e., an isolated stage), and that a distortion in stagnation pressure fixed in space is introduced far upstream. Let the subscript 1, 2, and 3 represent the regions upstream of the rotor, between the rotor and stator, and downstream of the stator respectively, and let the rotor be located at z = 0, the stator at z = a.

With reference to the analytical results of the previous Sections, we have:

Upstream of the Rotor;

$$\underset{\sim}{V}_1 = \bar{V}_z \hat{e}_z + \nabla \phi_1^u + \sum_{n=1}^{\infty} C_n e^{in\theta} \hat{e}_z , \tag{3.59}$$

where

$$\phi_1^u = \sum_{n=1}^{\infty}\sum_{p=1}^{\infty} A_{np_1}^u R_{np}(r) e^{in\theta} e^{\lambda_{np} z} . \tag{3.60}$$

In the gap between the rotor and stator,

$$\underset{\sim}{V}_2 = \overline{V}_z \hat{e}_z + \overline{V}_{\theta 2} \hat{e}_\theta + \nabla \phi_2^u + \nabla \phi_2^d + \sum_{n=1}^{\infty} P_{n2} e^{in\bar{\alpha}_2^d} \hat{e}_z + \sum_{n=1}^{\infty} G_{n2} e^{in\bar{\alpha}_2^d}, \tag{3.61}$$

where

$$\phi_2^u = \sum_{n=1}^{\infty}\sum_{p=1}^{\infty} A_{np2}^u R_{np}(r) e^{in\theta} e^{\lambda_{np}(z-a)} = \sum_{n=1}^{\infty}\sum_{p=1}^{\infty} A_{np2}^{*u} R_{np}(r) e^{in\theta} e^{\lambda_{np} z} \tag{3.62}$$

$$\phi_2^d = \sum_{n=1}^{\infty}\sum_{p=1}^{\infty} A_{np2}^d R_{np}(r) e^{in\theta} e^{-\lambda_{np} z} + \sum_{n=1}^{\infty}\sum_{p=1}^{\infty} Z_{np_2}(z) R_{np}(r) e^{in\theta}, \tag{3.63}$$

with

$$A_{np_2}^{*u} = A_{np2}^u e^{-\lambda_{np} a}. \tag{3.64}$$

Downstream of the Stator,

$$\underset{\sim}{V}_3 = \overline{V}_z \hat{e}_z + \overline{V}_{\theta 3} \hat{e}_\theta + \nabla \phi_3^d + \sum_{n=1}^{\infty} P_{n3} e^{in\bar{\alpha}_3^d} \hat{e}_z + \sum_{n=1}^{\infty} G_{n3} e^{in\bar{\alpha}_3^d}, \tag{3.65}$$

where

$$\begin{aligned} \phi_3^d &= \sum_{n=1}^{\infty}\sum_{p=1}^{\infty} A_{np3}^d R_{np}(r) e^{in\theta} e^{-\lambda_{np}(z-a)} + \sum_{n=1}^{\infty}\sum_{p=1}^{\infty} Z_{np3}(z) R_{np}(r) e^{in\theta} \\ &= \sum_{n=1}^{\infty}\sum_{p=1}^{\infty} A_{np}^{*d} R_{np}(r) e^{in\theta} e^{-\lambda_{np} z} + \sum_{n=1}^{\infty}\sum_{p=1}^{\infty} Z_{np3}(z) R_{np}(r) e^{in\theta} \end{aligned} \tag{3.66}$$

with

$$A_{np3}^{*d} = A_{np3} e^{\lambda_{np} a} \tag{3.67}$$

We note that $Z_{np_2}(z)$ and $Z_{np_3}(z)$ assume the form

$$Z_{np_2}(z) = -\int_h^1 \frac{\left(r G_{rn_2} \frac{dR_{np}}{dr} + inK_{02} \frac{P_{n_2}}{r} R_{np}\right)}{\left(\lambda_{np}^2 + \frac{n^2 K_{02}^2}{r^4}\right)} e^{-\frac{inK_{02} z}{r^2}} \, dr \,. \tag{3.68}$$

and

$$Z_{np_3}(z) = -\int_h^1 \frac{\left(r G_{rn_3} \frac{dR_{np}}{dr} + inK_{03} \frac{P_{n_3}}{r} R_{np}\right)}{\left(\lambda_{np}^2 + \frac{n^2 K_{03}^2}{r^4}\right)} e^{-\frac{inK_{03}}{r^2}(z-a)} \, dr \,. \tag{3.69}$$

The unknowns $A^u_{np_1}$, P_{n_2}, G_{n_2}, $A^u_{np_2}$, $A^d_{np_2}$, P_{n_3}, G_{n_3}, and $A^d_{np_3}$ are to be determined from a set of eight independent matching conditions: four at the rotor at Z = 0 and four at the stator at Z = a. These matching conditions are provided by Eq. (3.32) to (3.35). As before application of these matching conditions will show that the functions $G_{n_2}(r)$, $G_{n_3}(r)$, P_{n_2} can be expanded in the form of Fourier Bessel Series as follows:

$$G_{rn_2}(r) = \sum_{p=1}^{\infty} G_{np_2} \frac{dR_{np}}{dr} \tag{3.70}$$

$$G_{rn_3}(r) = G_{rn_2}(r) e^{-\frac{inK_{02}a}{r^2}} + \sum_{p=1}^{\infty} G_{np_3} \frac{dR_{np}}{dr} \,, \tag{3.71}$$

$$P_{n_2} = G_{n_1} + \sum_{p=1}^{\infty} P_{np_2} R_{np}(r) \,, \tag{3.72}$$

and that

$$P_{n3} = P_{n2}\, e^{-\frac{in K_{02} q}{r^2}} , \tag{3.73}$$

since the stator does no work on the passing fluid.

Successive application of the matching conditions at the rotor and the stator leads to the following set of equations for the determination of unknowns:

$$\lambda_{np} A^{u}_{np1} + \lambda_{np} A^{d}_{np2} - \lambda_{np} A^{u}_{np2} e^{-\lambda_{np} q} - in K_{02} \sum_{q=1}^{\infty} G_{nq_2} X_{3npq_2}$$

$$- P_{np2} + \eta^2 K_{02}^2 \sum_{q=1}^{\infty} P_{nq_2} Y_{1npq_2} = -\eta^2 K_{02}^2 S_{1np2} , \tag{3.74}$$

$$A^{u}_{np1} - A^{d}_{np2} - A^{d}_{np2} e^{-\lambda_{np} q} + \sum_{q=1}^{\infty} G_{nq_2} X_{5npq_2} + in K_{02} \sum_{q=1}^{\infty} P_{nq_2} Y_{3npq_2} = -in K_{02} S_{3np2} , \tag{3.75}$$

$$A^{u}_{np1} - A^{d}_{np2} - A^{d}_{np2} e^{-\lambda_{np} q} + \sum_{q=1}^{\infty} G_{nq_2} X_{5npq_2} + in K_{02} \sum_{q=1}^{\infty} P_{nq_2} Y_{3npq_2} - i \frac{P_{nq_2}}{n\omega} = -in K_{02} S_{3np2} , \tag{3.76}$$

$$\lambda_{np} K_{02} A^{u}_{np1} - \omega \sum_{q=1}^{\infty} \lambda_{nq} T_{3npq} A^{u}_{nq1} - in A^{d}_{np2} - in A^{u}_{np2} e^{-\lambda_{np} q} + in \sum_{q=1}^{\infty} G_{nq_2} X_{5npq_2}$$

$$- \eta^2 K_{02}^2 \sum_{q=1}^{\infty} P_{nq_2} Y_{3npq_2} = \eta^2 K_{02} S_{3np2} - (\alpha_{np2} - \beta_{np2}) . \tag{3.77}$$

$$-\lambda_{np} A^{d}_{np2} e^{-\lambda_{np} q} + \lambda_{np} A^{u}_{np2} + in K_{02} \sum_{q=1}^{\infty} G_{nq_2} X^{(q)}_{3npq_2} - in K_{03} \sum_{q=1}^{\infty} G_{nq_2} X^{(q)}_{3npq_3} - \eta^2 K_{02}^2 \sum_{q=1}^{\infty} P_{nq_2} Y^{(q)}_{1npq_2}$$

$$+ \eta^2 K_{03}^2 \sum_{q=1}^{\infty} P_{nq_2} Y^{(q)}_{1npq_3} + \lambda_{np} A^{d}_{np3} - in K_{03} \sum_{q=1}^{\infty} G_{nq_3} X_{3npq_3} = \eta^2 K_{02}^2 S^{(q)}_{1np2} - \eta^2 K_{03}^2 S^{(q)}_{1np2} , \tag{3.78}$$

$$A^d_{np2}e^{-\lambda_{np}q} + A^u_{np2} - \sum_{q=1}^{\infty} G_{nq_2} X^{(a)}_{5npq_2} + \sum_{q=1}^{\infty} G_{nq_2} X^{(a)}_{5npq_3} - inK_{02}\sum_{q=1}^{\infty} P_{nq_2} Y^{(a)}_{3npq_2} + inK_{03}\sum_{q=1}^{\infty} P_{nq_2} Y^{(a)}_{3npq_3}$$

$$- A^d_{np3} + \sum_{q=1}^{\infty} G_{nq_3} X_{5npq_3} - G_{nq_3} = inK_{02} S^{(a)}_{3np2} - inK_{03} S^{(a)}_{3np3} , \qquad (3.79)$$

$$\lambda_{np}K_{03}e^{-\lambda_{np}q}A^d_{np2} - \lambda_{np}K_{03}A^u_{np2} - in\sum_{q=1}^{\infty} G_{nq_2} X^{(a)}_{5npq_3} - inK_{02}K_{03}\sum_{q=1}^{\infty} G_{nq_2} X^{(a)}_{3npq_2} + n^2K_{03}\sum_{q=1}^{\infty} P_{nq_2} Y^{(a)}_{3npq_3}$$

$$+ n^2K^2_{02}K_{03}\sum_{q=1}^{\infty} P_{nq_2} Y^{(a)}_{1npq_2} + inA^d_{np3} - in\sum_{q=1}^{\infty} G_{nq_3} X_{5npq_3} = -n^2K_{03}S^{(a)}_{3np3} - n^2K^2_{02}K_{03}S^{(a)}_{1np2} + \alpha^{(a)}_{np3} . \qquad (3.80)$$

where the summation index q runs from 1 to p. The integrals X_{3npq}, X_{5npq}, Y_{1npq}, Y_{3npq}, T_{snpq}, S_{inp}, s_{3np}, α_{np} and β_{np} are given below Eq. (3.47); but whenever subscript j occurs (j = 2,3) the K_0 should then be replaced by K_{0j} respectively. Similarly whenever the superscript (a) occurs, an additional factor exp $\{-inK_{02}\ a/r^2\}$ should be included in the integrand.

As before, the set of equations from (3.74) to (3.80) shows that the radial harmonics are all coupled; they form a 7p by 7p complex matrix equation which can be inverted for the determination of the sets of unknowns $\{A^u_{np1}\}$, $\{A^u_{np2}\}$, $\{A^d_{np2}\}$, $\{G_{np2}\}$, $\{P_{np2}\}$, $\{A^d_{np3}\}$, and $\{G_{np3}\}$. With their determination, the flow field and hence the pressure field are completely known. The addition of successive blade rows downstream will of course introduce as many as new equations as new unknown coefficients.

It is seen that the form of the results for even two blade rows is very involved and clumsy unless the axial gap is very small, when considerable simplification is possible. In practice, the axial gaps are ordinarily smaller than the bladegap, so that the variation of the exponential factors in the above expressions from one side of the gap to the other

will usually be negligible; i.e., they can be replaced by unity. Such an analysis is quite useful for examining the evolution of a distortion in stagnation pressure through a stage.

CHAPTER 4 - QUASI-STEADY AERODYNAMIC LOAD ON THE ROTOR IN ASYMMETRIC FLOW

4.1 Introduction

In Chapters 2 and 3, we have obtained solutions for the steady flow of an inviscid incompressible fluid through a rotating blade row represented by an actuator disc (for a two-dimensional and a three-dimensional as well as an annular cascade) with prescribed non-uniform inlet conditions which are fixed in space. The flow field has been pictured as threaded with vortex filaments which are either introduced upstream or spring from solid surfaces such as the blades forming the disc. The actuator disc concept has been imposed so as to suppress the individuality of each blade such that the flow appear to be steady as viewed from the absolute frame of reference. We have already noted that because the individual blades of the rotor are moving relative to a fixed circulation distribution and are therefore under the conditions of unsteady flow. In consequence, vorticies will be shed at their trailing edges in accordance with the theory of airfoils in unsteady flow. In addition, an unsteady streamwise component of vorticity is shed into the downstream flow as a result of the radial gradient of the circulation distribution. It is felt that such features of the flow and its vorticity may be better elucidated by considering the flow from the point of view of an observer rotating with the blades. In this rotating frame of reference, the flow appears unsteady.

4.2 The Shed Vorticity

Eq. (2.8) of Part I, is the Euler's equation for an inviscid incompressible fluid in the rotating frame of angular velocity $\underset{\sim}{\omega}$. The

corresponding Helmholtz equation is obtained by taking the curl of Eq. (2.8) in Part I; it is given by

$$\frac{\partial \underset{\sim}{\Omega}}{\partial t} + (\underset{\sim}{W}\cdot\nabla)\underset{\sim}{\Omega} = (\underset{\sim}{\Omega}\cdot\nabla)\underset{\sim}{W} ,$$

which, to the order ε, is

$$\frac{\partial \underset{\sim}{\Omega}}{\partial t} + (\underset{\sim}{\bar{W}}\cdot\nabla)\underset{\sim}{\Omega} = (\underset{\sim}{\Omega}\cdot\nabla)\underset{\sim}{\bar{W}} , \tag{4.1}$$

since the vorticity $\underset{\sim}{\Omega}$ is small. For the case of distorted flow through a rotor in an annular duct,

$$\underset{\sim}{\bar{W}}^{u} = (0, -\omega r, \bar{V}_z) , \tag{4.2}$$

$$\underset{\sim}{\bar{W}}^{d} = (0, \bar{V}_\theta^{d} - \omega r, \bar{V}_z)$$

$$= (0, \bar{V}_z K_0/r - \omega r, \bar{V}_z) . \tag{4.3}$$

for a free vortex mean flow. Writing Eq. (2.1) in its component form, we obtain,

$$\frac{D\xi}{Dt} = 0 , \tag{4.4}$$

$$\frac{D\eta}{Dt} = \begin{cases} 0 & z < 0 \\ -\dfrac{2K_0\bar{V}_z}{r^2}\xi & z > 0 \end{cases} \tag{4.5}$$

$$\frac{D\zeta}{Dt} = 0 , \tag{4.6}$$

where the operator D/Dt refers to differentiation with respect to time following the relative motion of fluid particle. The relative cylindrical

coordinate system (r,θ',z) used is one in which θ' is measured with respect to the rotating blade (Fig. I.1b). They are related to the absolute cylindrical coordinate system (r,θ,z) through

$$\theta' = \theta - \omega t \tag{4.7}$$

Thus the absolute vorticity which is rewritten below, may be obtained directly from Section 3.4 of Part II by substituting $(\theta' + \omega t)$ for θ and $(\bar{\alpha}^{d'} + \omega t)$ for $\bar{\alpha}^{d}$ where $\bar{\alpha}^{d'} = \bar{\alpha}^{d} - K_0 Z/r^2$.

TABLE I

	Upstream	Downstream
ξ	$\sum_{n=1}^{\infty} \frac{in}{r} C_n e^{in(\theta'+\omega t)}$	$\sum_{n=1}^{\infty} \frac{in}{r} P_n(r) e^{in(\bar{\alpha}^{d'}+\omega t)}$
η	$-\sum_{n=1}^{\infty} \frac{dC_n}{dr} e^{in(\theta'+\omega t)}$	$-\sum_{n=1}^{\infty} \left\{ \frac{inK_0}{r^2} G_n + \frac{2inK_0 Z}{r^3} P_n + \frac{dP_n}{dr} \right\} e^{in(\bar{\alpha}^{d'}+\omega t)}$
ζ	0	$-\sum_{n=1}^{\infty} \frac{inG_n}{r} e^{in(\bar{\alpha}^{d'}+\omega t)}$.

Eq. (2.4) indicates that the radial vorticity associated with a fluid particle will remain unchanged as the particle passes through the whole flow field including the blade passages at the disc. This is so for the case of a stator. However, for the case of the rotor, it is seen from TABLE I that there is a change of radial vorticity across the disc given by

$$\Delta\xi = \sum_{n=1}^{\infty} \frac{in}{r}(P_n - C_n)\, e^{in(\theta'+\omega t)}. \tag{4.8}$$

This is a consequence of the unsteadiness of the lift on the rotating blades, thus resulting in the shedding of vortices into the downstream flow in accordance with the Kelvin's Theroem. This has been anticipated earlier in Chapter 3 of Part II. We shall show this in the following.

Let $\gamma_T(r,\theta)$ denote the circulation distribution per unit circumferential length in the rotor disc at radius r. If $\Gamma(r,\theta)$, (Fig. II.6), is the circulation about each of the B blades on a rotor represented by the actuator disc, then

$$\gamma_T(r,\theta) = \frac{B\Gamma(r,\theta)}{2\pi r} = \sum_{n=0}^{\infty} \gamma_n(r)\, e^{in\theta} = \sum_{n=0}^{\infty} \gamma_n(r)\, e^{in(\theta'+\omega t)}, \tag{4.9a}$$

where we have written $\Gamma(r,\theta) = \Gamma_0 + \tilde{\Gamma}(r,\theta)$ with $\Gamma_0 = 2\pi r\, \bar{V}_\theta^d$ = constant so that $\gamma_0(r) = B\Gamma_0/2\pi r$.

Thus

$$\tilde{\gamma}_T(r,\theta) = \gamma_T(r,\theta) - \gamma_0(r) = \frac{B\tilde{\Gamma}(r,\theta)}{2\pi r} = \sum_{n=1}^{\infty} \gamma_n(r)\, e^{in(\theta'+\omega t)}, \tag{4.9b}$$

Consider an airfoil moving through air at rest. At a particular time t_0, the airfoil is at A, and the shed vortices will remain at A as the airfoil moves away from A to B, at time t. Hence, at this time t, the vorticity at A is that due to the shed vortex from the airfoil at a time S/U earlier, where U is the speed of the airfoil, and S is the distance between A and B. In other words, the shed vortex needs a time lapse (= S/U) in order to make its presence felt at a particular point. We will exploit this fact in an attempt to relate the change in radial component of vorticy.

The mean flow is steady in both the absolute and relative frames of reference. Thus, viewing from the relative frame, the streamlines appear to be lines of constant ($r\theta' - Z \tan \beta_1$) in the upstream flow region and lines of constant ($r\theta' - Z \tan \beta_2$) in the downstream flow region (Fig. II.7), where β_1, and β_2 are given by

$$\tan\beta_1 = -\frac{\omega r}{\bar{V}_z} \quad , \tag{4.10}$$

and

$$\tan\beta_2 = \frac{\bar{V}_\theta - \omega r}{\bar{V}_z} = \frac{K_0}{r} - \frac{\omega r}{\bar{V}_z} \tag{4.11}$$

Note that we have unrolled a cylindrical plane of constant r in obtaining Fig. II.7.

According to Kelvin's Theorem, there is a shed circulation equal and opposite to the rate of change of circulation about any airfoil with an unsteady lift. Thus, the vorticity associated with a fluid particle at a point (r,θ,z) at time t is related to the negative of the shed circulation at $(r,\theta'_0,0)$ at time t_0, where

$$t - t_0 = \frac{z}{\bar{V}_z} \tag{4.12}$$

and

$$r\theta' - z\tan\beta_2 = r\theta_0' \tag{4.13}$$

Hence, we can write

$$\Omega r_{shed}(r,\theta',z) = -\frac{\partial}{\partial z}\left[\gamma_T(r,\theta_0',0)\right]$$

$$= -\frac{\partial t}{\partial z}\frac{\partial}{\partial t}\left[\gamma_T(r,\theta_0',0)\right]. \tag{4.14}$$

Since we imagine that the space downstream of the actuator disc is densely filed with infinitesimal vorticies. But,

$$\frac{\partial z}{\partial t} = \bar{V}_z \tag{4.15}$$

so that

$$\Omega r_{shed}(r,\theta',z) = -\sum_{n=1}^{\infty} \frac{in\omega}{\bar{V}_z}\gamma_n e^{in(\theta_0'+\omega t_0)}, \tag{4.16}$$

where we have used Eq. (4.9). Note that since variables are dimensionless, $\bar{V}_z$ is effectively of value unity. Substituting for θ_0' and t_0 from Eqs. (4.12) and (4.13), (4.16) becomes,

$$\Omega r_{shed}(r,\theta',z) = -\sum_{n=1}^{\infty} in\omega\gamma_n e^{in\left[(\theta' - \frac{z\tan\beta_2}{r}) + \omega(t - \frac{z}{\bar{V}_z})\right]}$$

$$= -\sum_{n=1}^{\infty} in\omega\gamma_n e^{in(\theta' - \frac{k_0 z}{r^2} + \omega t)}. \tag{4.17}$$

where we have made use of Eq. (4.11).

By setting Z = 0, and using Eq. (4.9) and (3.53) of Part II, we obtain the shed vorticity as

$$\Omega_{r_{shed}} = -\sum_{n=1}^{\infty} \frac{in}{r} (P_n - C_n) e^{in\theta} \quad , \tag{4.18}$$

thus, confirming that the shed circulation due to the fluctuating lift accounts for the change of radial vorticity across the disc.

We have noted that the distortion of the radial vortex filament by the free vortex swirl in the tangential direction gives rise to a growing tangential component of vorticity. This can readily be obtained from Eq. (4.5), the integration of which along the relative streamline gives

$$\begin{aligned} \eta - \eta_{z=0} &= -\zeta \frac{2K_0}{r^2} \bar{V}_z t \\ &= -z \frac{2K_0}{r^2} \sum_{n=1}^{\infty} \frac{in}{r} P_n e^{in(\bar{\alpha}^{d'} + \omega t)} \quad , \end{aligned} \tag{4.19}$$

since the RHS of Eq. (4.5) remains constant along the relative streamline. It is noted that Eq. (4.19) corresponds to the growth term in the expression for the tangential vorticity.

4.3 The Trailing Shed Vorticity

The non-growth tangential component of vorticity downstream of the rotor contains a term

$$-\sum_{n=1}^{\infty} \frac{dP_n}{dr} e^{in(\bar{\alpha}^{d'} + \omega t)} \quad ,$$

part of which, by virtue of Eq. (3.43) of Part II, comes from vortex filaments introduced far upstream of the rotor. Thus, the difference at

$Z = 0$,

$$-\sum_{n=1}^{\infty}\left(\frac{dP_n}{dr}-\frac{dC_n}{dr}\right)e^{in(\theta'+\omega t)}$$

must have sprung from the solid surfaces of the blades forming the disc. By making use of Eqs. (3.53) and (3.54) of Part II, we obtain

$$-\sum_{n=1}^{\infty}\left(\frac{dP_n}{dr}-\frac{dC_n}{dr}\right)e^{in(\theta'+\omega t)} = \omega\frac{B}{2\pi}\frac{\partial\tilde{\Gamma}(r,\theta)}{\partial r} = \sum_{n=1}^{\infty} in\omega G_n e^{in(\theta'+\omega t)}, \tag{4.20}$$

thus confirming that it arises from the variation of blade circulation.

Since the growing tangential component of vorticity is related to the distortion of radial vorticity by free-vortex mean swirl in the tangential direction, it can be neglected in the present consideration. The axial and tangential components (minus that of the upstream one) of the vorticity are now reducible to a single component lying along the relative streamline given by

$$\Omega_S = -\sec\beta_2\sum_{n=1}^{\infty}\frac{in}{r}G_n e^{in(\alpha^{d'}+\omega t)}. \tag{4.21}$$

This streamwise vorticity Ω_S is Beltrami-like in character in the rotating frame and it represents the unsteady trailing shed circulation from the blades. Thus, we may therefore identify it as a Beltrami component of vorticity if we move with the rotor.

It should be noted that, in the absolute frame, Ω_S is not Beltrami vorticity since it does not point in the direction of the absolute flow in spite of the fact that it reamins, constant along the streamline of the mean absolute flow and is directly related to the trailing shed circulation.

CHAPTER 5 - NUMERICAL EXAMPLES ON DISTORTED FLOW THROUGH A BLADE ROW

5.1 Introduction

Numerical examples on distorted flow through an isolated stator and an isolated rotor are worked out here. They are intended to elucidate the general features of the flows as described by the two-dimensional theory and three-dimensional theory, and also to show the magnitude of the effects that can arise in such flows. The numerical examples are based on sinusoidal inlet distortion in stagnation pressure as input. Table II indicates the conditions for which the numerical examples have been obtained; they will be discussed in the following

TABLE II: NUMERICAL EXAMPLES

n	$h=r_h/r_t$	K_0	ω	disturbance amplitude*
1	0.4	0.4	0	0.1
5	0.4	0.4	0	0.1
1	0.4	0.3	2.04	0.1
1	0.4	1.0	1.7	0.1

*disturbance amplitude = $\delta P_t/\rho\bar{V}_z^2$

5.2 An Isolated Stator

The stator considered is of the free-vortex type with a hub-to-tip ratio of 0.4 and a mean flow angle of 45° at the hub. The upstream perturbation in stagnation pressure is given by

$$\delta P_t = 0.1 \cos\theta, \tag{5.1}$$

where we have measured pressure in units of $\rho\bar{V}_z^2$.

Figure II.8 shows the mere convection of the circumferential pattern of stagnation pressure by the mean swirling flow downstream of the stator. The amplitude is 0.1 since the flow passes through the stator without any change in stagnation pressure.

As already noted, Fig. II.9a shows the three-dimensional prediction of the presistence of the static pressure perturbations at the tip downstream of a stator. The magnitude of these pressure disturbances in fact increases slightly with the axial distance Z before beginning at $Z \simeq 2$, to decay as Z^{-1} in accordance with Eq. (3.57) of Part II. The two-dimensional strip theory predicts the absence of these downstream static pressure perturbations; and the three-dimensional rectilinear cascade theory predicts the presence of a potential pressure field which decays exponential with distance downstream of the stator; hence it cannot describe the persistent behavior of the static pressure perturbations shown in Fig. II.9a. The physical mechanism repsonsible for this feature of the flow is the presence of centrifugal force field in annular swirling flow. Comparison of Fig. II.9a with Fig. II.8 indicates that the static pressures are increasingly out of phase with the downstream stagnation pressure disturbances. Fig. II.9b shows the downstream static pressure disturbances is higher here at the hub because of the larger centrifugal force; otherwise the pattern of variation is similar to that at the tip.

The corresponding pattern of radial velocity variation is shown in Fig. II.10a. The amplitude of the radial velocity increases steadily with the axial distance Z until it reaches a maximum at $Z \simeq 2.5$ before beginning to decay to a value corresponding to the contribution from the shed

circulation. The behavior of this three-dimensional effect (which can not be predicted from the three-dimensional rectilinear cascade theory) can readily be explained in terms of the downstream development of the vorticity field described earlier. The distortion of the radial vortex filaments by the swirl leads to a tangential component of vorticity and hence secondary vorticity. Initially, the secondary flow induced by the secondary vorticity grows in strength thus leading to a growing component of radial velocity. Ultimately, the winding up of the radial vortex filaments around the axis produces a mutually destructive induced field leading to the decay of radial velocity to the value of the contribution from the shed circulation. The corresponding variation of axial velocity is shown in Fig. II.10b.

In addition to the pressure and velocity perturbations, the other quantity of interest in turbomachinery applications is the flow angle because of its effect on the performance of the downstream blade-row.Fig.II. 11 shows the flow angle variation in the tangential and axial direction at the hub. The flow angle perturbation is zero at the exit of the blade row because we have assumed the leaving angle to be constant [Eq. (3.35) of Part II with $\omega = 0$). The amplitude of the flow angle perturbation increases from $Z = 0$ onward until it reaches a maximum magnitude of 49 at $Z \simeq 2.0$; from then on it decreases again.

It has already been noted that the secondary flow (and hence the radial velocity) associated with the streamwise (or θ,z) components of vorticity, as they develop just behind and downstream of the disc, can lead to significant three-dimensional effects. A more quantitative view of this result is provided in Fig. II.12 in which the Beltrami component

of the vorticity (i.e., the shed circulation) is plotted for various azimuthal and spanwise positions just downstream of the disc. The Figure reveals (at least for n = 1) that the three-dimensional effects can be expected to be the strongest near the hub; in fact numerical results tend to indicate so.

The radial variation of the static pressure field at various circumferential stations for a particular axial location is shown in Fig. II.13a to Fig. II.13d. Careful observation indicates that except for that part near the hub (roughly for values of r from 0.4 to 0.55), the radial variation of static pressure is quite linear. This linear behavior becomes more pronounced further downstream. The deviation from this linear behavior near the disc may be attributed to contribution from the irrotational disturbances. It is possible that one may devise an approximate theory based on the linearity of static pressure (and hence the axial and tangential velocity perturbations) with radius. Such an approximate theory may not be quite good in the hub vicinity. The linear behavior of the perturbation quantities with radius may be a result of the dominance of the first radial eigenmode over all the other modes. However, such conclusions must not be carried over the the case of a distortion with higher harmonics.

Figures II.14a to II.14c give the downstream static pressure perturbations resulting from an inlet distortion of a higher harmonic (n = 5) approaching a stator. It is seen that the amplitude of the disturbances decays much more rapidly, verifying the n-dependence indicated in Eq. (3.57) of Part II. Because the argument of the exponential factor in the integrand in Eq. (3.31) of Part I has been increased by an increase in n,

consequently its asymptotic behavior is reached in a shorter axial distance.

5.3 An Isolated Rotor

The upstream incoming flow has a single lobed sinusoidal total pressure distortion pattern. Fig. II.15 illustrates the predicted three-dimensional pressure perturbation downstream of the rotor. Results at both the hub, and tip are shown, and comparison with the two-dimensional theory is provided. While the two-dimensional and the three-dimensional theories agree reasonably well at the tip; this is not the case at the hub. In fact, the two-dimensional theory tends to somewhat exaggerate the predicted perturbations at the tip and misses them almost completely in the hub. There it is shown that the static pressure perturbations at the hub predicted by the three-dimensional theory persists as far as $Z = 2$, however, those predicted by the two-dimensional theory vanishes at about $Z = 0.5$.

Figure II.16a shows the change in stagnation pressure across a rotor using the three-dimensional and the two-dimensional theories at the hub and the tip. The comparison of two-dimensional predictions of stagnation pressure with the three-dimensional predictions are more successful than for the static pressure; nevertheless, some quantitative differences remain. It is noted that there is a marked change in the profile of stagnation pressure at the tip as it crosses the rotor. The phase of the stagnation pressure pattern is changed on crossing the rotor. Near the hub, the three-dimensional theory predicts the amplification of the stagnation pressure distortion, which the two-dimensional theory fails to predict. Comparison with Fig. II.15 shows a marked difference in phases between the static and stagnation pressures at the hub.

Figure II.16b shows the form of the upstream relative flow angles at

the plane of the rotor. Since the relative leaving angle, β_2 is constant by assumption, the relative angles upstream of the rotor tend to account for the downstream form of the stagnation pressure pattern at the rotor plane, since both the quantities are representative of work done. Comparison of Figs. II.16a and II.16b shows that this is approximately so. Fig. II.17 shows the form of the corresponding static pressure rise across the rotor in its plane.

Figure II.18 is a plot of the radial variation of the trailing shed vorticity at various circumferen ial positions on the downstream plane of the rotor (i.e., at $Z = 0^+$). In analogy with Fig. II.12 of an isolated stator case, the vorticity is the strongest in the hub region. This accounts for some strong three-dimensional effects in the hub region.

The above illustrations seem to emphasize the conclusion already arrived at for the stator case; namely, the two-dimensional theory, which does not include the centrifugal effects, the shed circulation and the secondary vorticity, cannot describe the flow phenomena adequately. It is noted that the consequences appear to be especially significant in the hub region.

CHAPTER 6 - COMPARISON OF ANALYTICAL AND EXPERIMENTAL RESULTS

6.1 Introduction

In the previous Chapter, numerical examples were worked out to examine the features of the distorted flow through an isolated stator and rotor. The main differences among the theories (i.e., the two-dimensional, the three-dimensional rectilinear, and the annular cascade theories) were pointed out. From these numerical examples, one may conclude that the centrifugal effects should be included in the analysis of any flow through a turbomachine. The failure of the two-dimensional theory to predict some important features of the flow was pointed out as well. In this Chapter, we will examine the degree to which the theory can describe a swirling flow in an annular duct by comparing the analytical results with the available experimental results. A set of experimental data for a flow downstream of a row of inlet guide vanes with a graded gauze screen just upstream is made available by Greitzer and Strand[57]. Another important set of three-dimensional experimental results has recently been obtained by Rizvi[60] on a single rotating row of a free vortex axial compressor with inlet distortion screens placed far upstream.

6.2 An Isolated Vane Row

The experimental studies were carried out by Greitzer and Strand[57] on an annular cascade wind tunnel at the Whittle Laboratory of the Engineering Department, Cambridge University. The test rig facility is shown in Fig. II.19. The vane row, inducing a downstream swirl, was preceeded by honey comb flow straightener followed by the distortion screen, which produces a sinusoidal stagnation pressure distortion just upstream of the vane row.

The annular test section has a hub-to-tip ratio of 0.43. The vane row produces a flow with a constant mean outflow angle of 47.7° as shown in Fig. II.20, and therefore is not of the free-vortex type.

All the measurements were taken with a single sinusoidal total stagnation pressure distortion pattern, they were taken at several radial and axial locations. It is deduced from these experimental data that the distortion in stagnation pressure at the exit of the vane row is approximately given by

$$\frac{\delta P_t}{\frac{1}{2}\rho \bar{V}_z^2} = 0.42 \cos\theta . \tag{6.1}$$

Figure II.21 shows a plot of the product of the radius and the mean tangential velocity with radius. The value $\bar{V}_\theta r$ is not a constant since the vane row is of the nonfree-vortex type. However, a spanwise average of $\bar{V}_\theta r$ can be determined (shown as broken line in Fig. II.21). The spanwise average of $\bar{V}_\theta r / \bar{V}_z r_T$ is found to be 0.76 and will be used as the value for K_0 for subsequent use in obtaining numerical data from the theory. The maximum deviation of the actual value of $(\bar{V}_\theta r)$ from its spanwise average is about 18%. Furthermore, the gradient of $(\bar{V}_\theta r)$ with respect to r, which is proportional to the strength of the shed circulation, is quite gentle except for the portion close to the tip. In consequence, the flow field may be considered to be made up of (i) the free-vortex-mean flow with a mean outflow angle of 37.3° at the tip, (ii) the perturbation flow due to axisymmetric disturbances for deviation from the free-vortex design, and (iii) the non-axisymmetric perturbation flow introduced by the circumferential distortion in stagnation pressure.

The perturbed flow due to axisymmetric disturbances is described by the familiar actuator disc theory[1,4,18,34]; its main analytical results are summarized below (in dimensionless form):

$$\bar{V}_z = \begin{cases} 1+\sum_{p=1}^{\infty} \frac{B_p}{2} e^{\lambda_p z} \frac{1}{r}\frac{\partial}{\partial r}(r\Gamma_p(r)) & z<0 \\ 1+\sum_{p=1}^{\infty} \frac{B_p}{2}(2-e^{-\lambda_p z})\frac{1}{r}\frac{\partial}{\partial r}(r\Gamma_p(r)) & z>0 \end{cases} \tag{6.2}$$

$$\bar{V}_r = \begin{cases} -\sum_{p=1}^{\infty} \frac{B_p}{2} \lambda_p e^{\lambda_p z}\Gamma_p(r) & z<0 \\ -\sum_{p=1}^{\infty} \frac{B_p}{2} \lambda_p e^{-\lambda_p z}\Gamma_p(r) & z>0 \end{cases} \tag{6.3}$$

where $\Gamma_p(r)$ is a linear combination of the Bessel Functions of the first and second kind with order p. It is given by

$$\Gamma_p(r) = \left[J_1(\lambda_p r) - \frac{J_1(\lambda_p)}{Y_1(\lambda_p)} Y_1(\lambda_p r)\right] \Big/ \sqrt{N_p} \ , \tag{6.4}$$

where

$$N_p = \int_h^1 r\left[J_1(\lambda_p r) - \frac{J_1(\lambda_p)}{Y_1(\lambda_p)} Y_1(\lambda_p r)\right]^2 dr \tag{6.5}$$

The coefficient Bp is found by matching of the flow at the actuator disc; it is given by

$$B_p = \frac{1}{\lambda_p^2}\int_h^1 \frac{1}{r}\left(\frac{\bar{V}_\theta r}{\bar{V}_z}\right)\frac{d}{dr}(\bar{V}_\theta r)\Gamma_p(r)\,dr \ . \tag{6.6}$$

The eigenvalues λp are the roots of the equation

$$J_1(\lambda_p)Y_1(\lambda_p h) - J_1(\lambda_p h)Y_1(\lambda_p) = 0 \tag{6.7}$$

which guarantees the vanishing of radial velocity at the hub and the shroud.

We note that because of the boundary conditions at the hub and shroud, the slope of the curve (i.e., d/dr $(\bar{V}_\theta r)$ in Fig. II.22 must vanish at the hub and shroud, otherwise a radial flow there is implied. Thus, the functional form of $(\bar{V}_\theta r)$ can conveniently be described by

$$(\bar{V}_\theta r) = \sum_{j=1}^{N} a_{j-1} \cos\left[\pi (j-1)\left(\frac{r-h}{1-h}\right)\right] . \tag{6.8}$$

The coefficients a_{j-1} (or equivalently the degrees of freedom) are determined from Fig. II.21. For each value of r between 0.43 and 1, there is a corresponding value of $(\bar{V}_\theta r)$ so that by permitting N degrees of freedom, the set of coefficients a_{j-1} can be determined. For 24 degrees of freedom, the values of a_{j-1} are shown in TABLE III.

TABLE III

a_0	0.75935	a_6	-0.00813	a_{12}	0.00290	a_{18}	-0.00052
a_1	-0.10046	a_7	0.00763	a_{13}	-0.00299	a_{19}	-0.00081
a_2	-0.06073	a_8	-0.00241	a_{14}	0.00250	a_{20}	-0.00060
a_3	0.00906	a_9	0.00037	a_{15}	-0.00051	a_{21}	0.00037
a_4	-0.02450	a_{10}	0.00118	a_{16}	0.00061	a_{22}	0.00035
a_5	0.01943	a_{11}	-0.00374	a_{17}	0.00005	a_{23}	-0.00000

Thus, knowing $(\bar{V}_\theta r)$, the axisymmetric disturbances are completely determined through the use of actuator disc theory.

The non-axisymmetric disturbances due to the stagnation pressure distortion are determined through the use of the theory developed in Chapter 3 of Part II. By making use of the available experimental information and analytical results, it is found that the downstream stagnation pressure pattern would vary in accordance with

$$\delta P_t = 0.21 \cos\left(\theta - \frac{K_0 Z}{r^2}\right) . \tag{6.9}$$

where we have normalized the pressure by $(\rho \bar{V}_z^2)$. This pattern of variation is confirmed by Figure II.22 which shows the axial variation of the circumferential pattern of stagnation pressure distortion; its swirl downstream with the mean flow is in agreement with Strand's measurement. Fig. II.23 shows the comparison between the three-dimensional predictions and the experimental data for various radial locations at Z = 0.62. The agreement is excellent. Similarly, there is agreement in the comparisons made in Fig. II.24. However, there is descrepancy between the theory and experiment at r = 0.49; this is probably due to viscous effects such as the growth of boundary layer in the hub region. A similar trend is also observed in Fig. II.25 except those at r = 0.94 in the tip region and r = 0.6 in the tip region. These discrepancies are probably due to viscous origin again such as boundary layer growth in the hub and tip regions.

Figure II.26 shows the axial velocity perturbations from Strand's experiment[57], and from the three-dimensional theory, up to Z = 2.57. Figs. II.27, II.28, and II.29 show the comparison between theory and experiment for various radial stations at Z = 0.62190, 1.417, and 2.5735 respectively. The agreement between theory and experiment is excellent with the exception of those (i) at r = 0.488 for Z = 1.417, (ii) at

r = 0.598, and (iii) r = 0.496 for Z = 2.5735. The discrepancy is the biggest in (iii). It is noted that these radial locations are within the hub region and possibly it is due to the boundary layer effect.

In Fig. II.30, the results arising from the three-dimensional prediction of the persistence of the static pressure perturbations are compared with Strand's data. We emphasize again that such predictions are out of reach of the two-dimensional theory. Here, there is good agreement up to $Z \simeq 1.4$. Beyond this point, considerable scatter in the results occur in contrast to the still well-organized pattern of stagnation pressure and axial velocity perturbations beyond the corresponding point. Figs. II.31 show a fairly good comparison between theory and experiment for the circumferential variation of static pressure at various radial stations for Z = 0.6219. However, those in Figs. II.32 are not so good.

Figs. II.32, II.34, and II.35 show the corresponding variation of the flow angle perturbations. Again, the agreement between theory and experiment is good except in the vicinity of the hub.

Finally, we point out that in making the above comparisons, we choose to place the disc at a position corresponding to the trailing edge of Strand's blade row. This choice seems to be consistent with the solidity and aspect ratio of the stator blading used in the experiment.

CHAPTER 7 - CONCLUSIONS: PART II

From the analytical study and comparison with experiments described in preceeding Chapters, we are able to conclude that significant differences exist among the possible analysis considered, i.e., the two-dimensional strip theory, the three-dimensional rectilinear cascade theory, and the three-dimensional (3-D) annular cascade theory. The first two approaches are unable adequately to describe several key features of the flow occurring in axial turbomachines under practical loading conditions. In the first case, this is due in part to the inherent limitations of two-dimensionality assumption, with the consequent neglect of the effects of both shed circulation and centrifugal acceleration. On the other hand, the three-dimensional rectilinear theory, while allowing for appropriate variation of fluid properties in the spanwise direction and therefore for the trailing vorticity (shed circulation), still neglects centrifugal effects. As we have seen, various significant flow phenomena arise because of the simultaneous presence of the centrifugal force field and shed circulation. These phenomena are included in the three-dimensional annular analysis. As demonstrated by Dunham[56], for example, the difference between rectilinear and annular three-dimensional studies are likely to be significant when the blade row is highly loaded.

Specifically, we have seen in both Parts I and II that the pressure and vorticity disturbances are strongly coupled in the swirling flow. As Greitzer[57] has emphasized, this is to a large extent because of the presence of a centrifugal force field; the extent of the coupling and the magnitude of the associated flow disturbances increase with the strength

of the annular swirl. In swirling flow, many vorticity induced disturbances are not purely convected even approximately by the mean downstream swirl flow. By contrast, in a non-swirling flow, pressure and vorticity disturbances do not interact[21] and vorticity induced disturbances are purely convected by the mean flow.

In the case of a stator accepting distorted inlet flow, the 3-D annular cascade theory predicts a strong pressure field persisting for significant distance downstream of the blade row; in many cases, the amplitude of the static pressure perturbation increases before eventually decaying. For free vortex downstream swirl, this proceeds inversely with the axial distance from the blade row. Two-dimensional theory completely fails to predict this effect; rather it describes the downstream static pressure field as uniform, with the streamlines remaining parallel as a consequence. On the other hand, three-dimensional rectilinear cascade theory predicts an exponentially decaying (potential) pressure field. The theoretical predictions of the 3-D annular analysis for a stator are in good agreement with the experimental measurements carried out in an annular swirl flow rig.

In the case of a rotor, the two-dimensional and three-dimensional theories agree reasonably well at the tip. However, this is not the case at the hub, as the two-dimensional theory almost completely misses the perturbations there. In reference 59, comparisions of the theory with Rizvi's experimental data[60] were made. It was shown in that work that the two-dimensional theory is qualitatively incorrect near the hub, while the 3-D annular predictions follow the rotor measurements reasonably well.

This is true even though the inlet distortion used by Rizvi was rather more sharp and severe than that for which the present theory was originally intended. Further, we note that for a free vortex mean downstream flow, the perturbations are predicted to be strongest at the rotor hub. An asymmetric upstream flow sets up an asymmetric circulation distribution on the disc representing the rotor. Because each individual blade on the real rotor must move relative to this fixed (distorted) circulation pattern, and is therefore operating in an unsteady flow, unsteady vortices, oriented in the radial direction, are necessarily shed into the downstream flow field. This is in accordance with Kelvin's Theorem. At the same time, an associated streamwise component of vorticity is shed into the stream as a result of a radial gradient of circulation at the disc, or rotor plane.[59]

CHAPTER 8 - SUGGESTIONS FOR FUTURE WORK

We have treated an asymmetric flow through a single blade row in the actuator disc limit in some detail and have outlined how successive applications of the results can be used to treat a distorted flow through multiple-blade rows. It would be interesting to study the mutual interactions among the blade rows as a result of a distorted inlet flow in further detail and to compare it with the simplified models (such as the parallel compressor model), and any available experimental data.

Because of the necessity of high pseed flow (and therefore compressibility effects) in modern, compact and light weight engines for aircraft application, it is desirable to extend the present analysis of a distorted flow through blade rows to the compressible regime; at least in the actuator disc limit in the initial stage. The technique used will again rely on the ability to give a correct description of the vorticity so that the internal aerodyamics of the turbomachines may be described. This can readily be achieved by the use of the Clebsch-Hawthorne Formulation for the reduced flow outlined in Section 4.9 of Part I. Such an analysis would be of use for looking at the response of a transonic blade row to an inlet distortion in stagnation pressure.

The problem of an inlet distortion in stagnation temperature can be analyzed similarly too. But we note that, by the substitution principle of Munk and Prim[4,30], flows with the same distribution of stagnation pressure will have the same geometrical pattern of streamlines regardless of the distirbution of stagnation temperature. Thus for a flow with a distortion in stagnation temperature through a free vortex stator, because the stagnation pressure is everywhere constant, the downstream streamlines

are changed only by the trailing shed circulation resulting from the distorted flow upstream. However, the picture would be quite different in the case of the rotor; the introduction of an upstream distortion in stagnation temperature will result in non-uniform work done by the free vortex rotor, thus creating a downstream distortion in stagnation pressure giving rise to the presence of secondary vorticity as the flow swirls downstream. Thus a stagnation temperature distortion would be of much interest in the rotor case.

The next step in this analytical work would be a relaxation in the assumption of actuator disc concept by allowing for the finite discretion of the rotor blades; thus, each blade would be like a single airfoil flying in and out of a gust suffering a sudden change of aerodynamic load each time. Such an analysis would also allow for the treatment of a moving distortion.

Finally, in view of the present recognition of the importance of three-dimensional effects in swirling flow, the problem of rotating stall should be reexamined in this light. A treatment of rotating stall may necessitate the inclusion of blade row characteristics.

APPENDIX II.A

The inhomogeneous solution of Eq. (2.80):

On substituting

$$\phi_I^d = \sum_{n=1}^{\infty}\sum_{p=0}^{\infty} X_{np}(x)\, e^{iny} \cos\frac{p\pi}{l} z \tag{A.1}$$

in Eq. (2.80), of Part II, we obtain

$$\sum_{n=1}^{\infty}\sum_{p=0}^{\infty}(X''_{np} - \lambda_{np}^2 X_{np}) e^{iny}\cos\frac{p\pi}{l} z = \sum_{n=1}^{\infty} in\tan\bar{\alpha}_2 P_n(z)\, e^{in(y-x\tan\bar{\alpha}_2)} \tag{A.2}$$

$$-\sum_{n=1}^{\infty}\frac{dG_n(z)}{dz} e^{in(y-x\tan\bar{\alpha}_2)}$$

On making use of the orthogonality of trigonmentrical functions, we have

$$\frac{1}{2}(X''_{np} - \lambda_{np}^2 X_{np}) = in\tan\bar{\alpha}_2 e^{-inx\tan\bar{\alpha}_2}\int_0^1 P_n(z)\cos\frac{p\pi}{l} z\,dz - e^{-inx\tan\bar{\alpha}_2}\int_0^1 \frac{dG_n}{dz}\cos\frac{p\pi}{l} z\,dz$$

$$= e^{-inx\tan\bar{\alpha}_2}\left\{in\tan\bar{\alpha}_2\int_0^1 P_n(z)\cos\frac{p\pi}{l} z\,dz - \frac{p\pi}{l}\int_0^1 G_n(z)\sin\frac{p\pi}{l} z\,dz\right\}, \tag{A.3}$$

where we have imposed the condition that $G_n(Z)$ should vanish at $Z = 0$.

On solving Eq. (A.3) by the method of variation of parameters, we obtain

$$X_{np}(x) = -\frac{2e^{-inx\tan\bar{\alpha}_2}}{l(\lambda_{np}^2 + n^2\tan^2\bar{\alpha}_2)}\left\{in\tan\bar{\alpha}_2\int_0^1 P_n(z)\cos\frac{p\pi}{l} z\,dz - \frac{p\pi}{l}\int_0^1 G_n(z)\sin\frac{p\pi}{l} z\,dz\right\}. \tag{A.4}$$

APPENDIX II.B

On substituting Eq. (3.30) in Eq. (3.26) of Part II, we obtain

$$\sum_{n=1}^{\infty}\sum_{p=1}^{\infty} e^{in\theta}\left\{Z_{np}(z)\left(\frac{d^2R_{np}}{dr^2}+\frac{1}{r}\frac{dR_{np}}{dr}-\frac{n^2}{r^2}R_{np}\right)+\frac{d^2Z_{np}}{dz^2}R_{np}\right\}$$

$$=-\frac{1}{r}\frac{\partial}{\partial r}\left(r\sum_{n=1}^{\infty}G_n e^{in\bar{\alpha}^d}\right)-\frac{\partial}{\partial z}\left(\sum_{n=1}^{\infty}P_n e^{in\bar{\alpha}^d}\right) . \tag{B.1}$$

The normalized radial eigenfunction $R_{np}(r)$ must satisfy

$$\frac{d^2R_{np}}{dr^2}+\frac{1}{r}\frac{dR_{np}}{dr}+\left(\lambda_{np}^2-\frac{n^2}{r^2}\right)R_{np}=0 . \tag{B.2}$$

Hence for each n,

$$\sum_{n=1}^{\infty}\left(\frac{d^2Z_{np}}{dz^2}-\lambda_{np}^2Z_{np}\right)R_{np}=-\frac{1}{r}\frac{\partial}{\partial r}\left(rG_n e^{-inK_0z/r^2}\right)-\frac{\partial}{\partial z}\left(P_n e^{-inK_0z/r^2}\right). \tag{B.3}$$

On multiplying the equation by rR_{nj}, and integrating from r = h to r = 1 we obtain, by virtue of the orthogonality of the normalized functions R_{nj},

$$\frac{d^2Z_{np}}{dz^2}-\lambda_{np}^2Z_{np}=-\int_h^1 R_{np}\frac{\partial}{\partial r}\left[rG_n e^{-inK_0z/r^2}\right]dr-\int_h^1 rR_{np}\frac{\partial}{\partial z}\left[P_n e^{-inK_0z/r^2}\right]dr . \tag{B.4}$$

The first integral on the RHS may be integrated by parts to give

$$\frac{d^2Z_{np}}{dz^2}-\lambda_{np}^2Z_{np}=\int_h^1\left(rG_n\frac{dR_{np}}{dr}+\frac{inK_0}{r}P_nR_{np}\right)e^{-inK_0z/r^2}dr . \tag{B.5}$$

We note that when integrating the first integral by parts we have assumed $G_n = 0$ at hub and tip, as we have pointed out in Chapter 3 of Part II. On solving Eq. (B.5) by the method of variation parameters, we obtain the integral form of $Z_{np}(z)$ given in Eq. (3.31) of Part II.

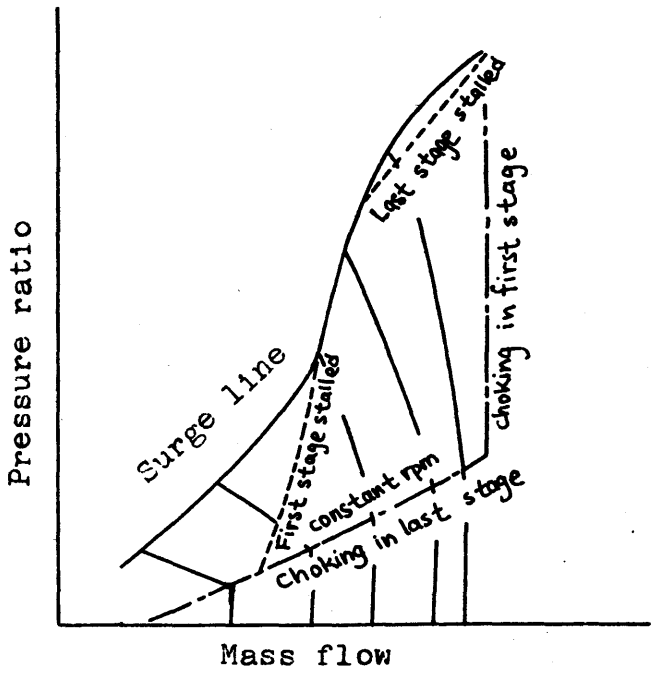

FIG. II.1: DIAGRAMMATIC REPRESENTATION OF THE CHARACTERISTICS OF A TYPICAL AXIAL COMPRESSOR.

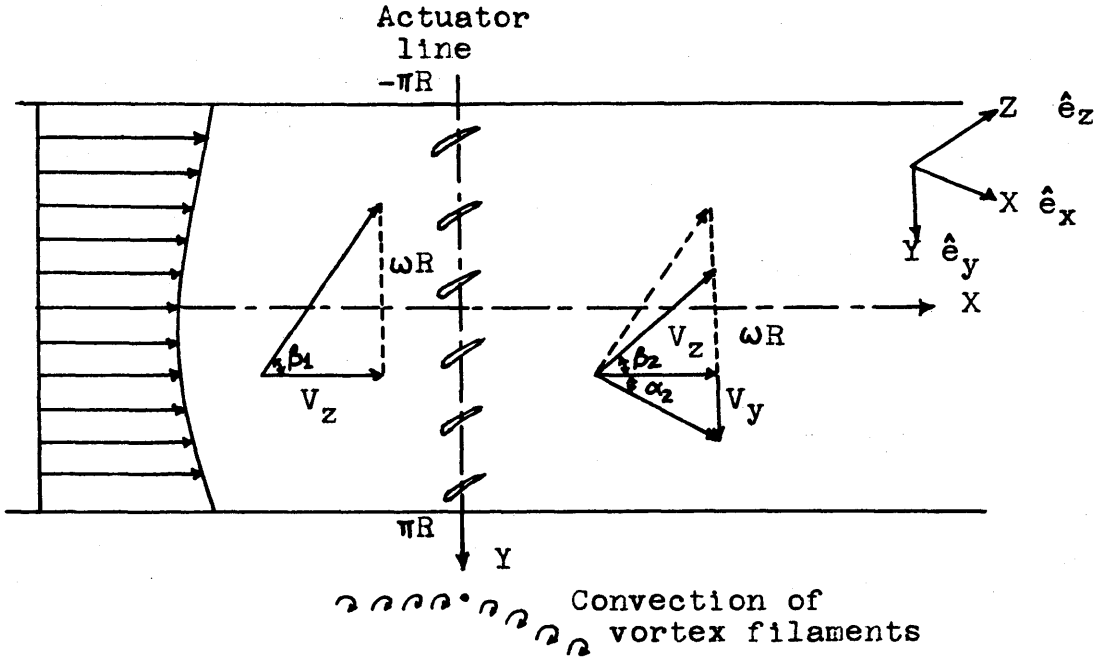

FIG. II.2: A DISTORTED FLOW THROUGH AN ISOLATED TWO-DIMENSIONAL CASCADES.

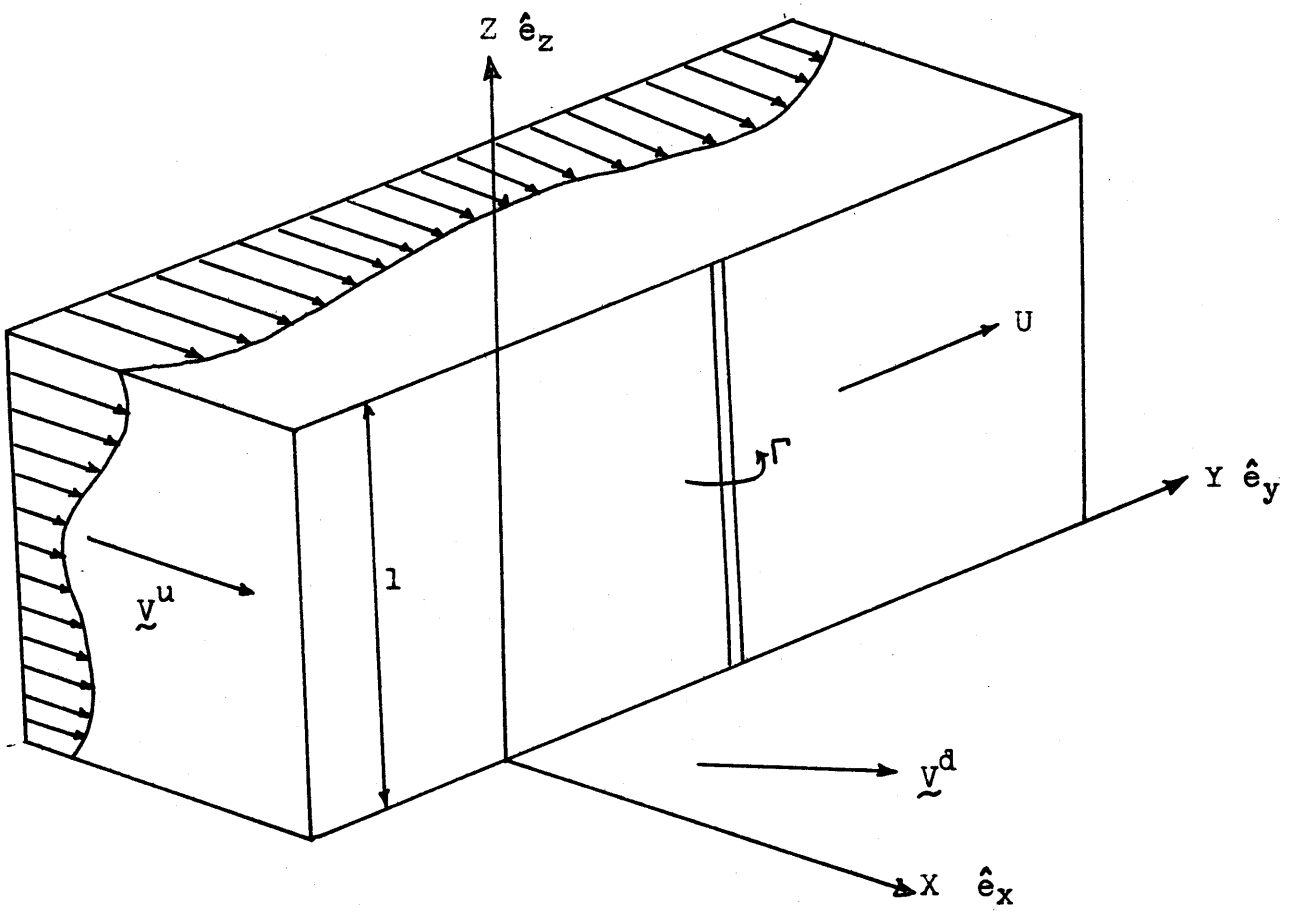

FIG. II.3: A DISTORTED FLOW THROUGH AN ISOLATED THREE-DIMENSIONAL RECTILINEAR CASCADES.

FIG. II.4: A DISTORTED FLOW THROUGH AN ISOLATED ANNULAR CASCADES.

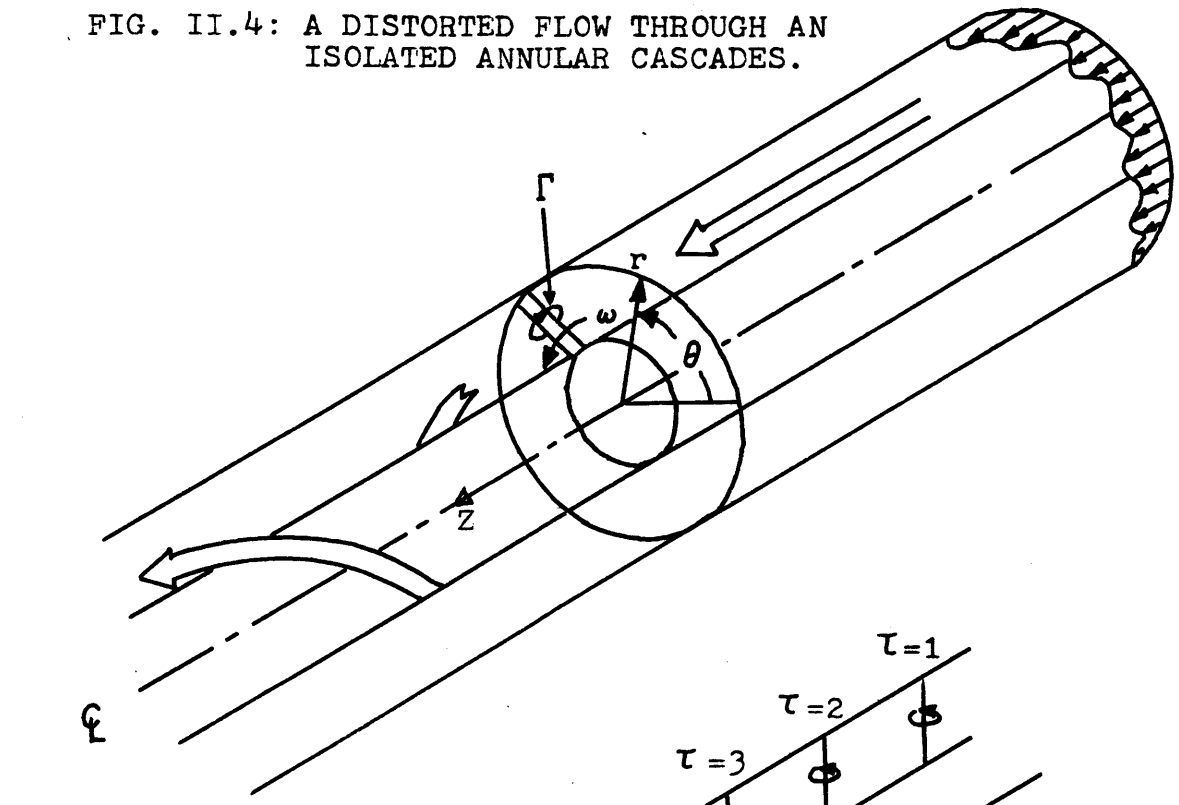

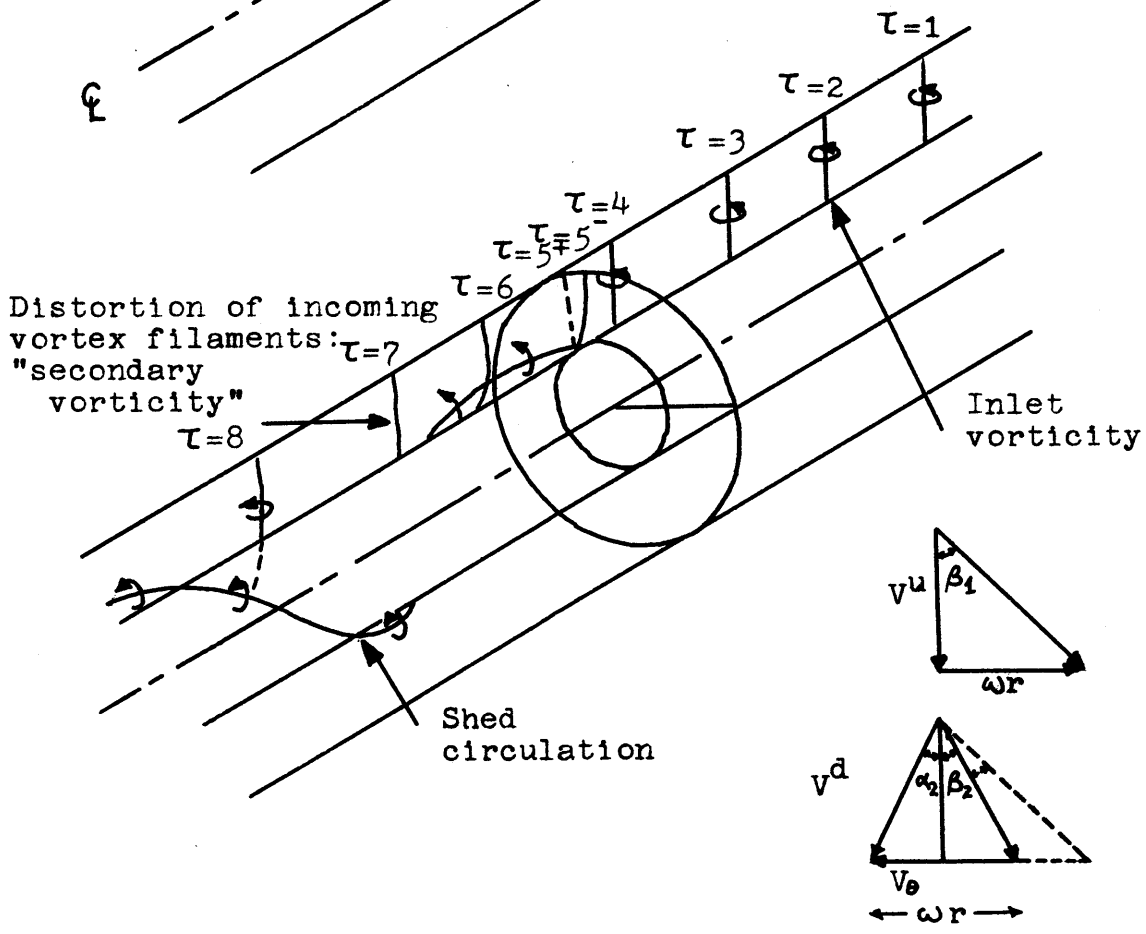

FIG. II.5: THE VORTEX FILAMENTS ASSOCIATED WITH A DISTORTED INLET FLOW.

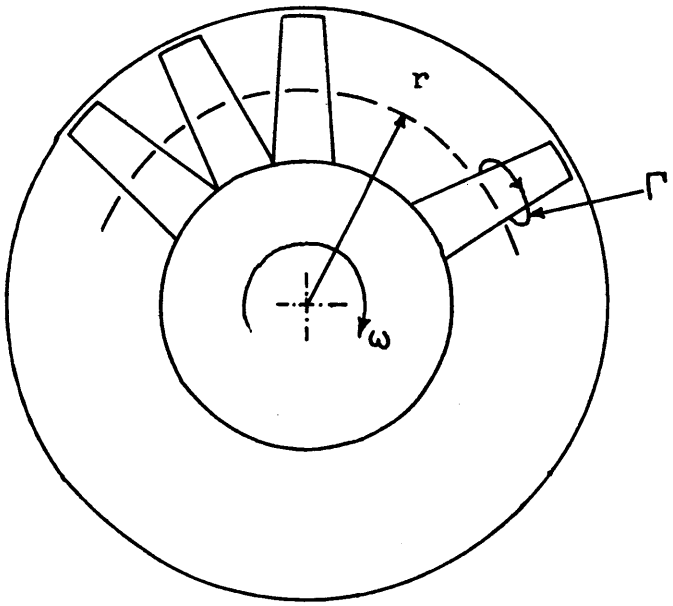

FIG. II.6: DEFINITION OF BLADE CIRCULATION.

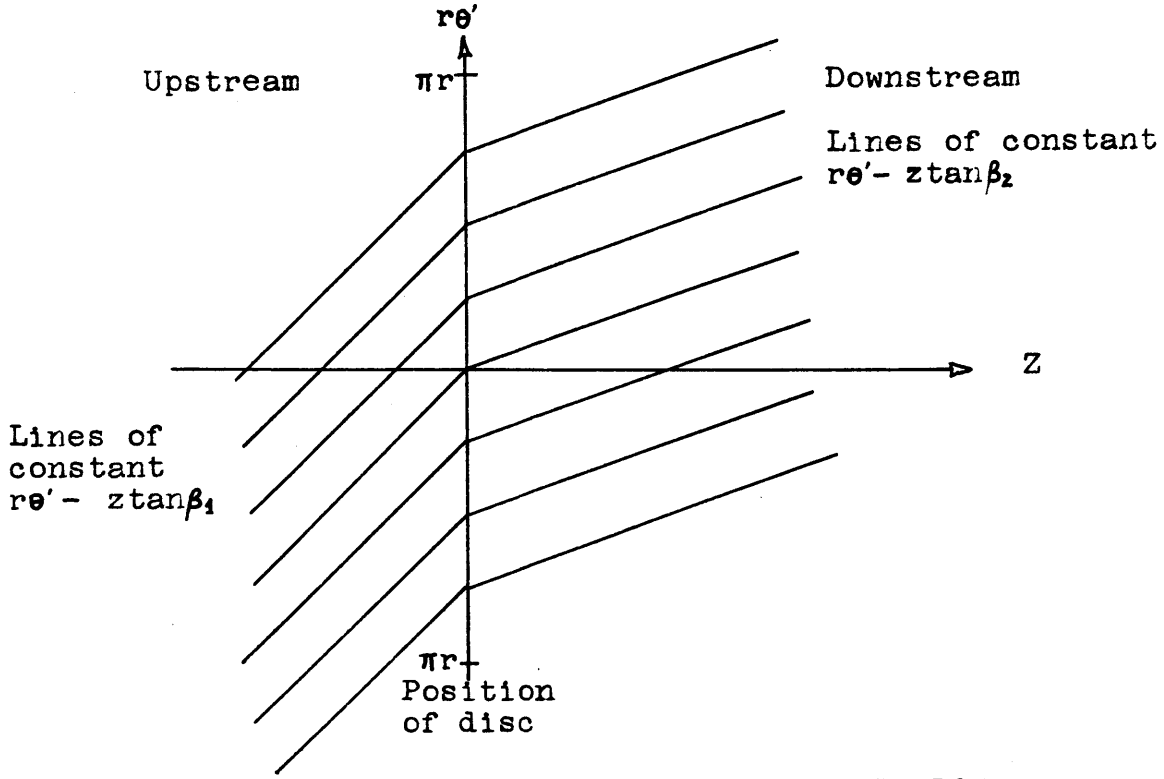

FIG. II.7: STREAMLINES OF THE MEAN RELATIVE FLOW.

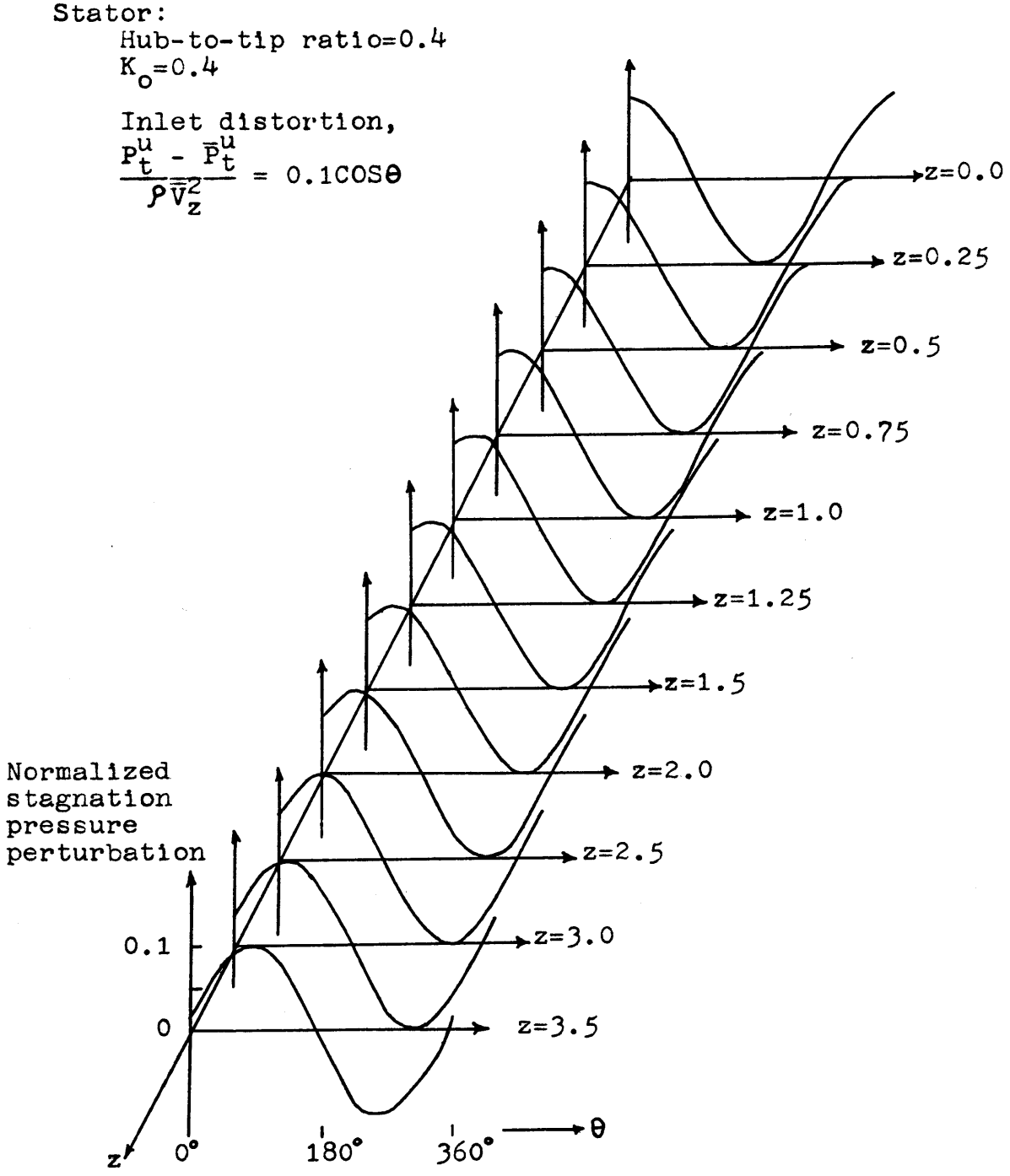

FIG. II.8: DOWNSTREAM VARIATION OF STAGNATION PRESSURE PERTURBATION AT THE TIP.

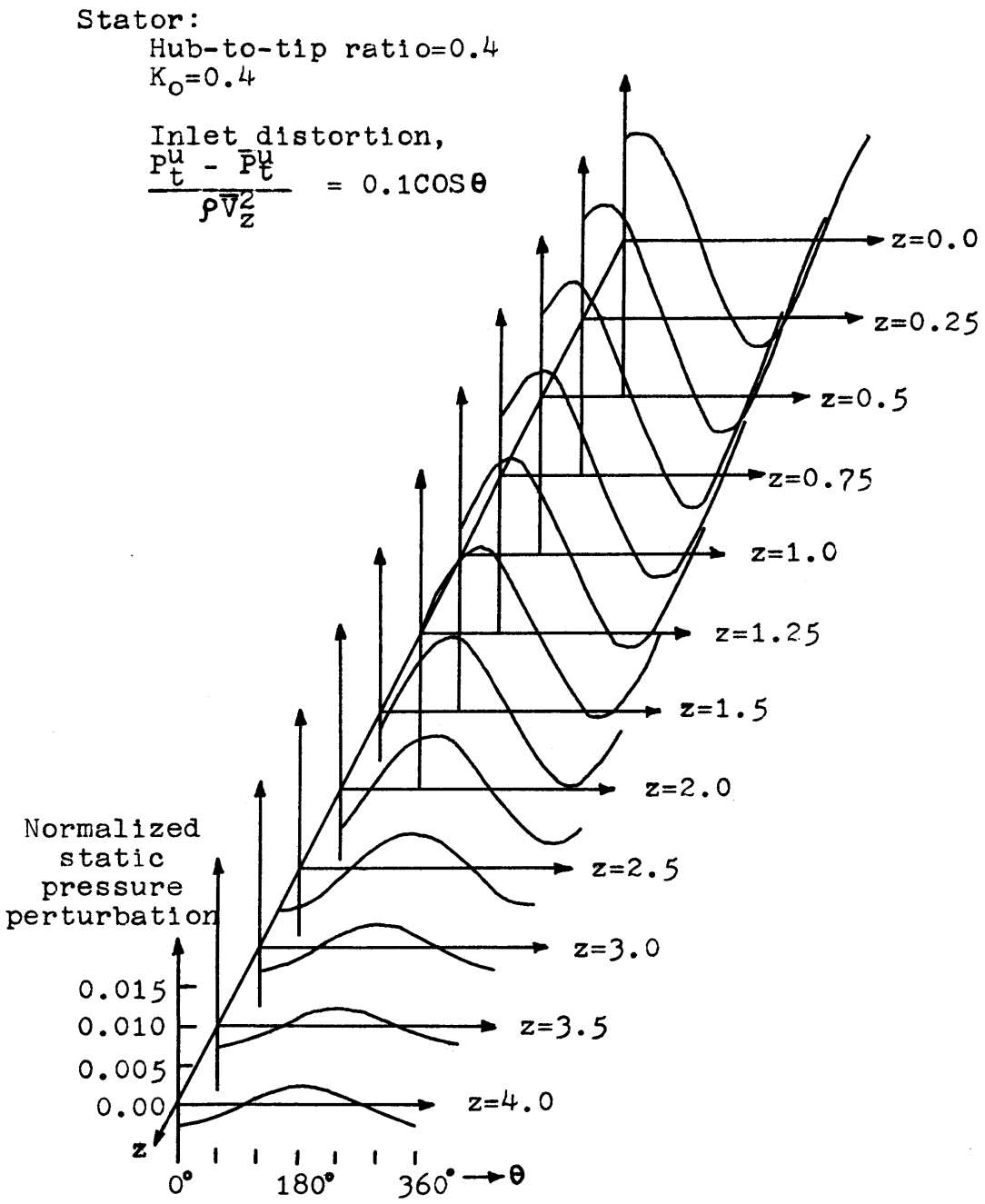

FIG. II.9a: DOWNSTREAM VARIATION OF STATIC PRESSURE PERTURBATION AT THE TIP.

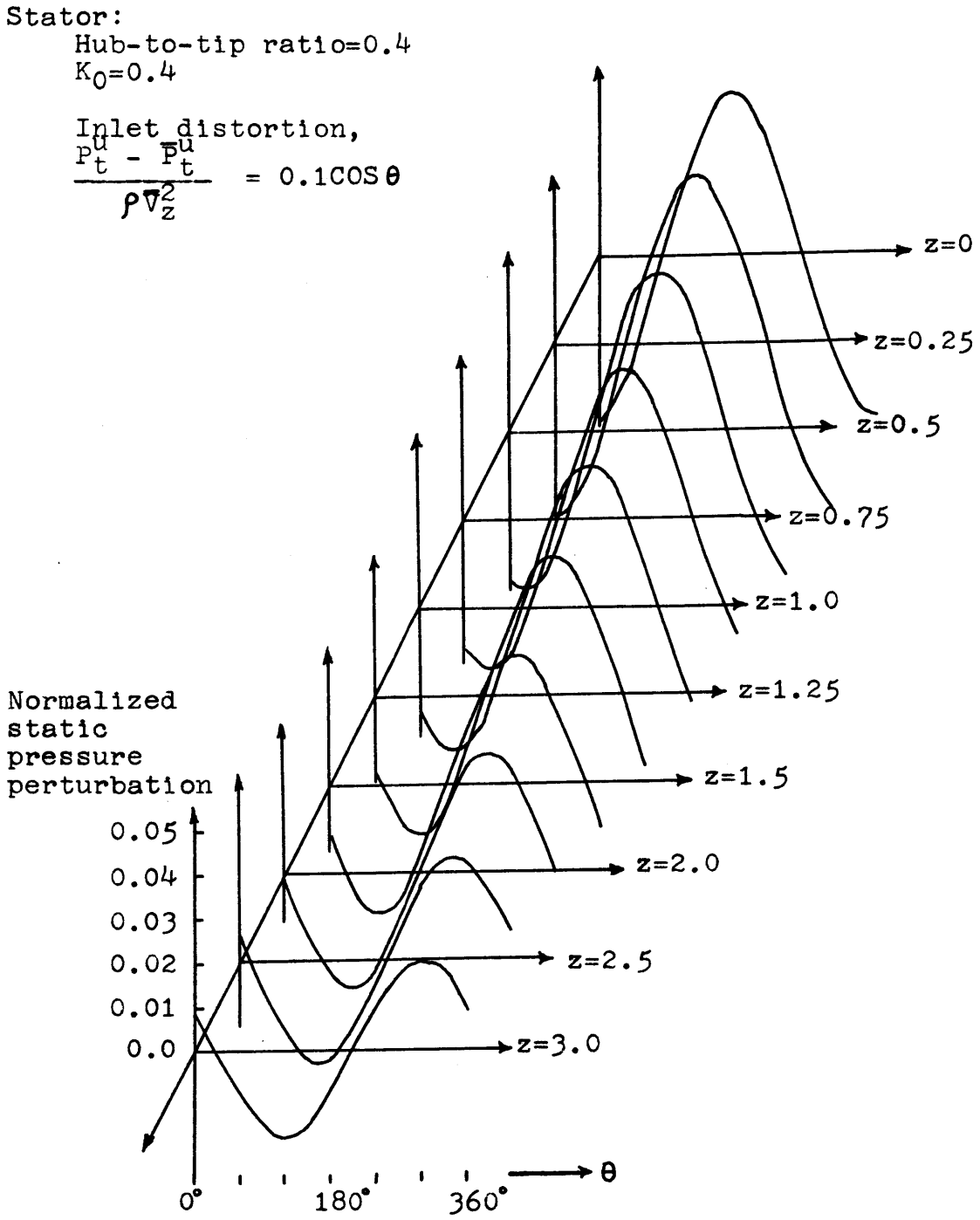

FIG. II.9b: DOWNSTREAM VARIATION OF STATIC PRESSURE PERTURBATION AT THE HUB.

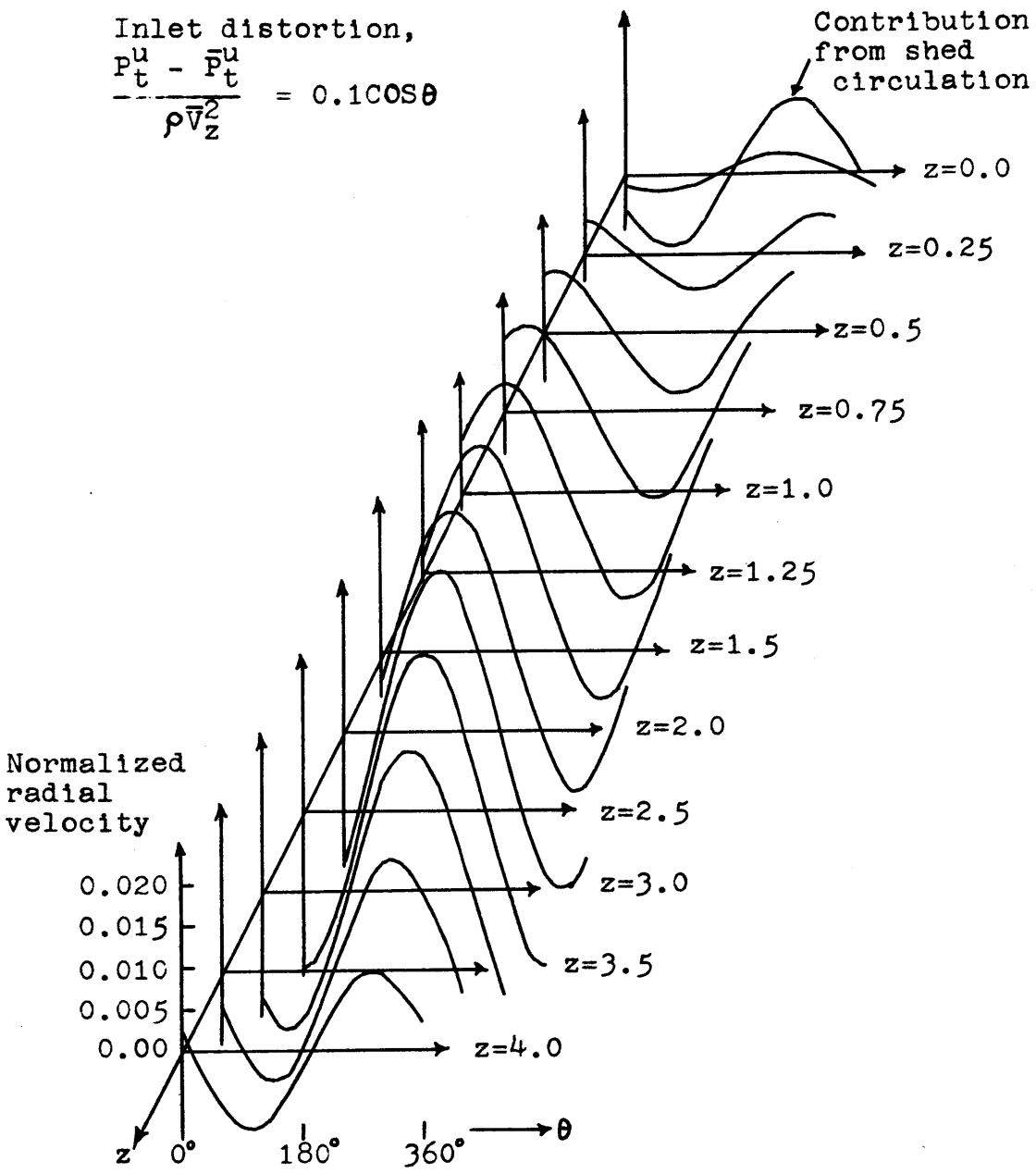

FIG. II.10a: DOWNSTREAM VARIATION OF RADIAL VELOCITY AT r/r_t=0.55.

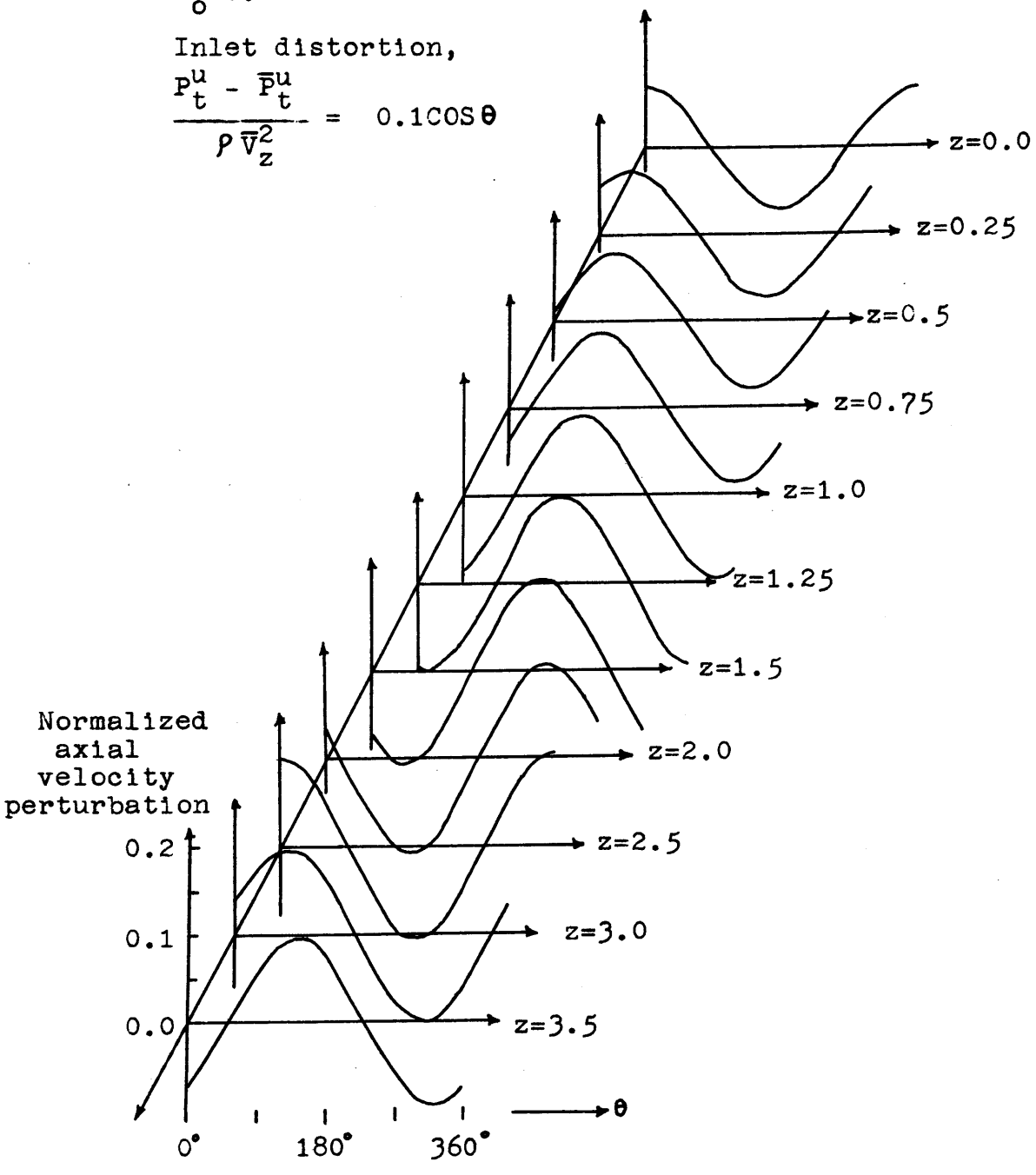

FIG. II.10b: DOWNSTREAM VARIATION OF AXIAL VELOCITY PERTURBATION AT THE HUB.

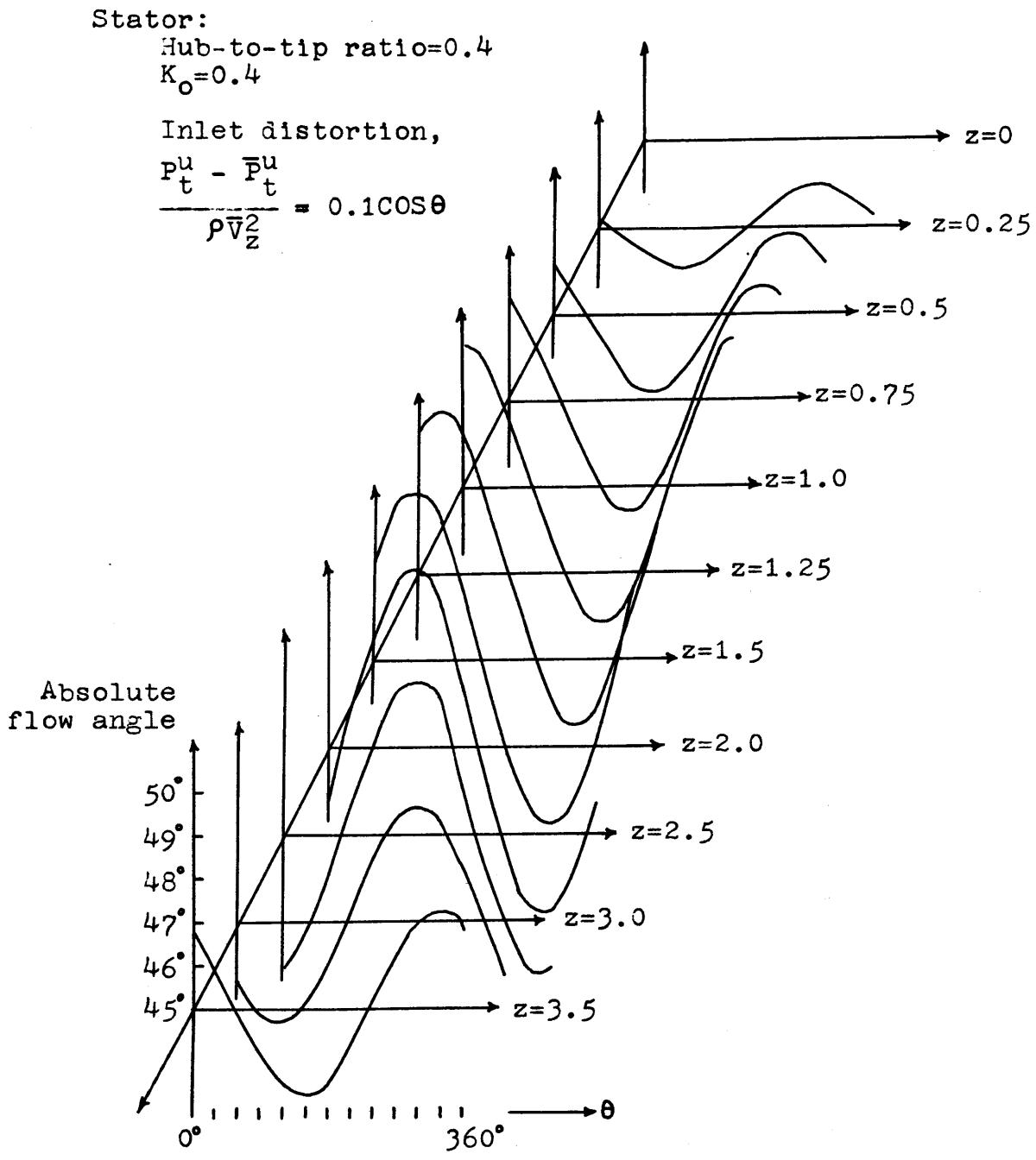

FIG. II.11: DOWNSTREAM VARIATION OF ABSOLUTE FLOW ANGLE AT THE HUB.

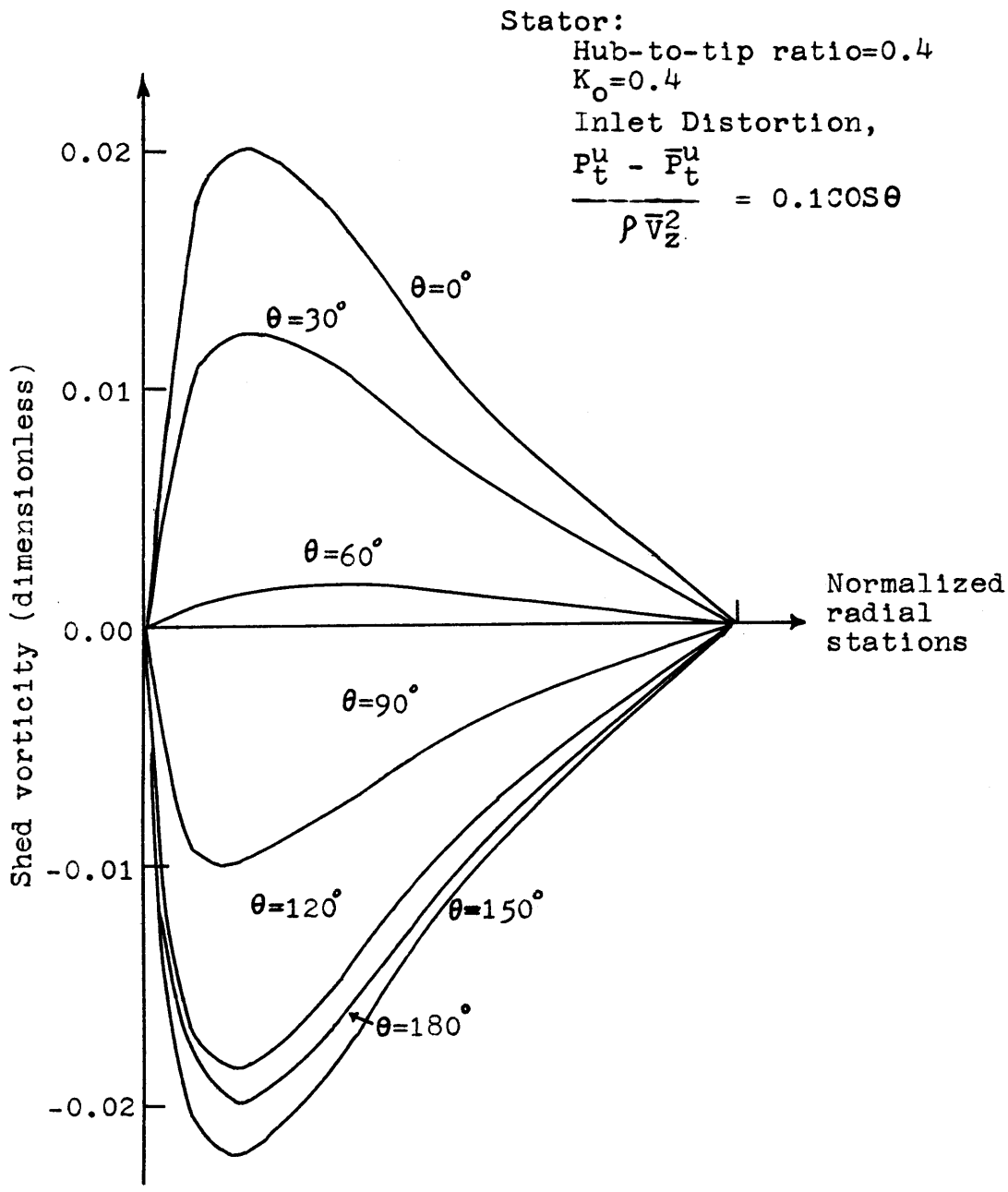

FIG. II.12: RADIAL DISTRIBUTION OF SHED CIRCULATION BEHIND THE STATOR.

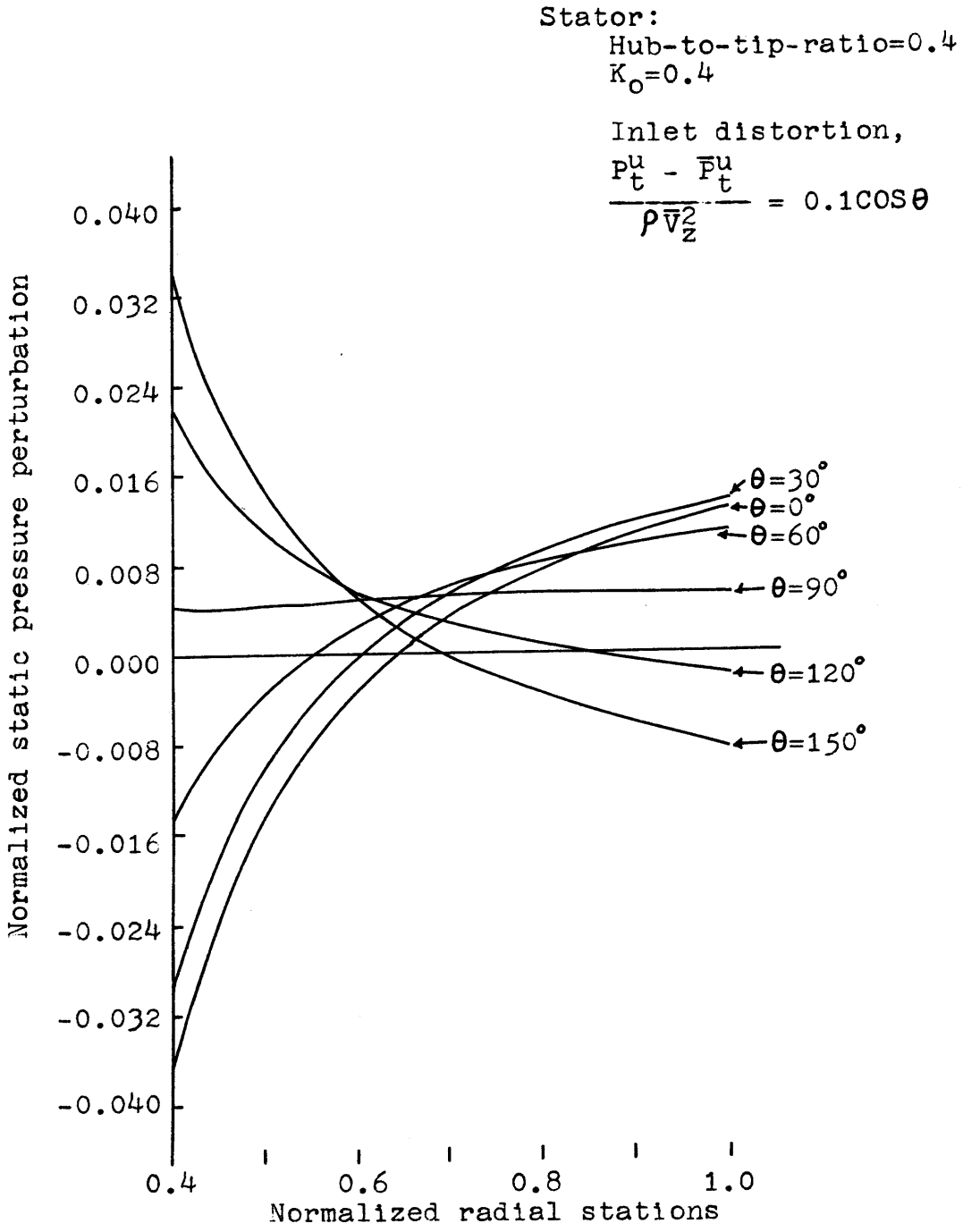

FIG. II.13a: RADIAL VARIATION OF DOWNSTREAM STATIC PRESSURE PERTURBATION AT Z=0.0

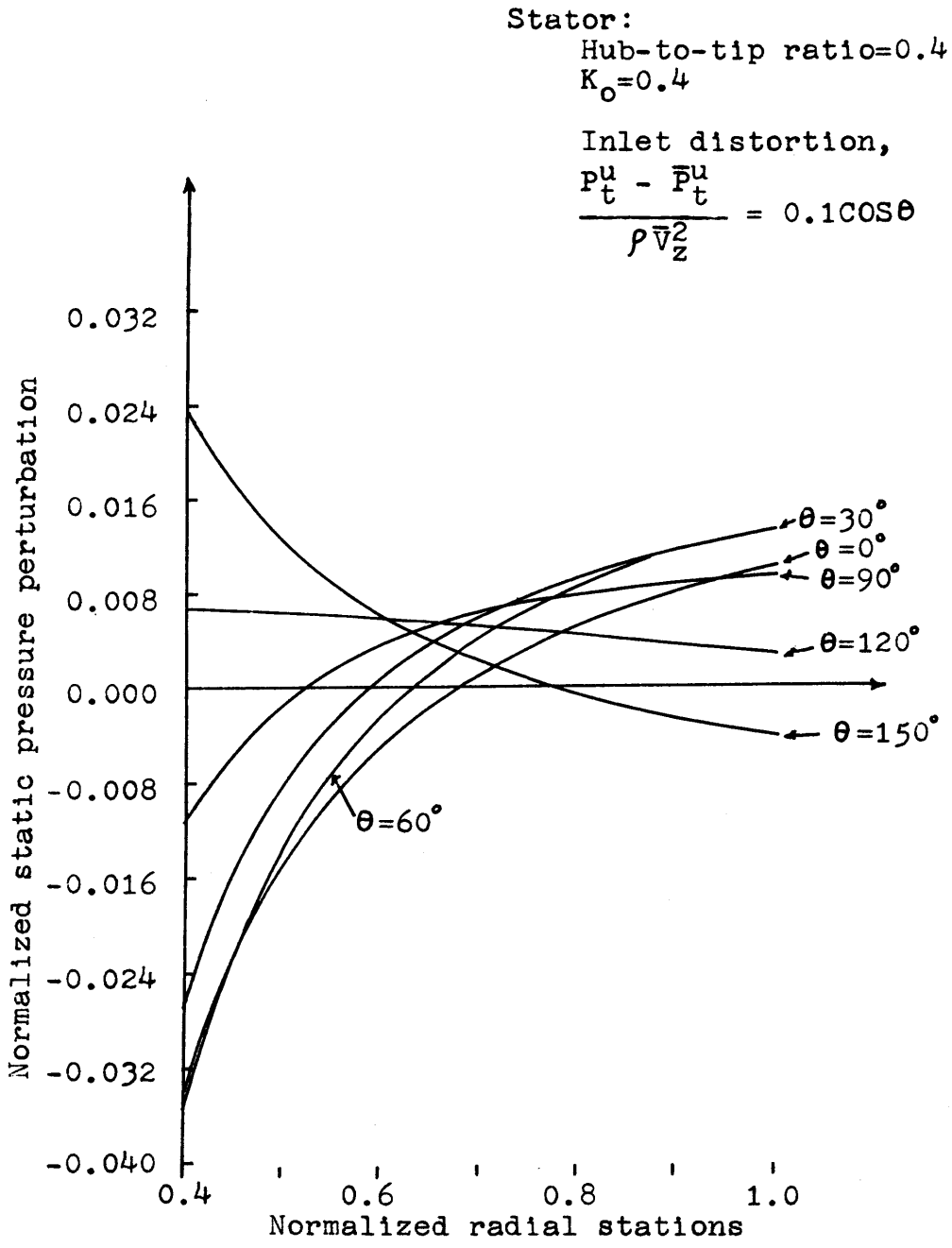

FIG. II.13b: RADIAL VARIATION OF DOWNSTREAM STATIC PRESSURE PERTURBATION AT Z=0.5.

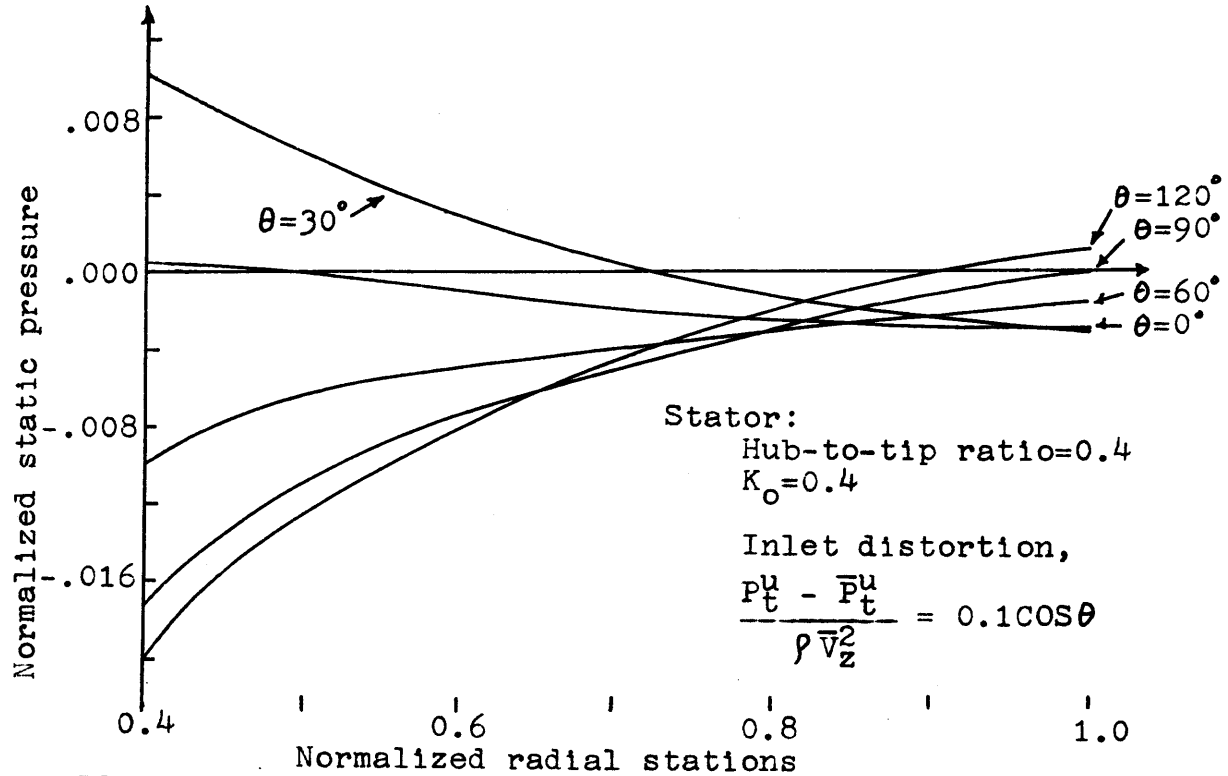

FIG. II.13c: RADIAL VARIATION OF DOWNSTREAM STATIC PRESSURE PERTURBATION AT Z=3.0.

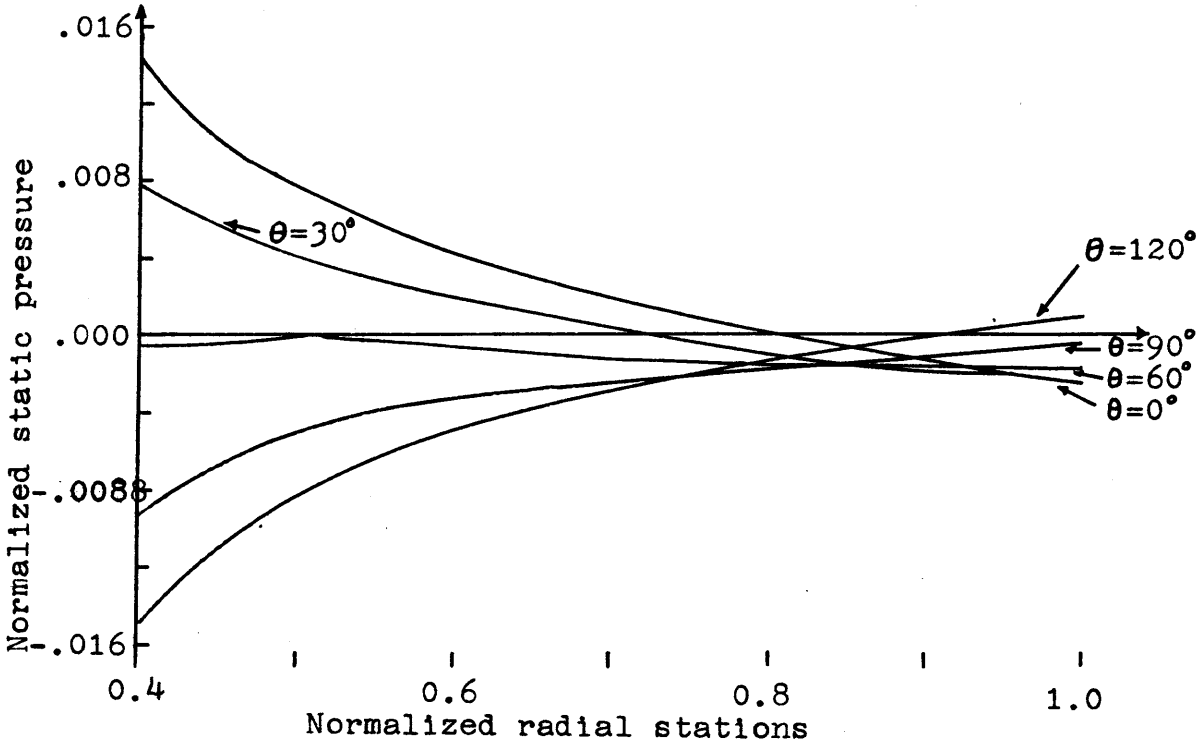

FIG. II.13d: RADIAL VARIATION OF DOWNSTREAM STATIC PRESSURE PERTURBATION AT Z=4.0.

Stator:

Hub-to-tip ratio=0.4

K_o=0.4

Inlet distortion,

$$\frac{p_t^u - \bar{p}_t^u}{\rho \bar{v}_z^2} = 0.1 \cos 5\theta$$

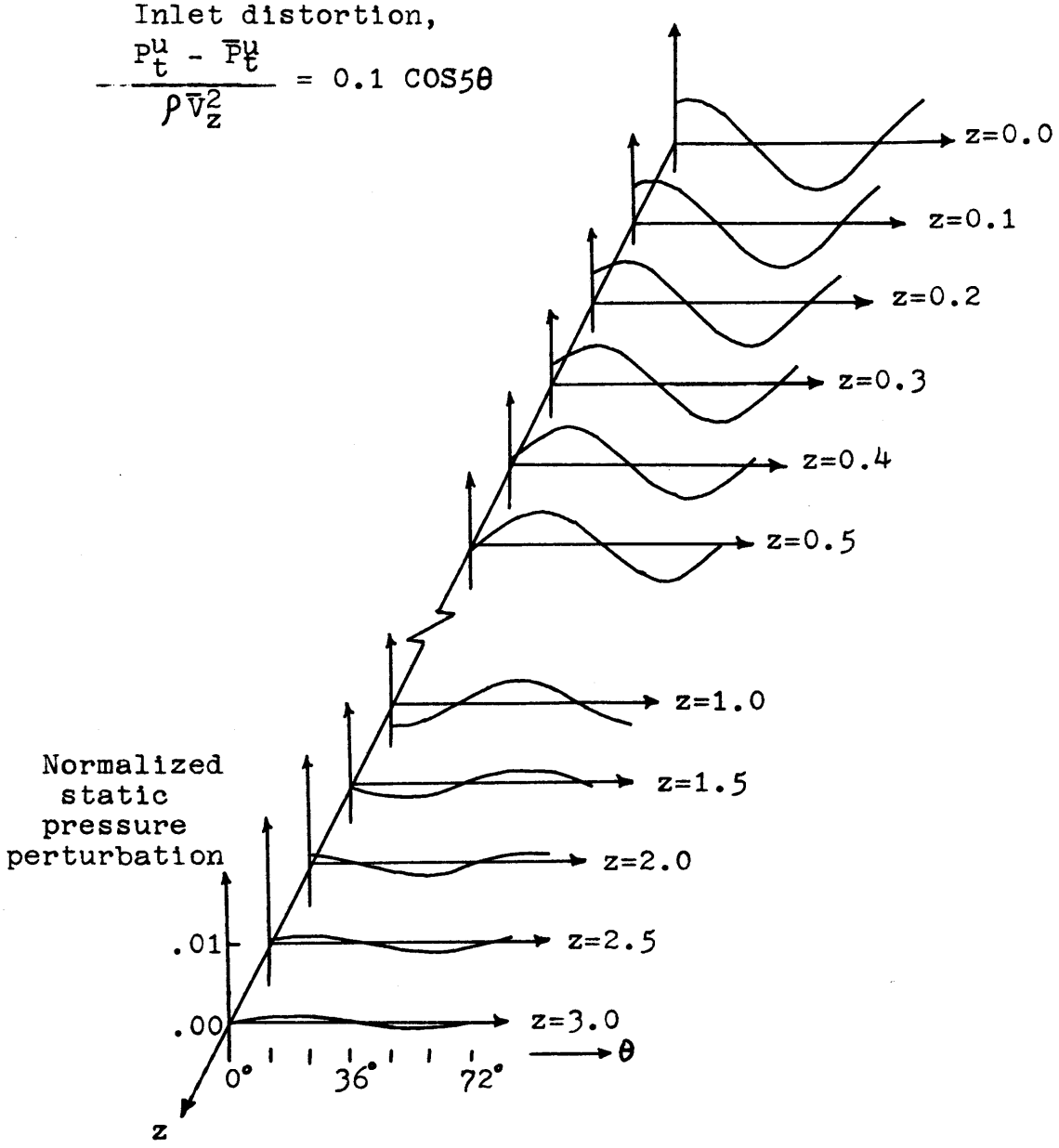

FIG. II.14a: DOWNSTREAM VARIATION OF STATIC PRESSURE PERTURBATION AT THE TIP.

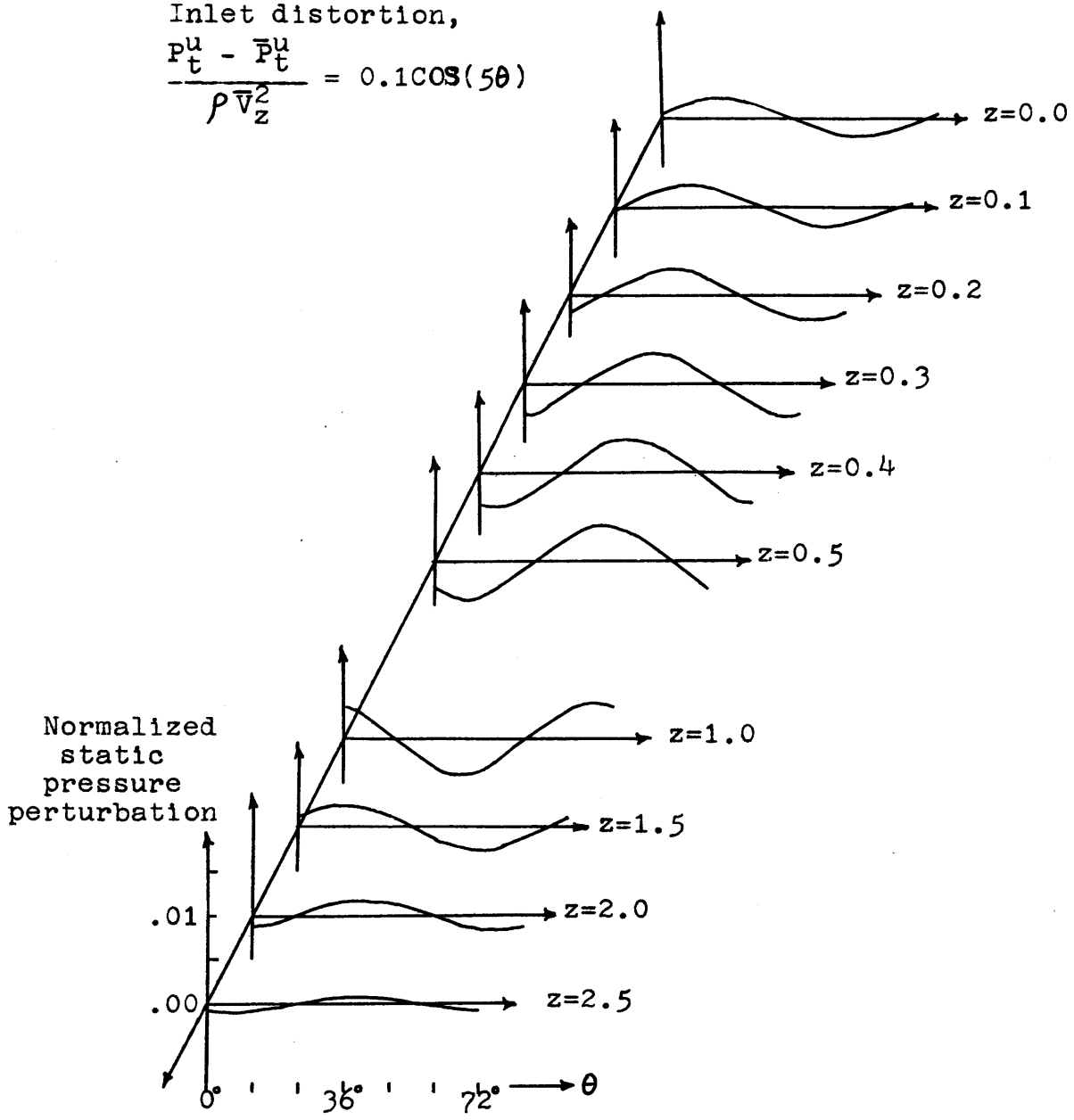

FIG. II.14b: DOWNSTREAM VARIATION OF STATIC PRESSURE PERTURBATION AT THE MID-SPAN.

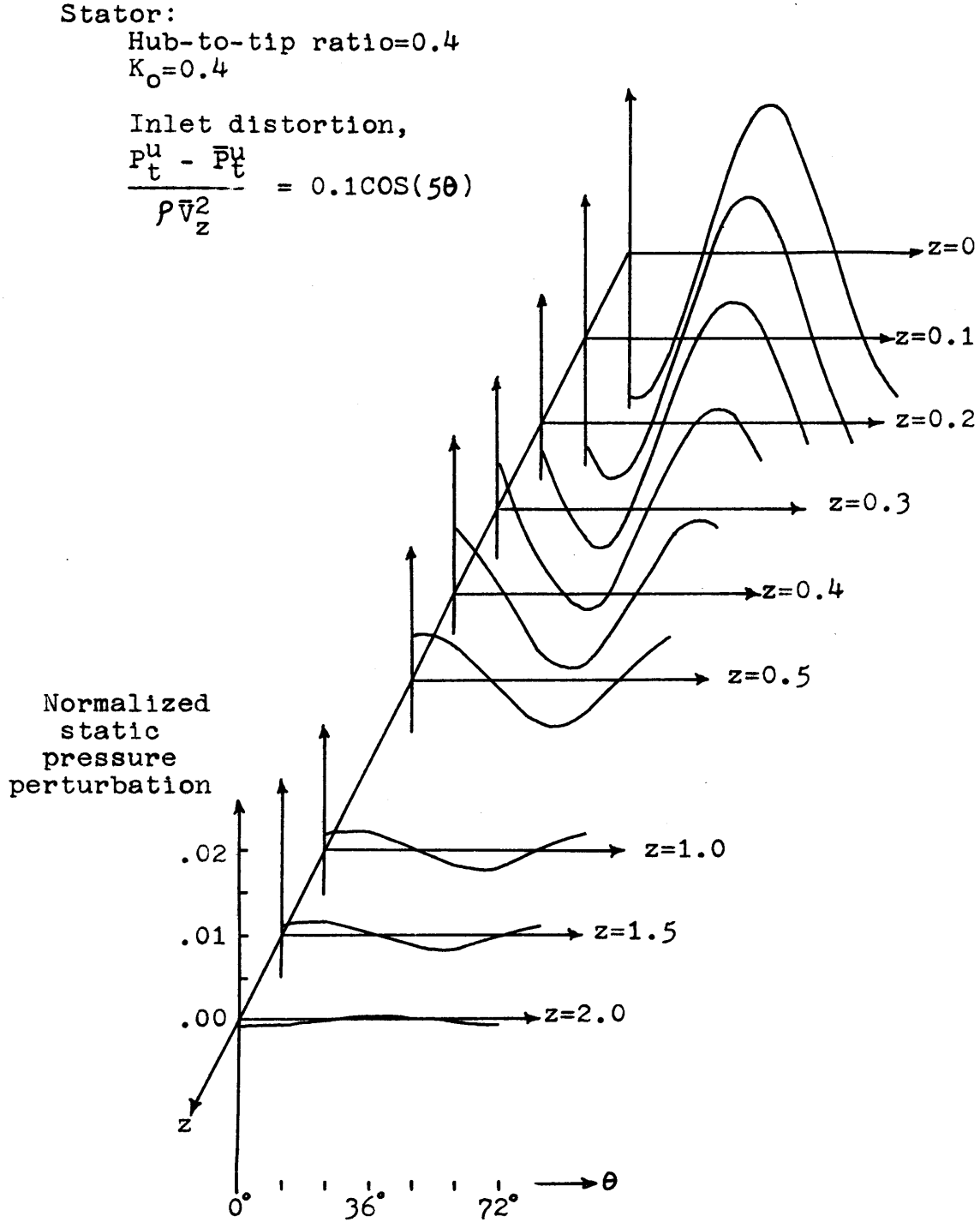

FIG. II.14c: DOWNSTREAM VARIATION OF STATIC PRESSURE PERTURBATION AT THE HUB.

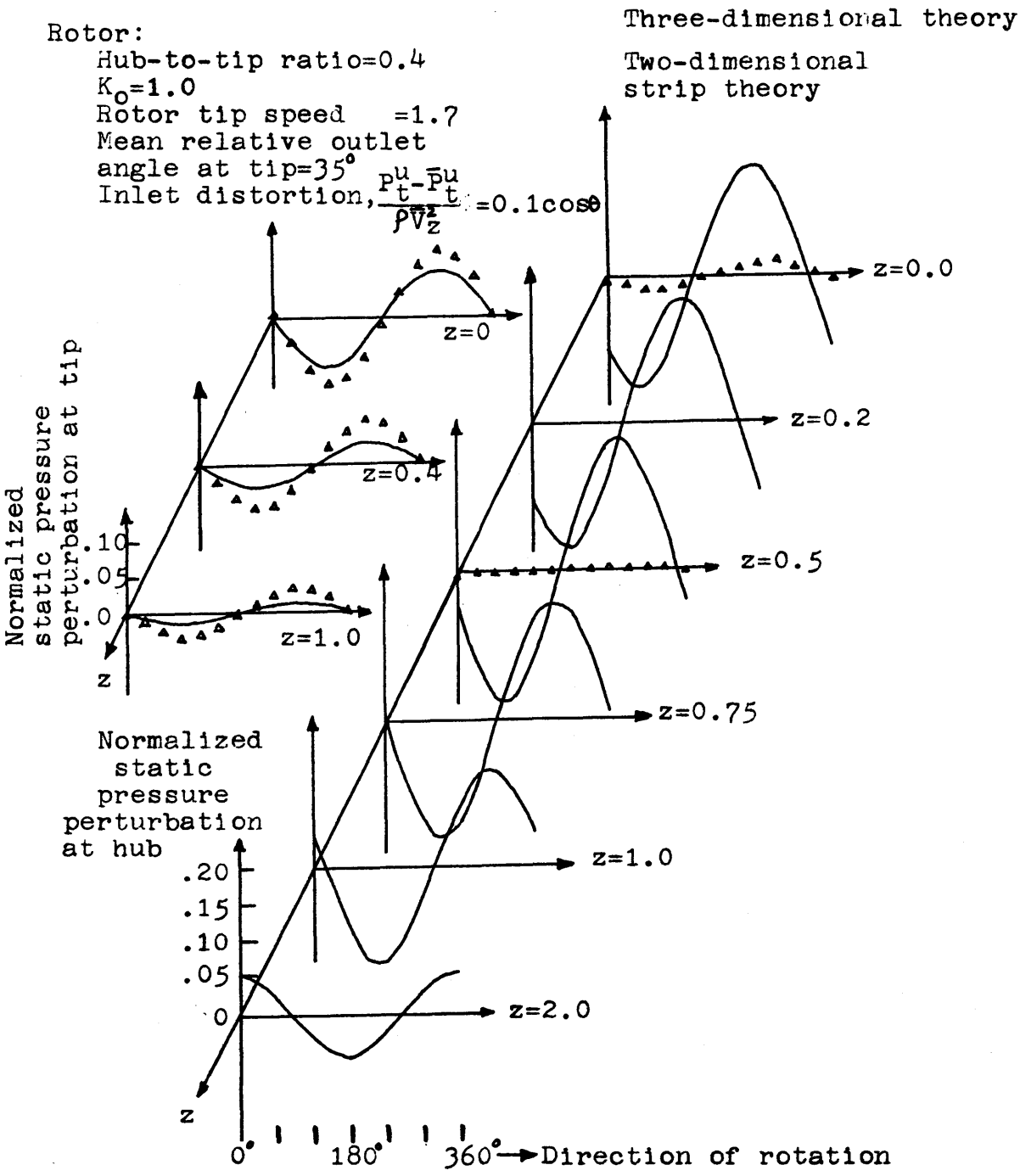

FIG. II.15: TWO-DIMENSIONAL AND THREE-DIMENSIONAL PREDICTIONS OF DOWNSTREAM STATIC PRESSURE DISTRIBUTION COMPARED AT HUB AND TIP.

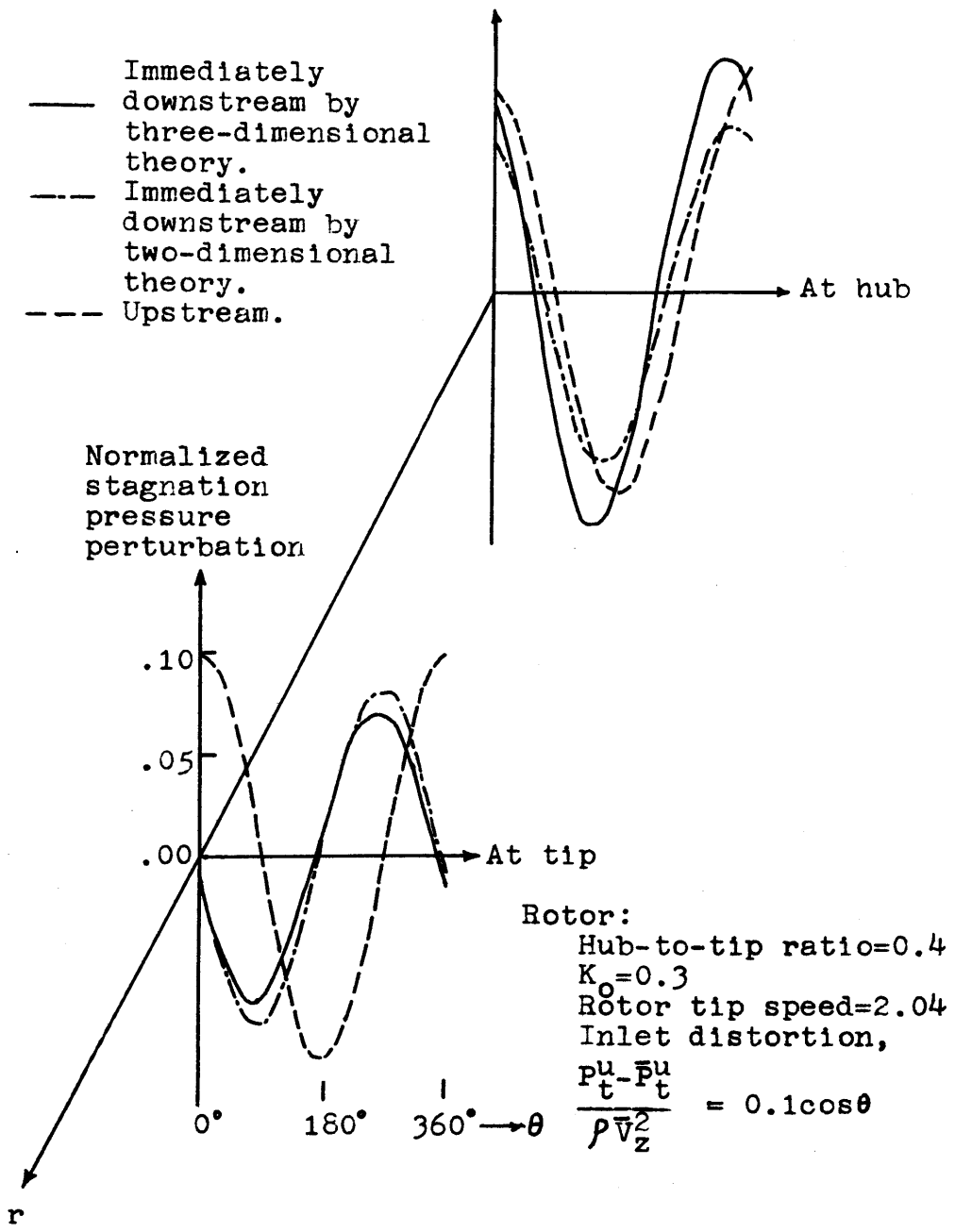

FIG. II.16a: TWO-DIMENSIONAL AND THREE-DIMENSIONAL PREDICTIONS OF STAGNATION PRESSURE PERTURBATION AT DISC, COMPARED AT HUB AND TIP.

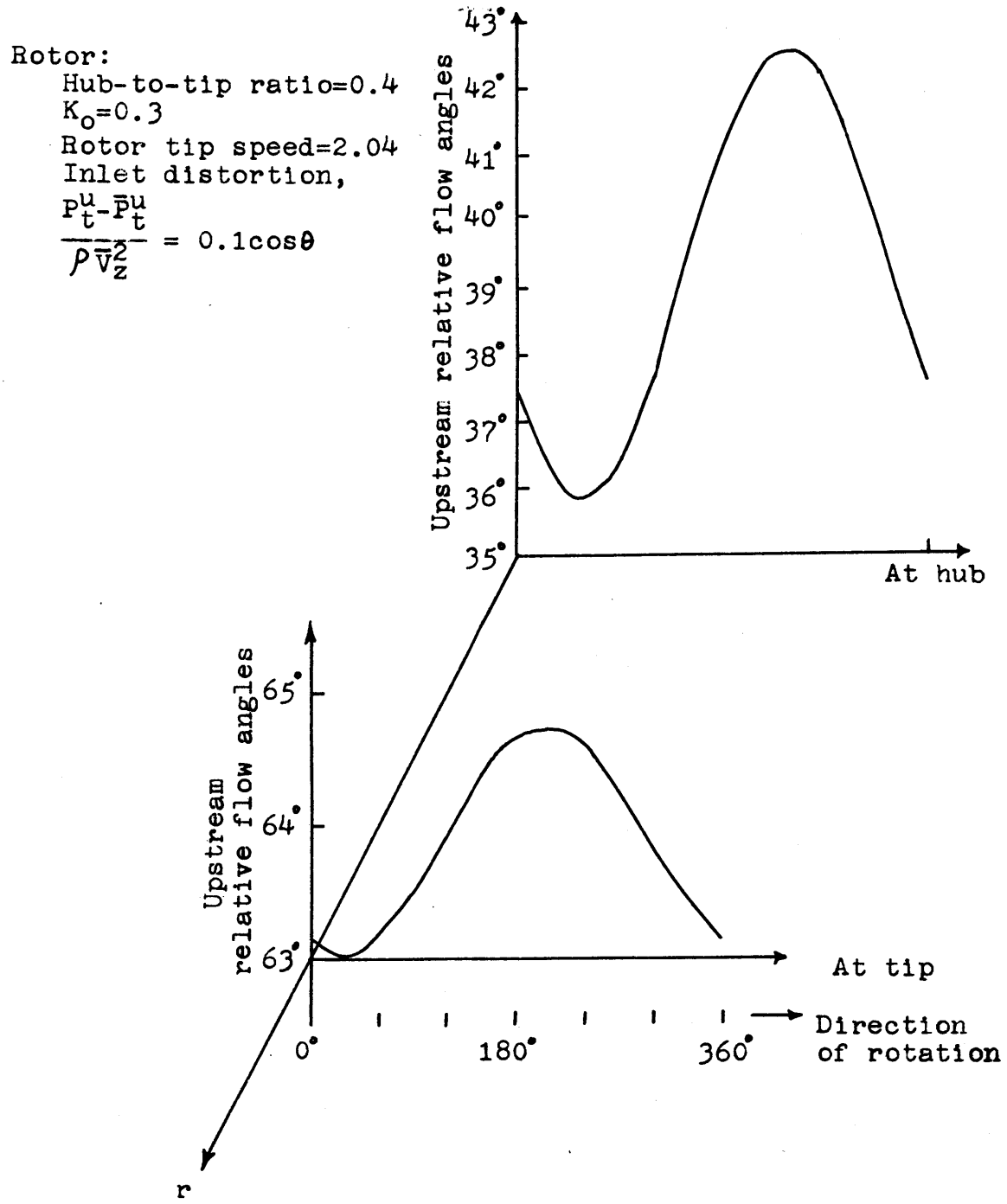

FIG. II.16b: CIRCUMFERENTIAL VARIATION OF UPSTREAM RELATIVE FLOW ANGLES AT DISC.

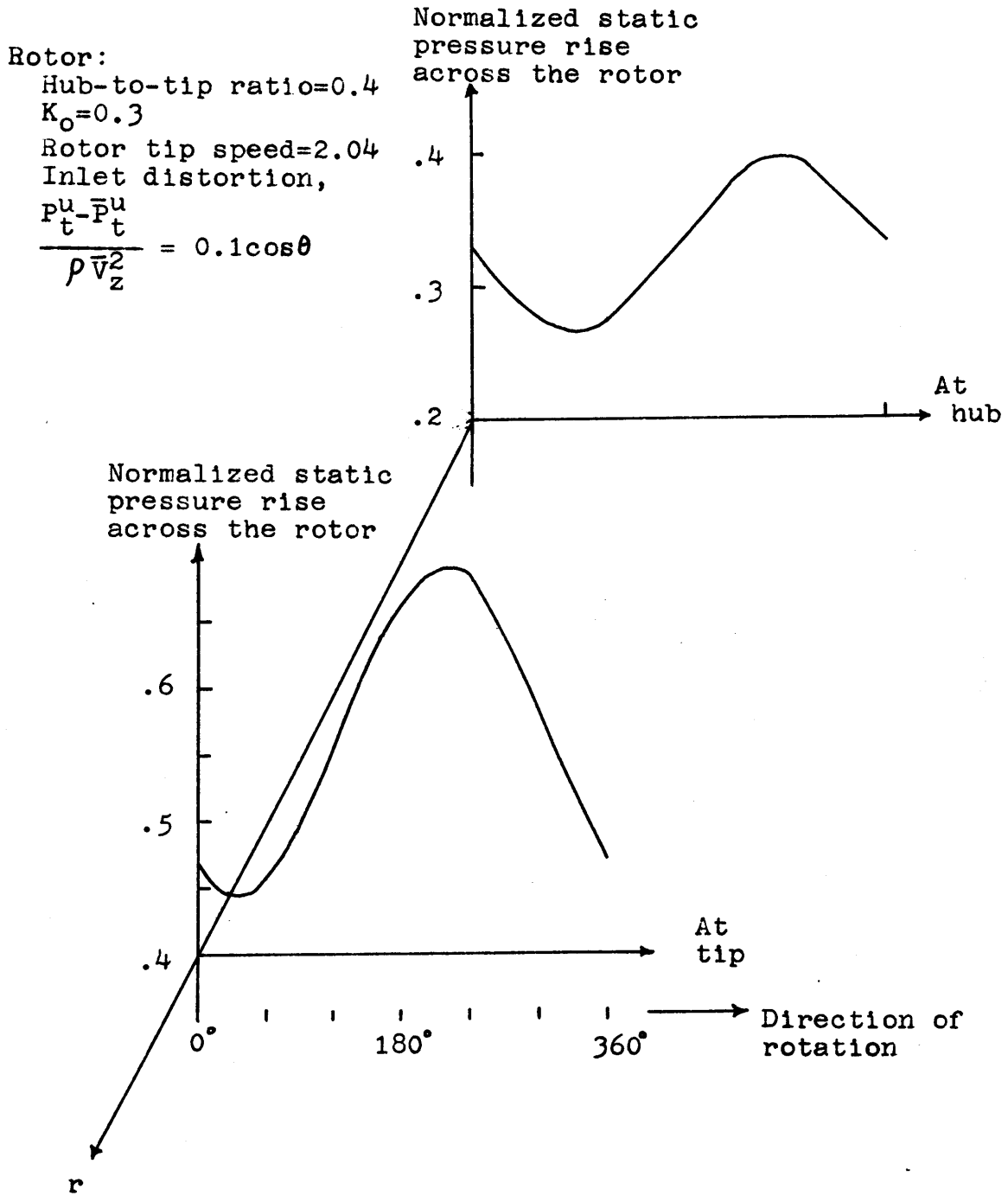

FIG. II.17: CIRCUMFERENTIAL VARIATION OF STATIC PRESSURE RISE ACROSS THE DISC AT THE HUB AND TIP.

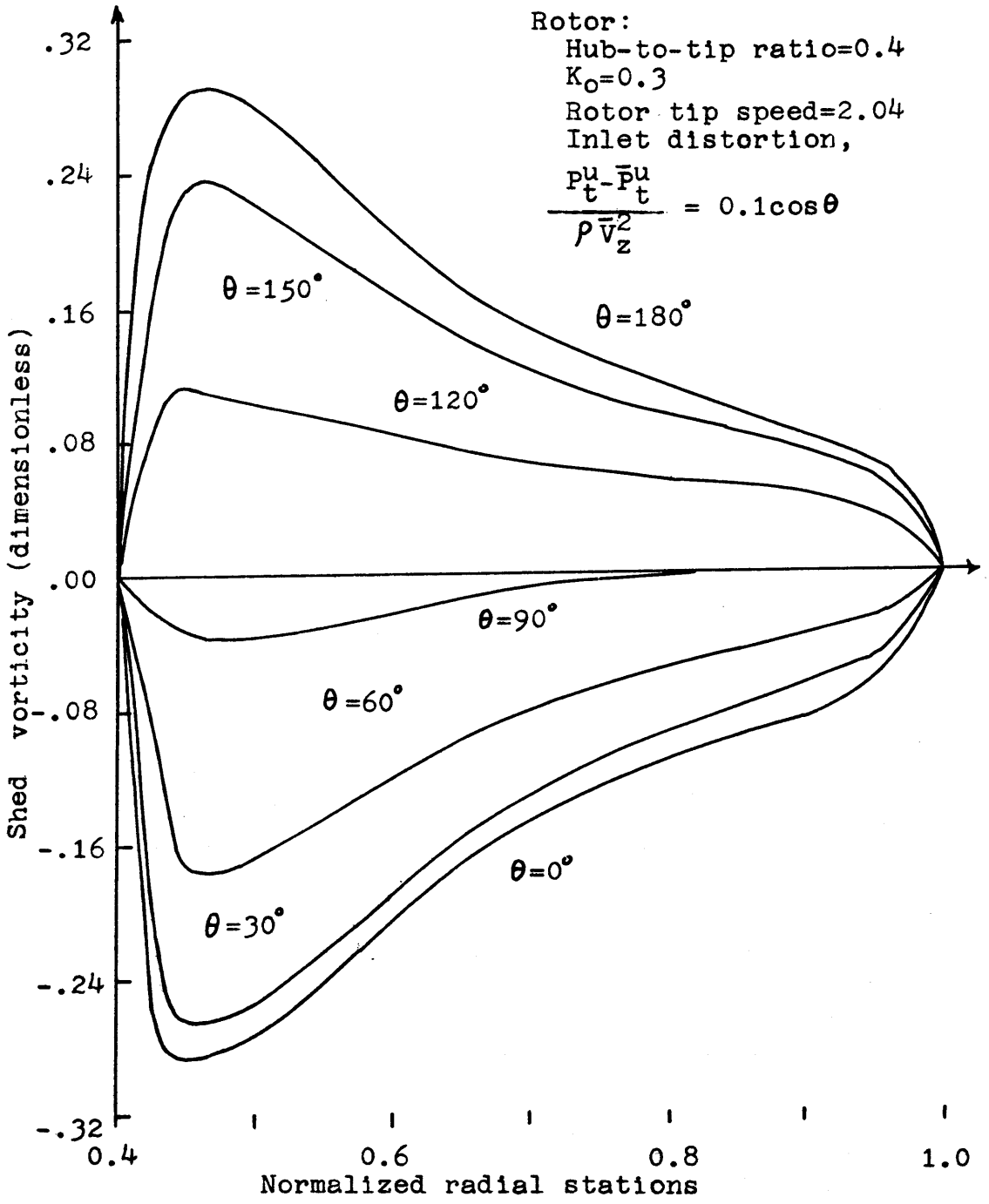

FIG. II.18: RADIAL DISTRIBUTION OF SHED CIRCULATION BEHIND THE ROTOR.

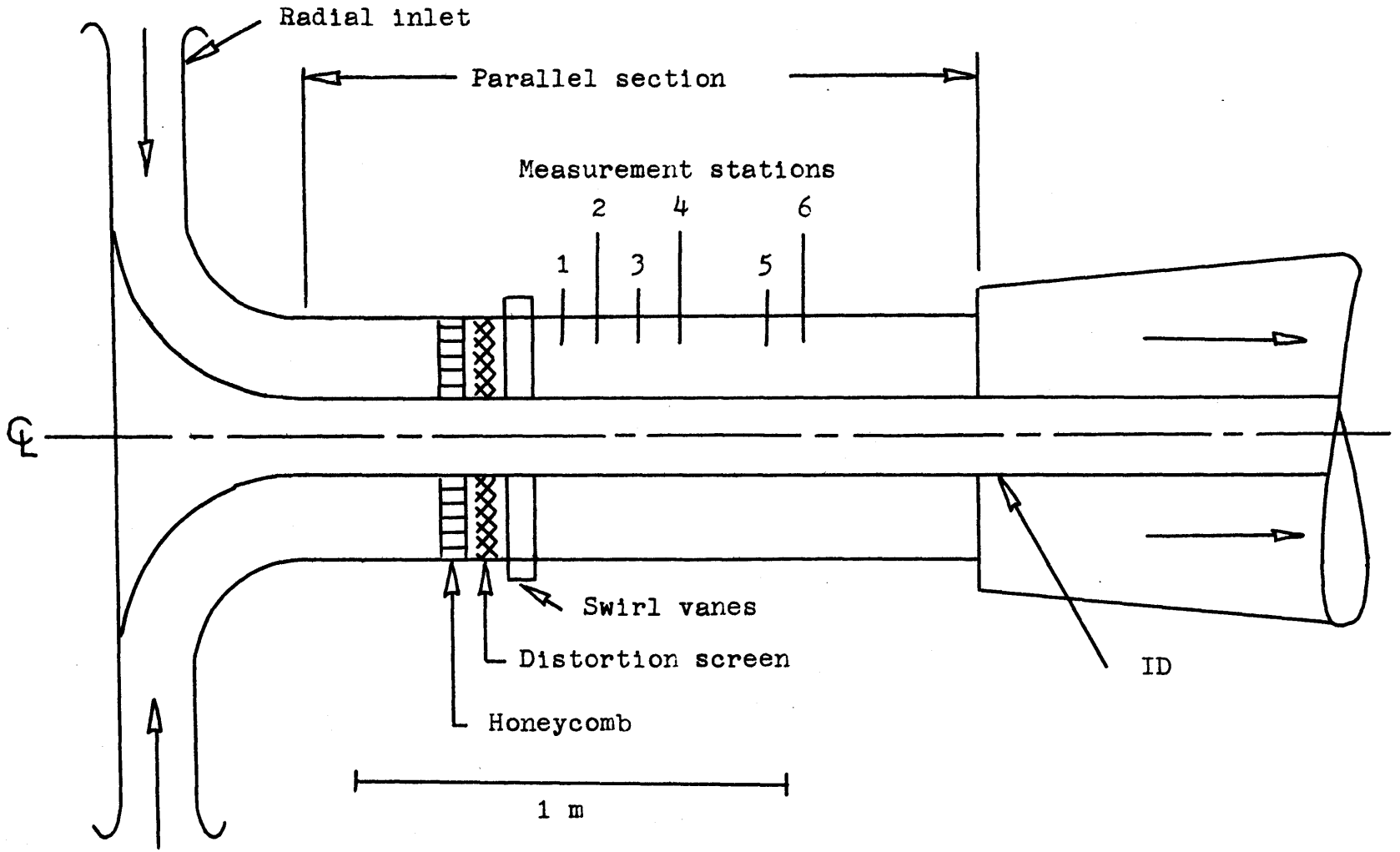

FIG. II.19: SECTION OF SWIRL FLOW RIG.

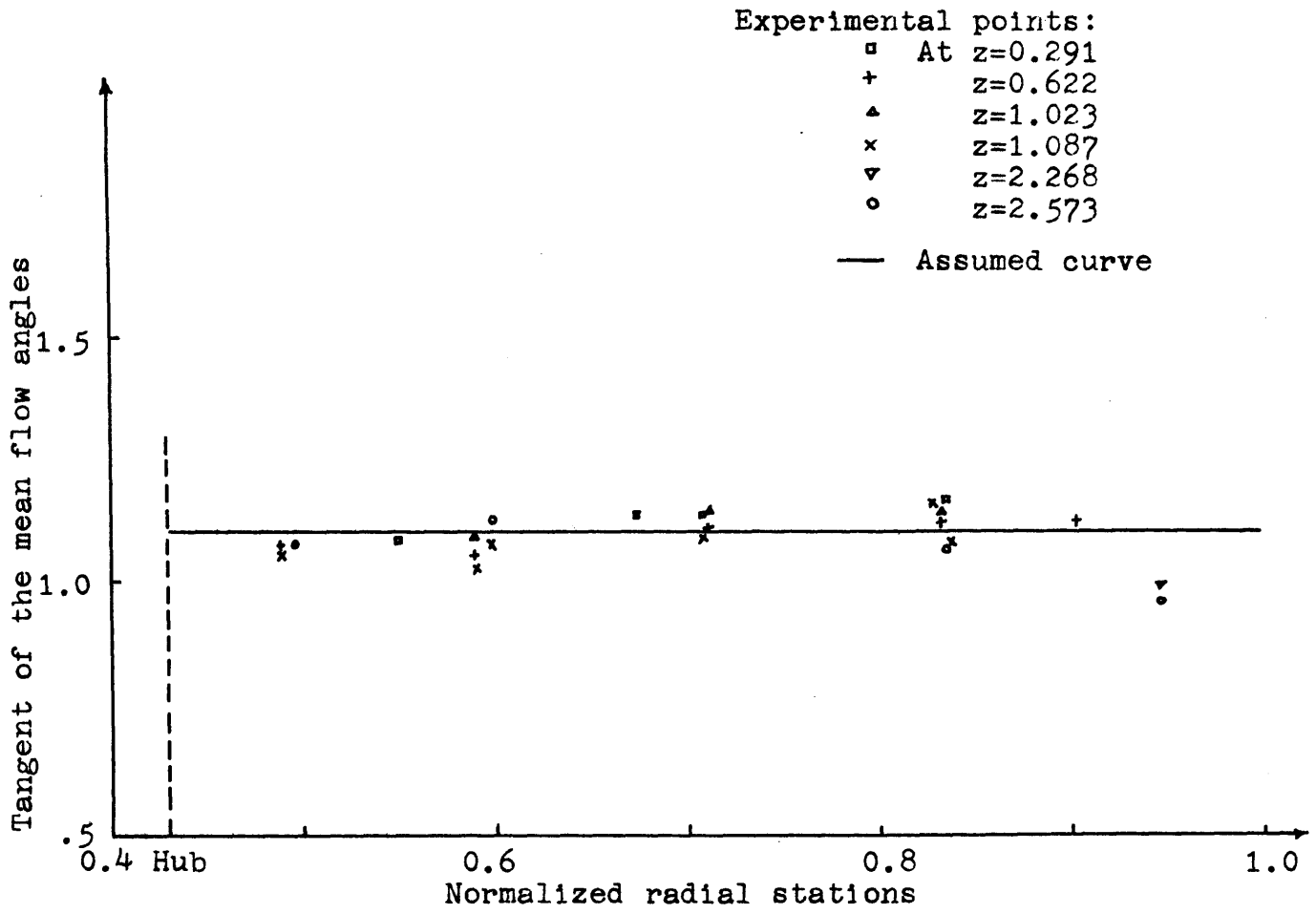

FIG. II.20: RADIAL DISTRIBUTION OF THE MEAN OUTLET FLOW ANGLES(MEASURED).

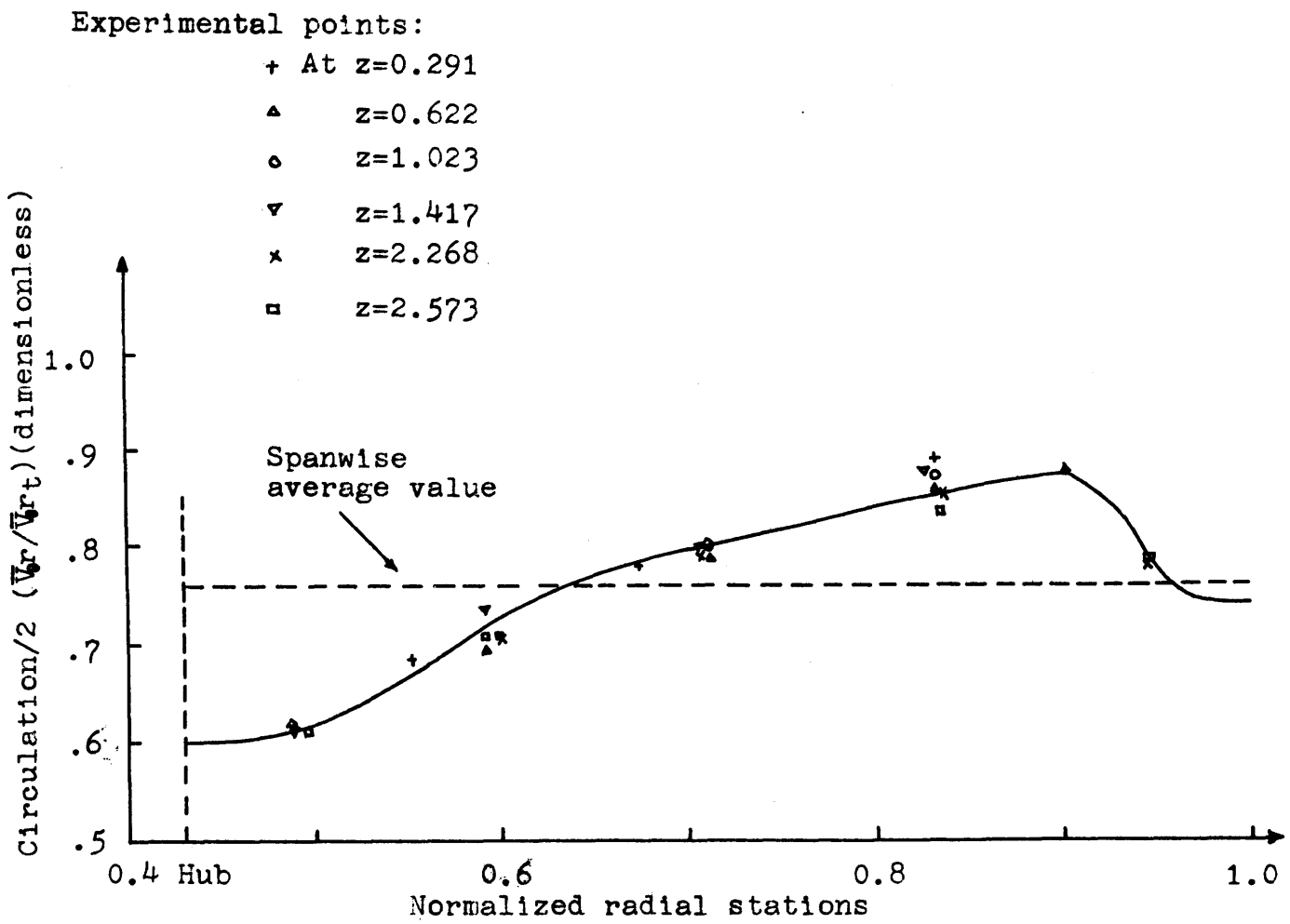

FIG. II.21: RADIAL DISTRIBUTION OF BLADE CIRCULATION AS OBTAINED FROM MEASURED DATA.

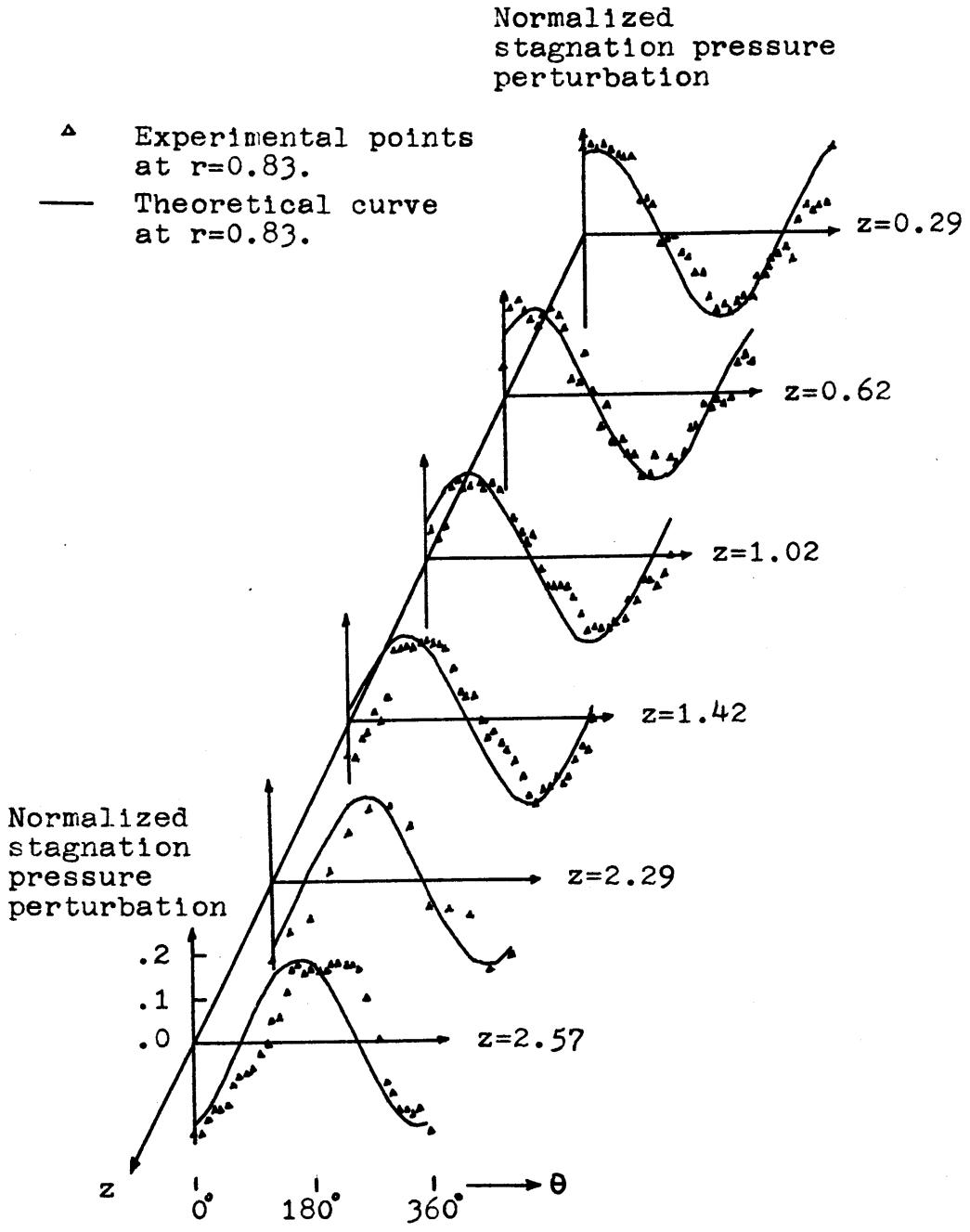

FIG. II.22: DOWNSTREAM CONVECTION OF STAGNATION PRESSURE DISTORTION AT r=0.83.

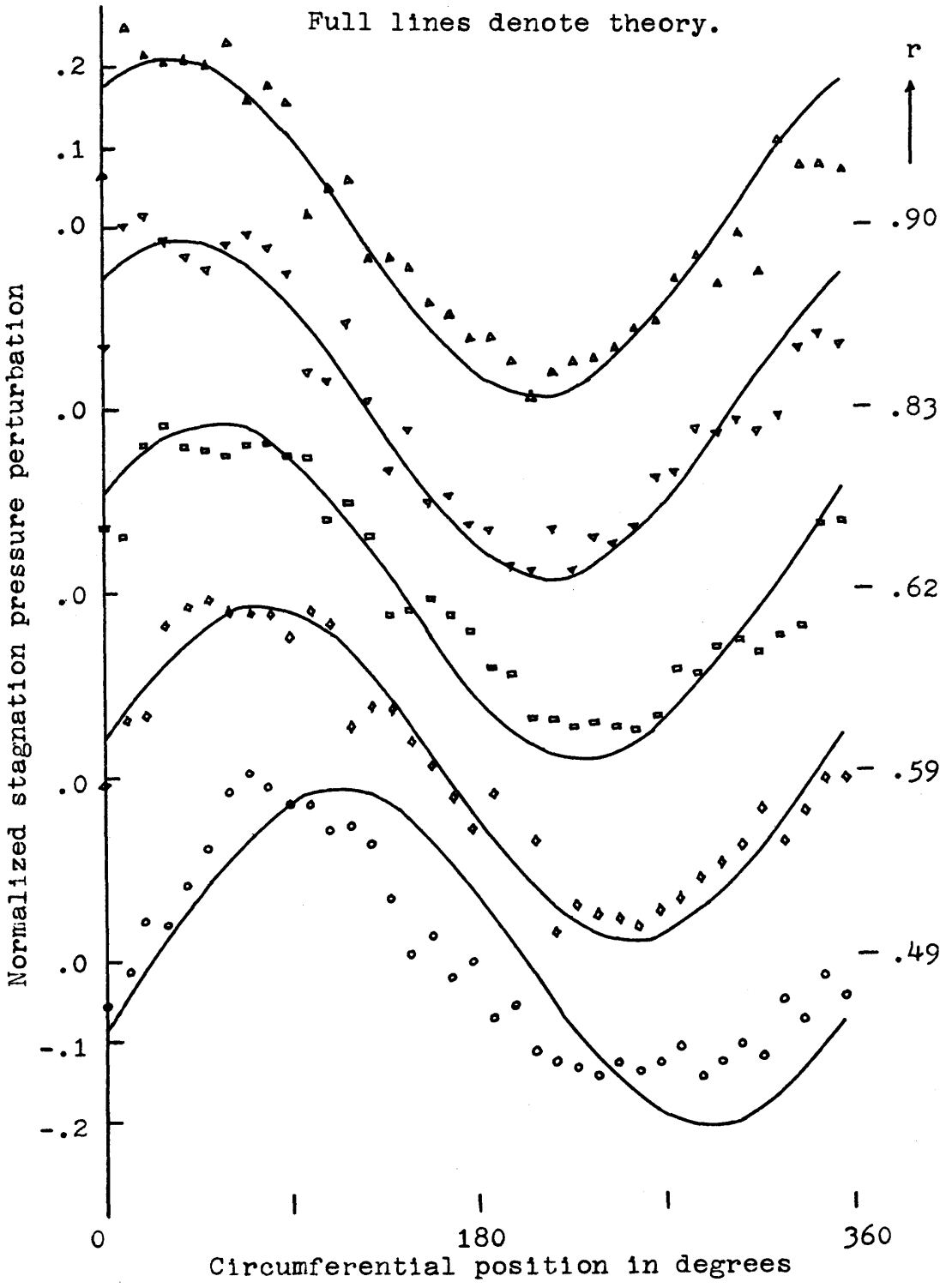

FIG. II.23: STAGNATION PRESSURE DISTRIBUTION AT DIFFERENT RADII FOR Z = 0.62.

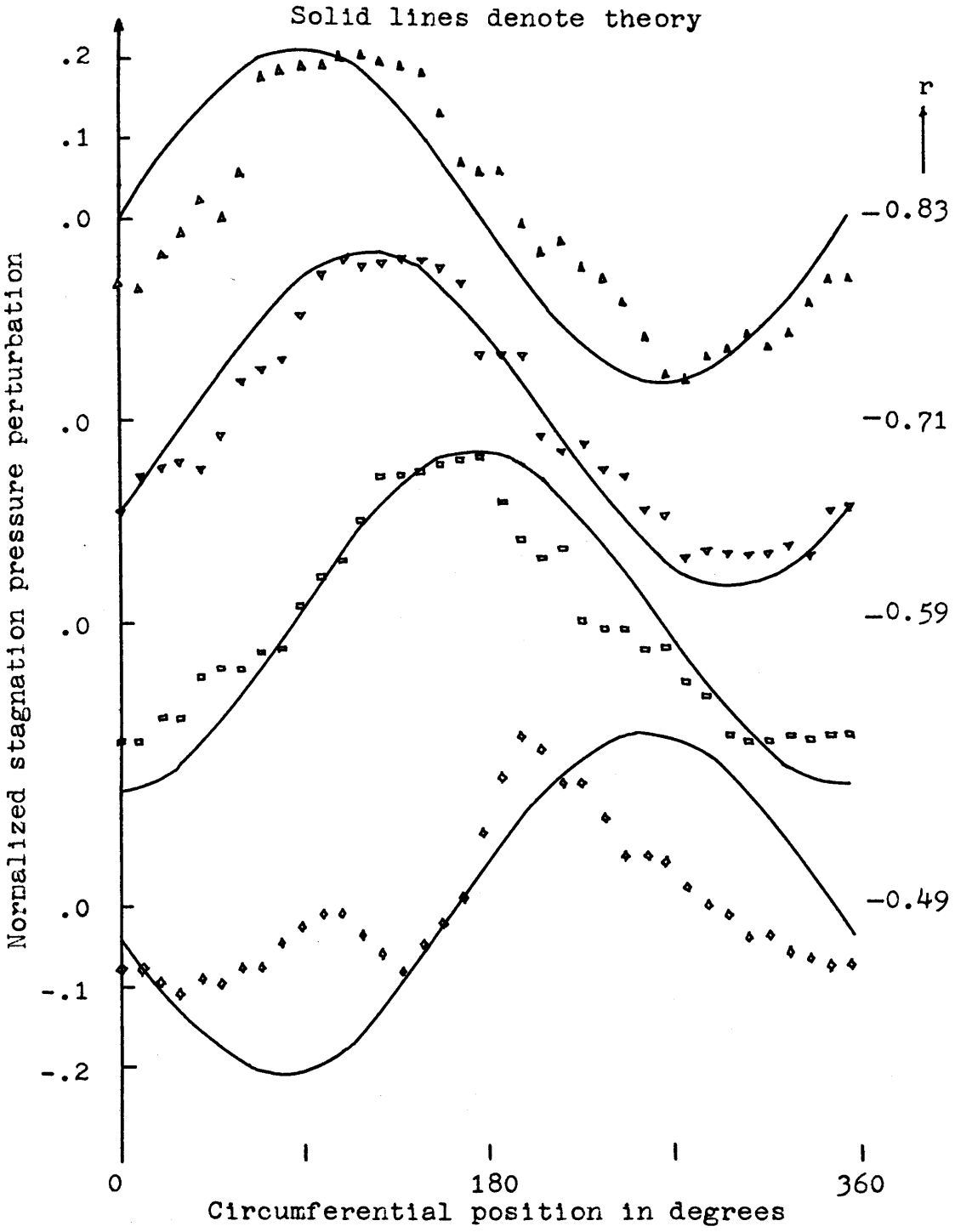

FIG. II.24: STAGNATION PRESSURE DISTRIBUTION AT DIFFERENT RADII FOR Z = 1.42.

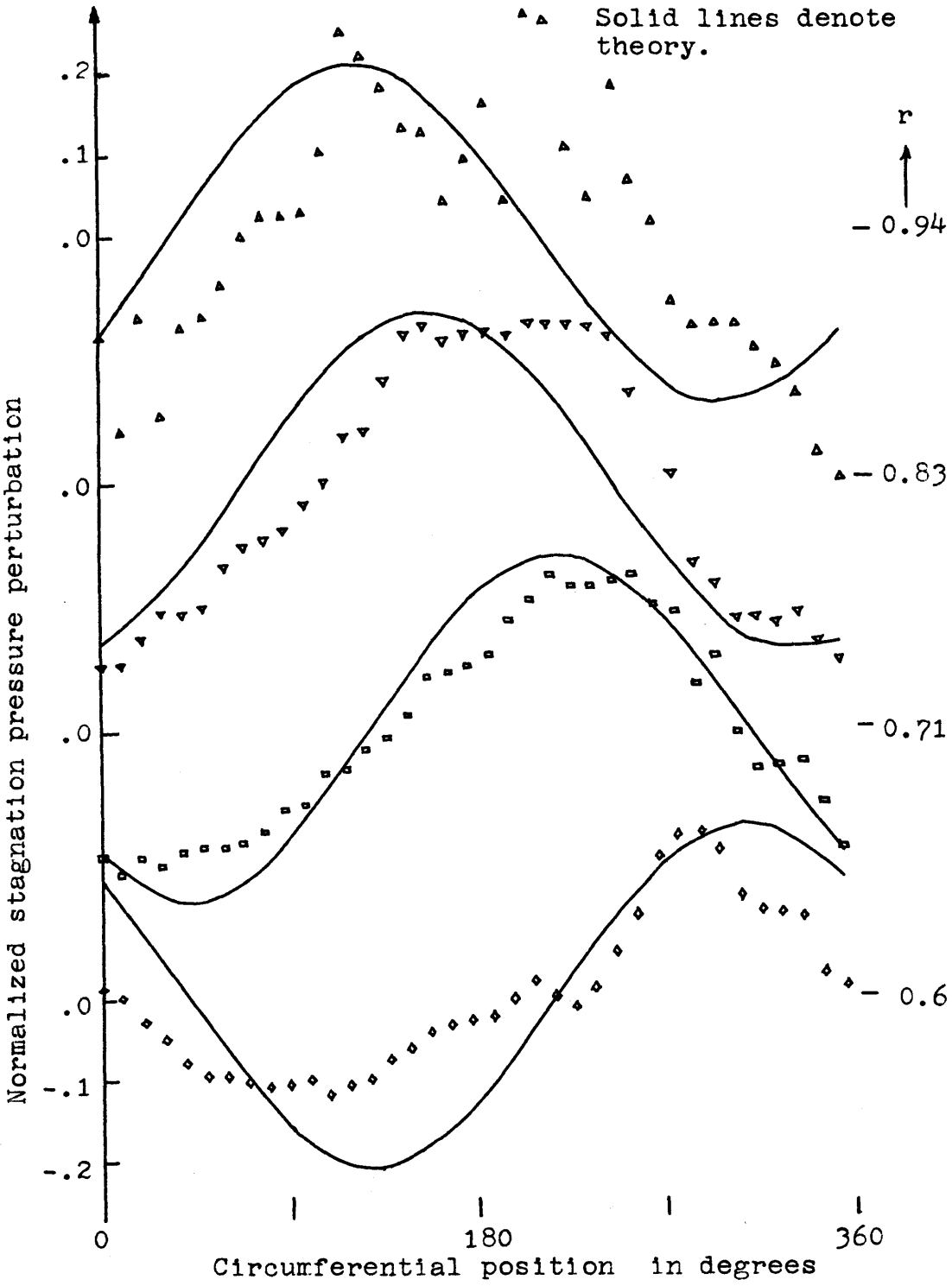

FIG. II.25: STAGNATION PRESSURE DISTRIBUTION AT DIFFERENT RADII FOR Z = 2.57.

Stator:
Hub-to-tip ratio=0.43
Mean outflow angle=48°

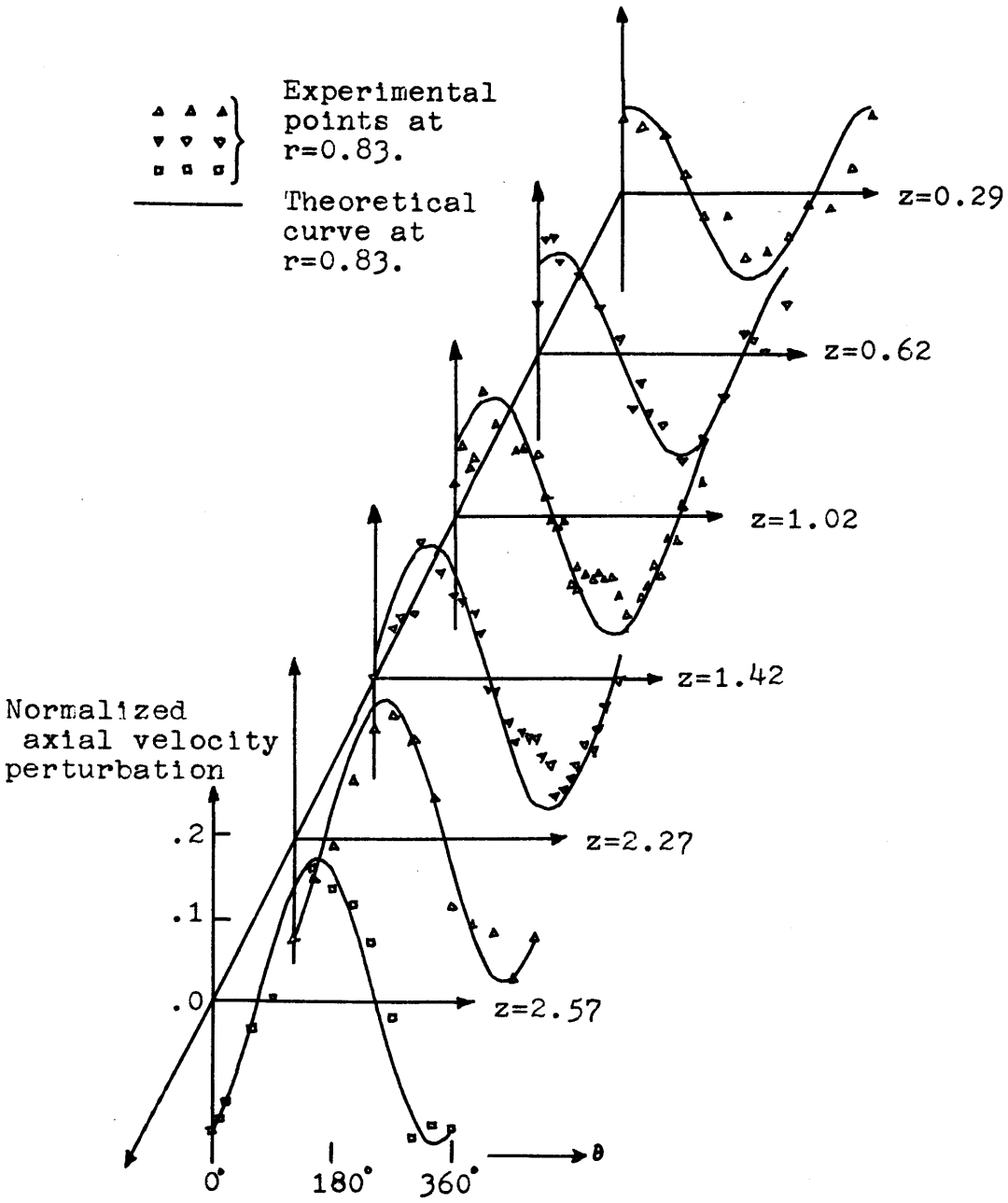

FIG. II.26: AXIAL VELOCITY DISTRIBUTION AT DIFFERENT AXIAL STATIONS FOR RADIUS r=0.83.

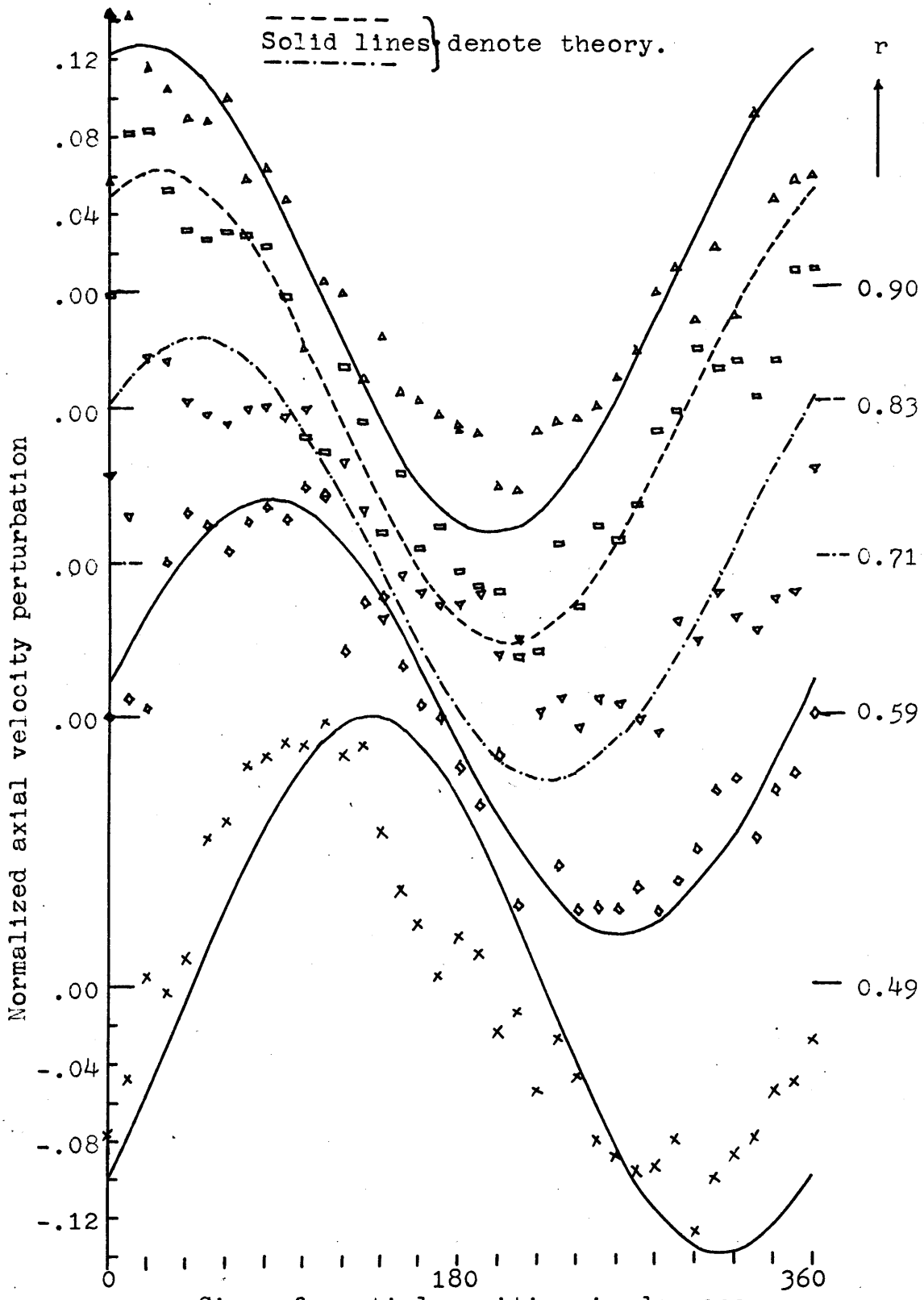

FIG. II.27: AXIAL VELOCITY DISTRIBUTION AT DIFFERENT RADII FOR AXIAL STATION Z = 0.62.

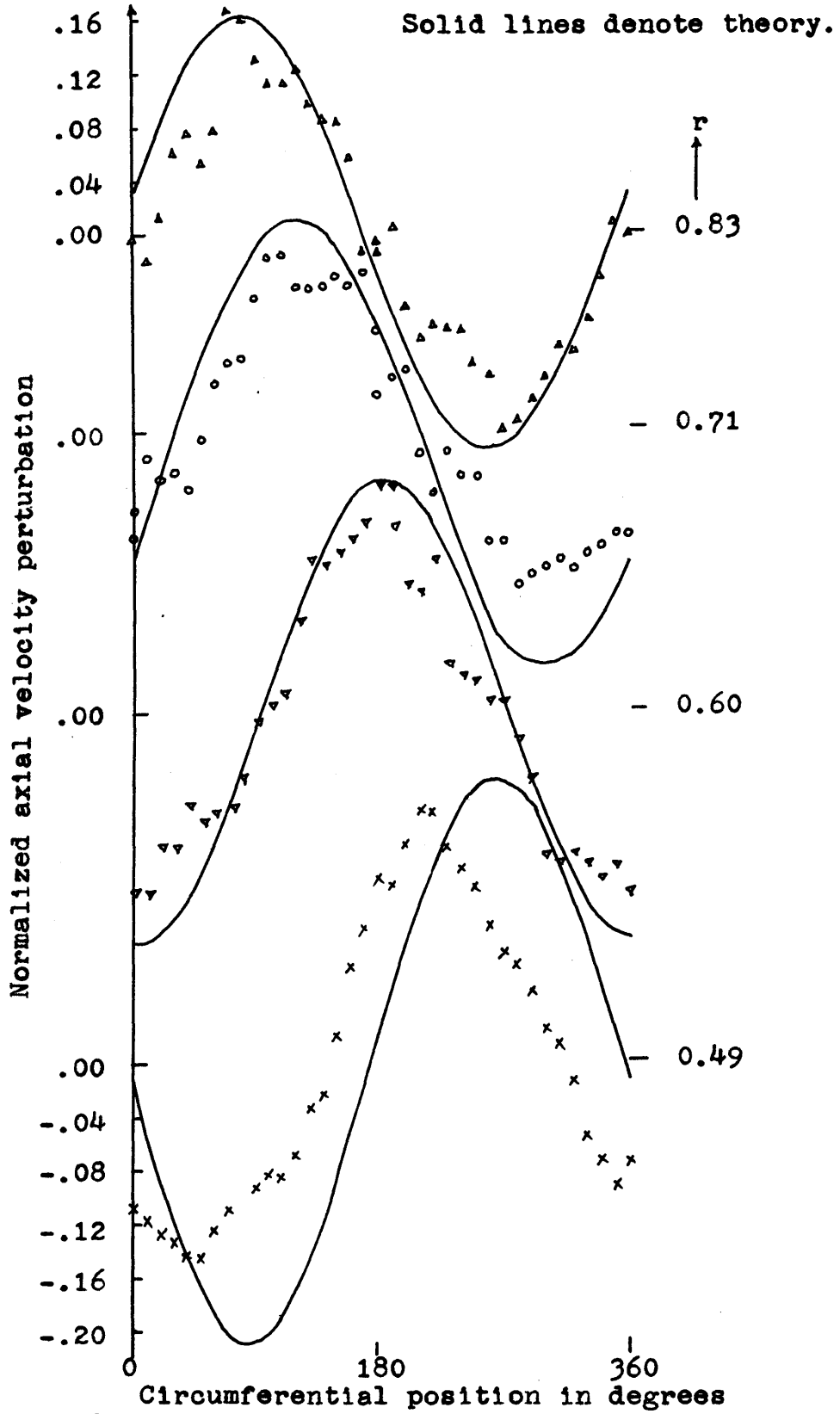

FIG. II.28: AXIAL VELOCITY DISTRIBUTION AT DIFFERENT RADII FOR AXIAL STATION Z = 1.42.

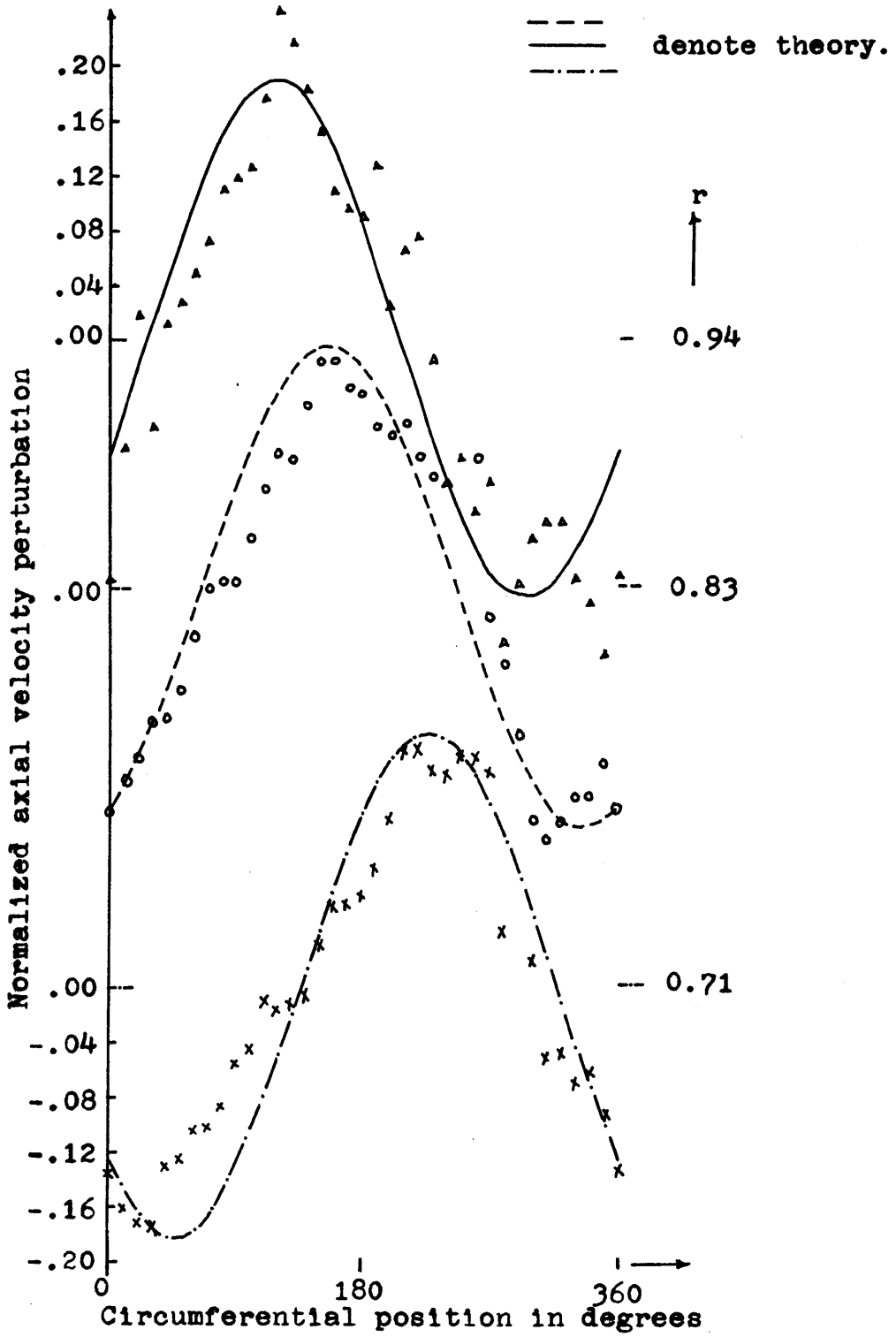

FIG. II.29: AXIAL VELOCITY DISTRIBUTION AT DIFFERENT RADII FOR AXIAL STATION z = 2.57.

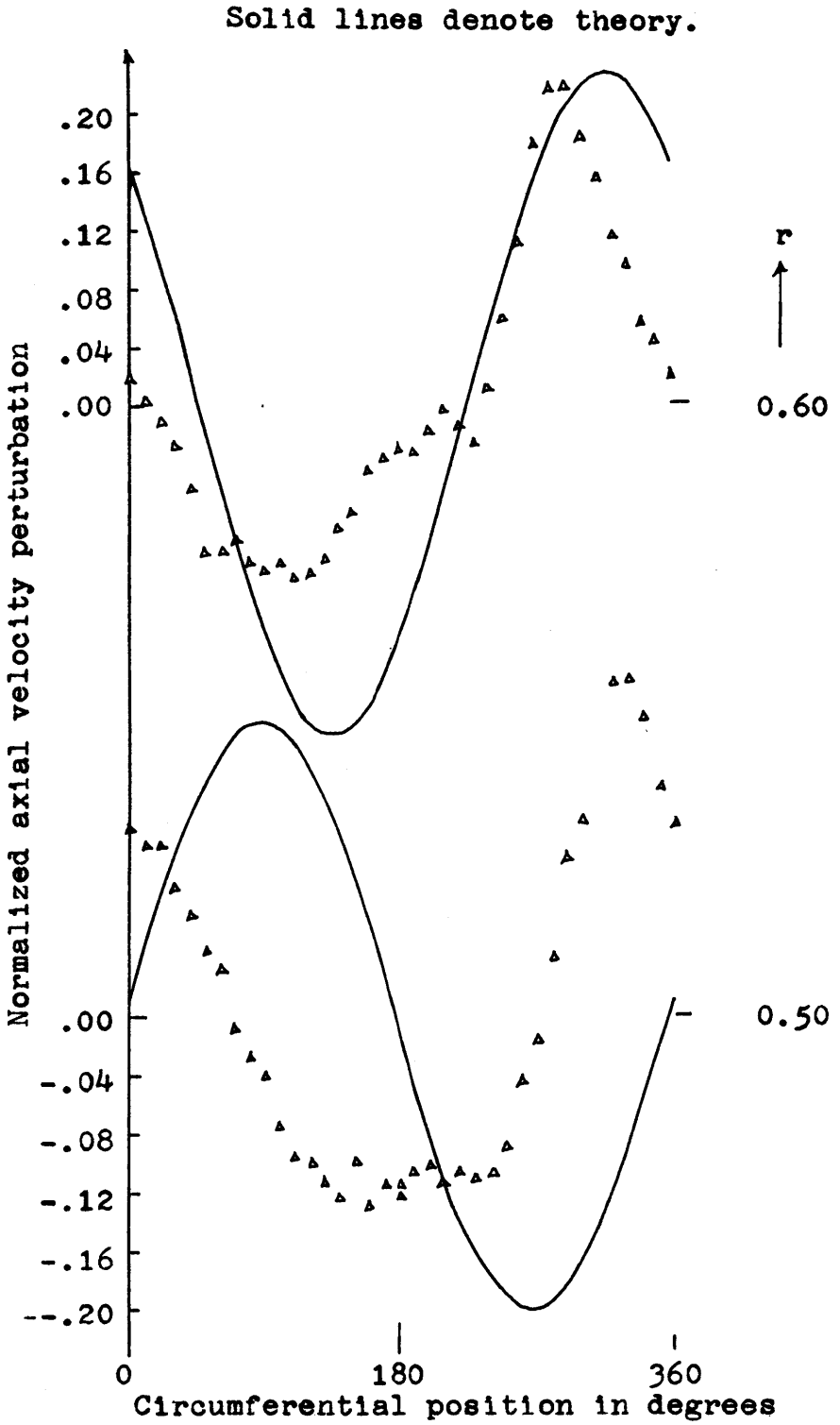

FIG. II.29: AXIAL VELOCITY DISTRIBUTION AT DIFFERENT RADII FOR AXIAL STATION Z = 2.57. (CONTINUATION)

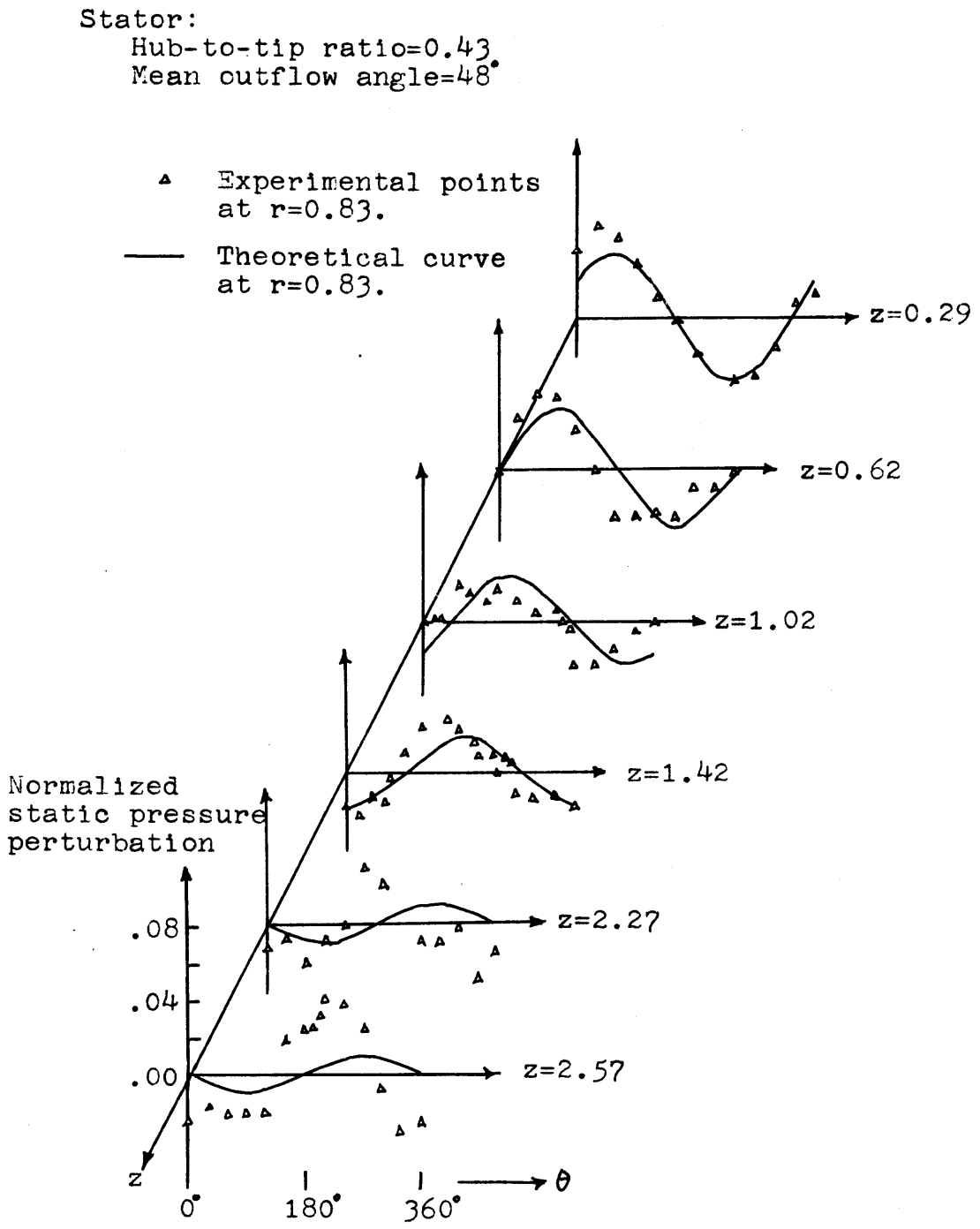

FIG. II.30: COMPARISON OF DOWNSTREAM STATIC PRESSURE PERTURBATIONS AT r=0.83: THEORY VS. EXPERIMENT.

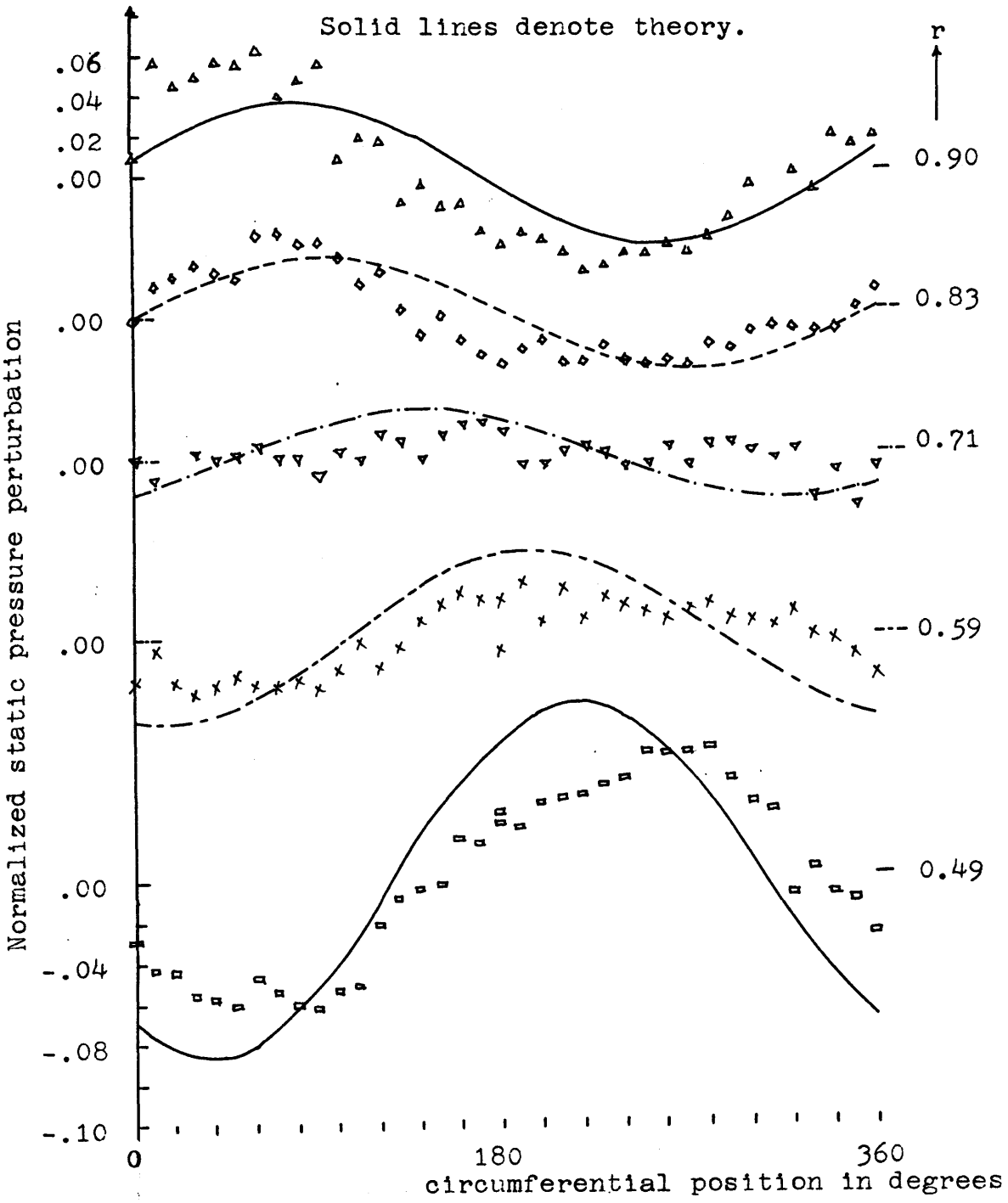

FIG. II.31: STATIC PRESSURE DISTRIBUTION AT DIFFERENT RADII FOR AXIAL STATION Z = 0.62.

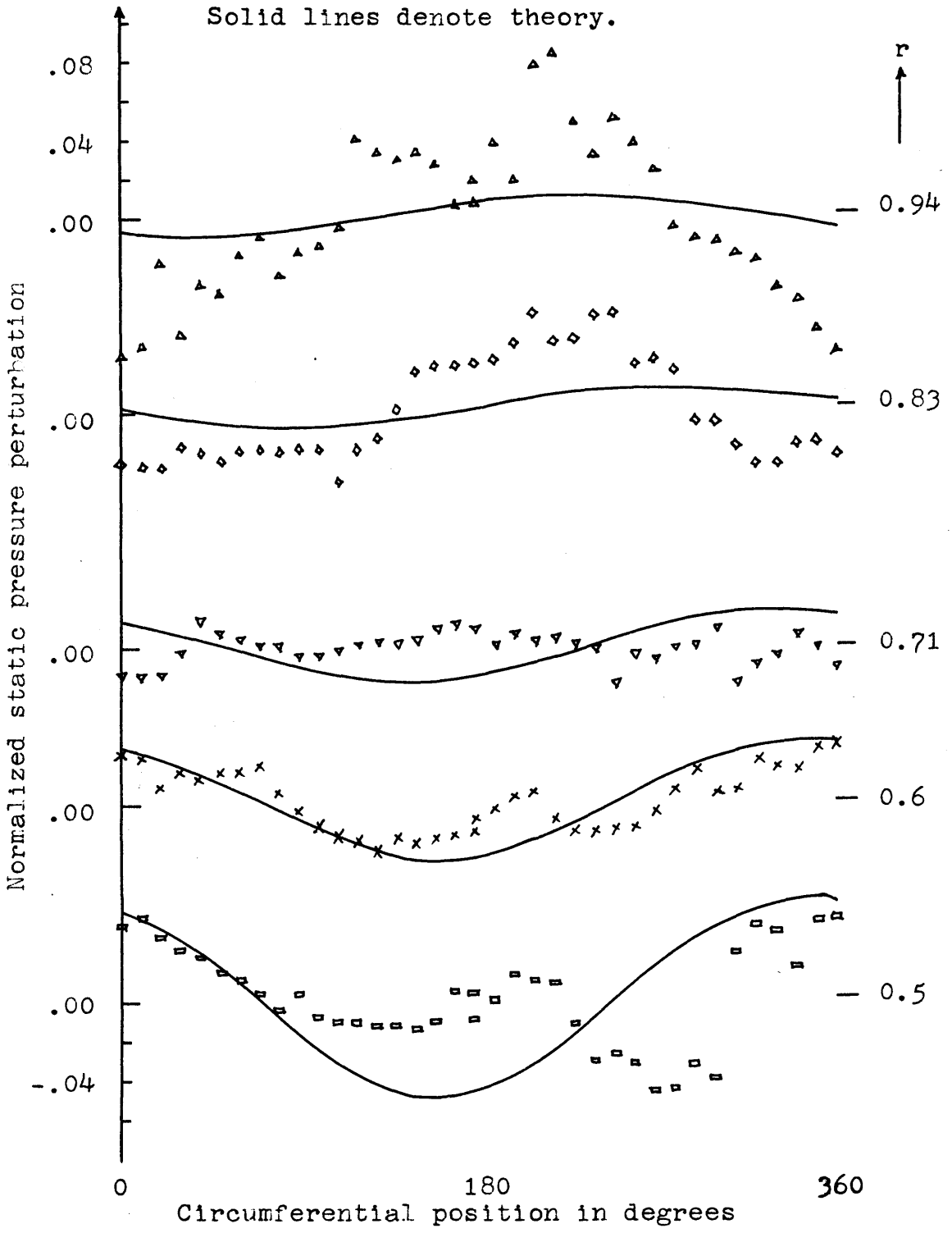

FIG. II.32: STATIC PRESSURE DISTRIBUTION AT DIFFERENT RADII FOR AXIAL STATION Z = 2.57.

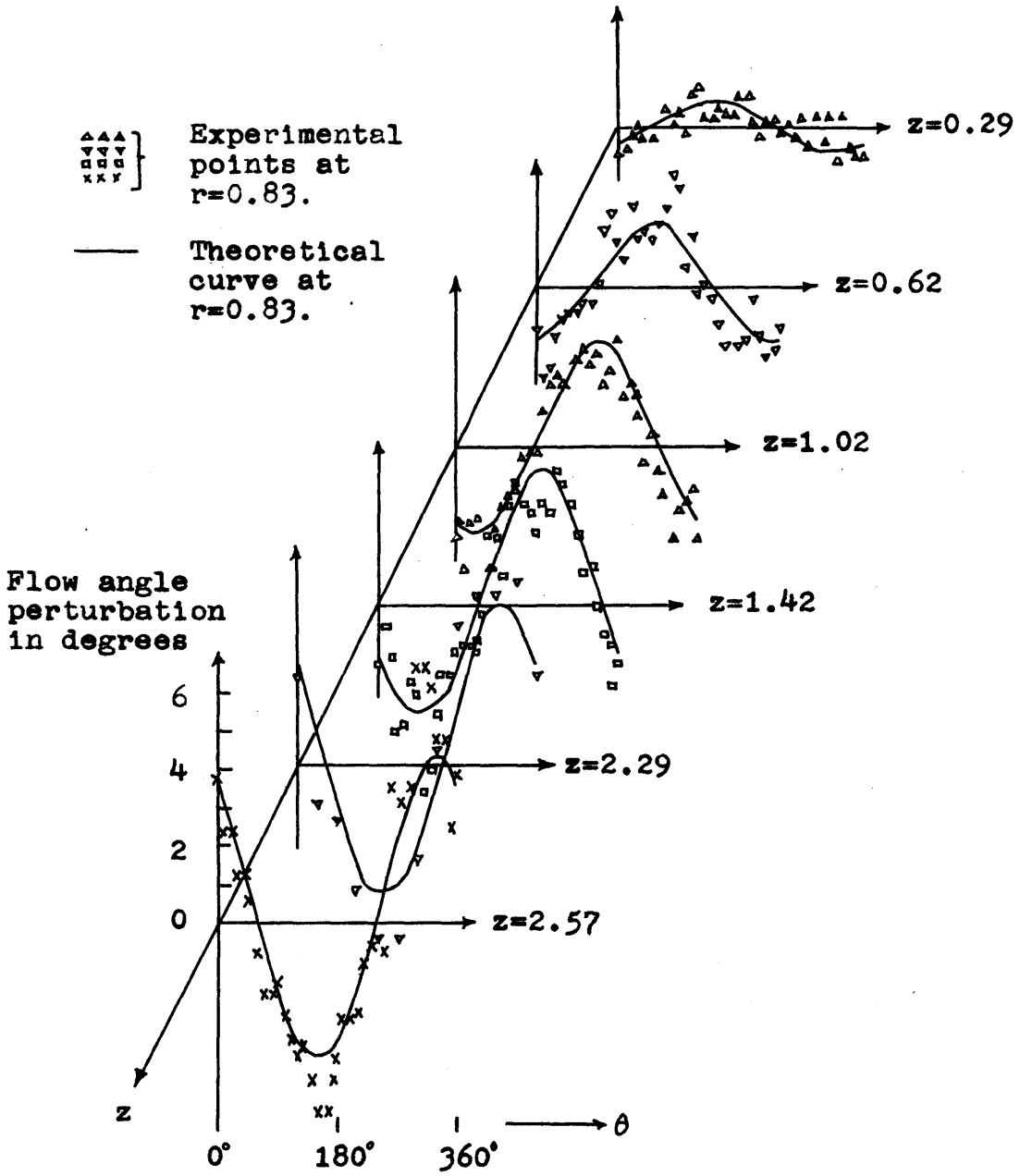

FIG. II.33: COMPARISON OF DOWNSTREAM FLOW ANGLE PERTURBATIONS AT RADIUS r = 0.83: THEORY VS. EXPERIMENT.

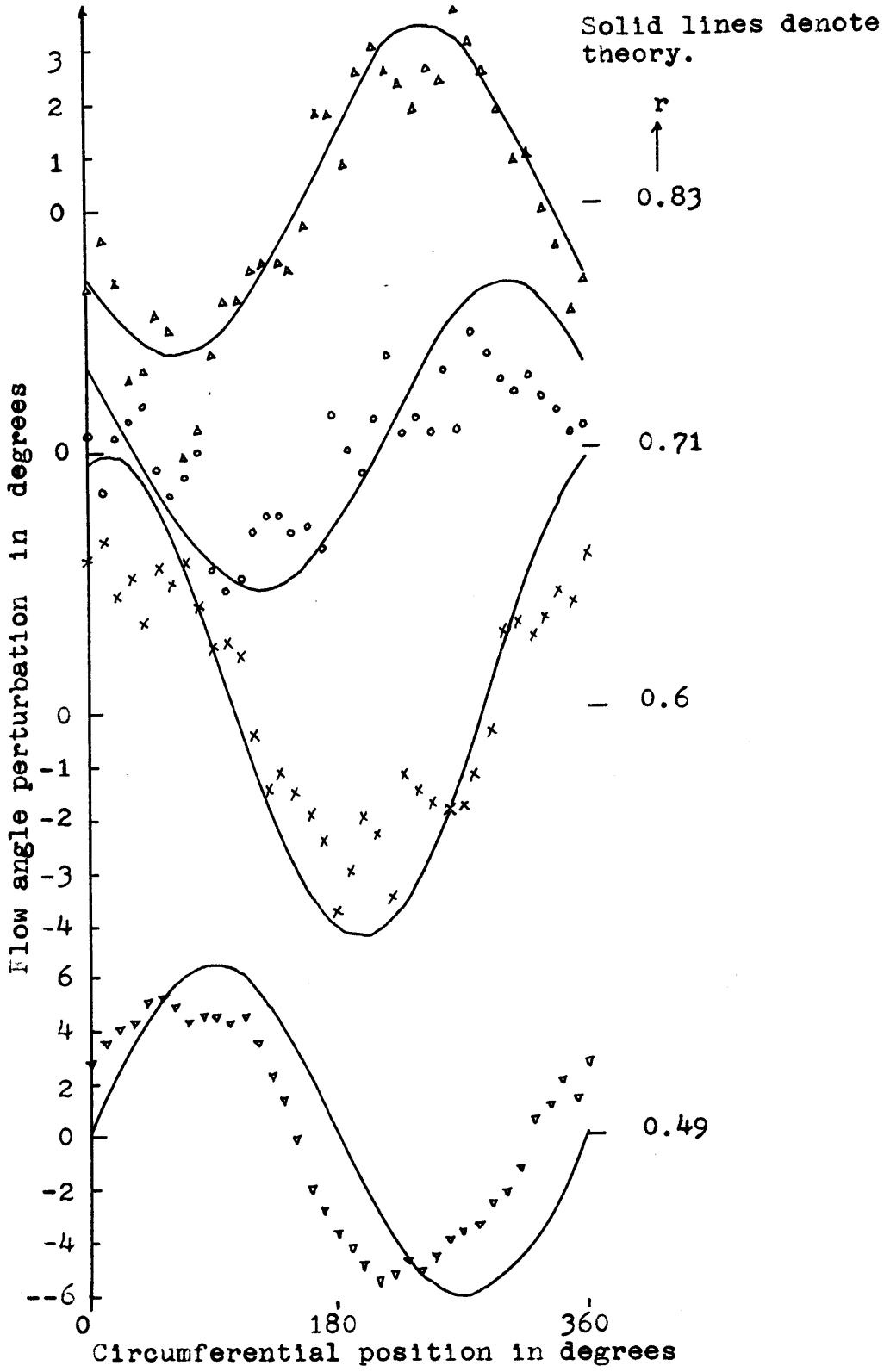

FIG. II.34: FLOW ANGLE DISTRIBUTION AT DIFFERENT RADII FOR AXIAL STATION Z = 1.42.

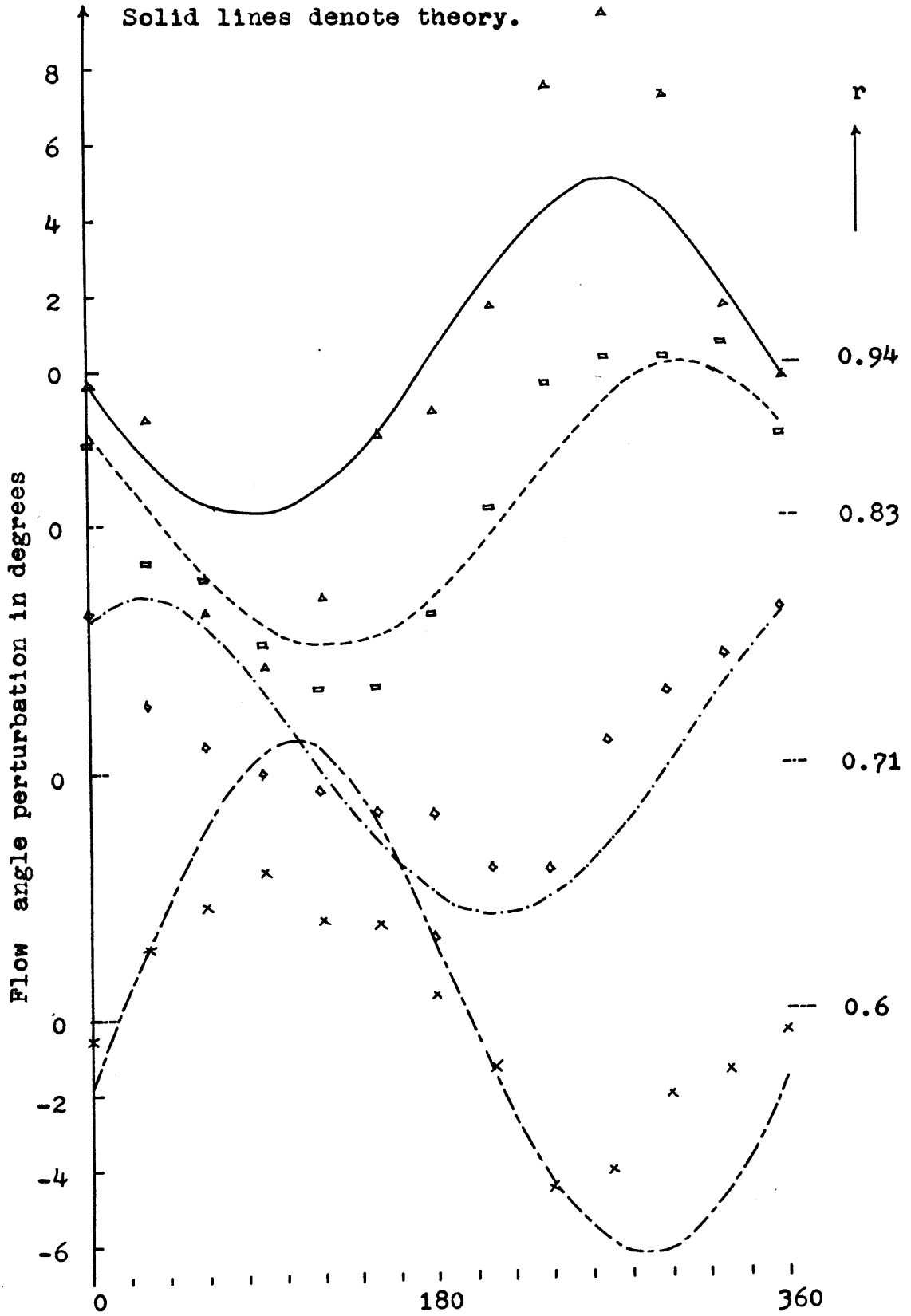

FIG.II.35: FLOW ANGLE DISTRIBUTION AT DIFFERENT RADII(Z=2.27).

REFERENCES

1. Marble, F. E., "Three-Dimensional Flow in Turbomachines," High Speed Aerodynamics and Jet Propulsion, 10, Sec. C, Princeton, 1964.

2. Hawthorne, W.R., "Rotational Flow Through Cascades," Parts I & II, Philosophical Transactions of the Royal Society, June, 1954.

3. Hawthorne, W.R., Novak, R.A., "The Aerodynamics of Turbomachinery," Annual Review of Fluid Mechanics, Vol. 1, 1969.

4. Hawthorne, W.R., "On the Theory of Shear Flow," MIT GTL Report #88, MIT, 1966.

5. Horlock, J.H., and B. Lakshminarayana, "Secondary Flow," Annual Review of Fluid Mechanics, 5, 247, 1973.

6. Wu, C.H., "A General Theory of Three-Dimensional Flow in Subsonic and Supersonic Turbomachines of Axial, Radial and Mixed Flow Types," NACA TN 2604, 1952.

7. McCune, J.E., "A Three-Dimensional Theory of Axial Compressor Blade Rows--Application in Subsonic and Supersonic Flows," J. of Aerospace Sci., 25, 9, Sept. 1958.

8. McCune, J.E., "The Transonic Fluid of an Axial Compressor Blade Row," J. of Aerospace Sci, 25, 10, Oct. 1958.

9. Davidson, R.E., "Linearized Potential Theory of Propeller Induction In A Compressible Flow," NACA TN 2983, 1953.

10. Okuroumu, O., and McCune, J.E., "Three-Dimensional Vortex Theory of Axial Compressor Blade Rows at Subsonic and Transonic Speeds," AIAA J., 8, 7, July 1970.

11. Okuroumu, O., and McCune, J.E., "The Lifting Surface Theory of Axial Compressor Blade Rows, Part I - Subsonic Compressor," AIAA J., 12, 10, 1974.

12. Okuroumu, O., and McCune, J.E., "The Lifting Surface Theory of Axial Compressor Blade Rows, Part II - Transonic Compressor," AIAA J., 12,10 1974.

13. McCune, J.E., and Dharwadkar, S.P., "Lifting Line Theory for Subsonic Axial Compressor Rotors," MIT GTL Report #110, 1972.

14. Falc̃ao, A.F., "Three-Dimensional Flow Analysis in Axial Turbomachines," Ph.D. Thesis, Cambridge, University, 1970.

15. Namba, M., "Lifting Surface Theory ofr a Rotating Subsonic or Transonic Blade Row," ARC R&M, #3740, 1974.

16. McCune, J.E., and Hawthorne, W.R., "The Effects of Trailing Vorticity on the Flow Through Highly-Loaded Cascades," J. of Fluid Mech., 74, Part 4, April 1976.

17. Morton, K.B., "Three-Dimensional Compressible Flow Through Highly Loaded Rectilinear Cascasdes," S.M. Thesis, Dept. of Aero & Astro, 1974.

18. Cheng, W.K., "A Three-Dimensional Theory of the Velocity Induced by a Heavily-Loaded Annular Cascade of Blades," M.S.Thesis, Dept. of Aero & Astro, MIT, June 1975.

19. Adebayo, A.O. and McCune, J.E., "Three-Dimensional Beltrami Flow in Turbomachinery with Strong Arbitrary Swirl," MIT GTL Report #132, 1977.

20. Cheng, W.K., "Uniform Inlet Three-Dimensional Transonic Beltrami Flow Through a Ducted Fan," MIT GTL Report #130, 1977.

21. Kerrebrock, J.L., "Small Disturbances in Turbomachine Annuli With Swirl," GTL Report #125, MIT, 1975. Also AIAA J, 15, 6, June 1977.

22. Lamb, H., "Hydrodynamics," Sixth Ed., Cambridge, Univ. Press, 1932.

23. Darwin, C., "Note on Hydrodynamics," Proc. Cambridge Phil. Soc., 49 342-254, 1953.

24. Lighthill, M.J., "Drift," J. Fluid Mech., 1, 31-53 (1956); note also "Corregenda to Drift", J. Fluid. Mech., 2, 311-2 (1957).

25. Hawthorne, W.R., "Engineering Aspects," Chapter 1, Research Frontiers in Fluid Dynamics, R.T. Seeger and G. Temple Eds., Interscience, NY, 1965.

26. McCune, J.E., "Three-Dimensional Flow in Highly-Loaded Axial Turbomachines," M.S. No. 56180(22S2), ZAMP, Nov. 1977.

27. Johnson, I., and Bullock, R., Eds., "Aerodynamic Design of Axial Flow Compressors," NASA SP-36, NASA 1965.

28. Sears, W.R., "Some Recent Developments in Airfoil Theory," J. of Aero. Sci., 23, 5, May 1956.

29. McCune, J.E., "Three-Dimensional Inviscid Flow Through a Highly-Loaded Transonic Compressor Rotor," Proc. Workshop of Transonic Flow Through Turbomachinery, T.C. Adamson, Ed., 1977.

30. Munk, M., and Prin, R.C., "On the Multiplicity of Steady Gas Flows Having the Same Streamline Pattern," Proc. Nat. Acad. Sci., U.S., 33, 5, 1947.

31. Nemenyi and R. Prim, "Some Geometric Properties of Plane Gas Flow,"

J. of Math. & Phys., 27, 1948.

32. Yih, C.S., "Dynamics of Non-Homogeneous Fluids," Macmillan, NY, 1965.

33. Hawthorne, W.R., Ringrose, J., "Actuator Disc Theory of the Compressible Flow in Free Vortex Turbomachinery," Proc. Inst. Mech. Engrs. Feb. 1963.

34. Chen, L.T., and McCune, J.E., "Comparison of Three-Dimensional Quasi-Linear Large Swirl Theory with Measured Outflow from a High Work Compressor Rotor," MIT GTL Report #128.

35. Epstein, A.H., "Quantitative Density Visualization in a Transonic Compressor Rotor," Ph.D. Thesis, MIT, Sept. 1975.

36. Thompkins, Jr., W.T., "An Experimental and Computational Study of the Flow in a Transonic Compressor Rotor," Ph.D. Thesis, MIT June 1976.

37. Bellman, D.R., & D.L. Hughes, "The Flight Investigation of Pressure Phenomena in the Air Intake of an F-11A Airplane, AIAA Paper 69-488, presented at the Fifth Propulsion Joint Specialist Conf. Colorado, 9-13 June, 1969.

38. Burcham,F.W., Jr., and D.R. Bellman, "A Flight Investigation of Steady State and Dynamic Pressure Phenomena in the Air Inlets of Supersonic Aircrafts," Paper #24, AGARD, Propulsion and Energetics Panel 38th Meeting, Sandefjord, Norway, Sept. 1971.

39. Valentine, H.H., and W.T. Beale, "Experimental Investigation of Distortion Removal Characteristics of Several Free Wheeling Fans," NACA RM 57 112, 1958.

40. Walker, C.L., J.N. Sivo, and E.T. Jansen, "Effect of Unequal Airflow Distribution From Twin Inlet Ducts on Performance of an Axial-Flow Turbojet Engine," NACA RM E54E13, 1954.

41. Wenzel, L.M., Experimental Investigation of the Effects of Pulse Pressure Distortions Imposed on the Inlet of a Turbofan Engine," NASA TMX-1928, Nov. 1969.

42. Wallner, L.E., Conrad, E.W., and Prince W.R., "Effect of Uneven Air-Flow Distribution to the Twin Inlets of an Axial Flow Turbojet Engine," NACA RM E 52 K 06, 1953.

43. Turner, R.C., Ritchie, J., and Moss G.E., "The Effect of Inlet Circumferential Maldistribution on Axial Compressor Stage," ARC R&M 3066, 1957.

44. Harry, D.P, and Lubick, R.J., "Inlet Air Distortion Effects on Stall, Surge, and Acceleration Margin of a Turbojet Engine Equipped with Variable Compessor Inlet Guide Vanes," NACA RM E54K26, 1955.

45. Whitehead, D.S., Vibration of Cascade Blades Treated by Actuator Disc Methods," Proc. I. Mech. E., 173, 21, 255.

46. Ehrich, F., "Circumferential Inlet Distortion in Axial Flow Turbomachinery, " Jnl. Aero. Soc., 24, 6, 413-17, June 1957.

47. Katz, R., "Performance of Axial Compressors with Asymmetric Inlet Flows," Daniel and Guggenheim Jet Propulsion Centre, Cal. Inst. of Tech, Report, June 1958 (AFOSR-TR-58-59 AD 162-112).

48. Rannie, W.D., and Marble, F.E., "Unsteady Flows in Axial Turbomachines," ONERA, Comptes Rendus des Journes Internationales de Sciences Aeronautiques, Part 2, pp. 1-21, Paris, May 27-29, 1957. Also Daniel and Florence Guggenheim Jet Propulsion Centre, Cal. Inst. Tech., USA Report, May 1957.

49. Doyle, M.D.C., Dixon, S.L., and Horlock, J.H., "Circumferential Asymmetry in Axial Compressors," J. R. Aero. Sci., 70, 956-957, Oct. 1966.

50. Hsuan Yeh, "An Actuator Disc Analysis of Inlet Distortion and Rotating Stall in Axial Flow Turbomachines," J. Aero/Space Sci., 26, 11, 739-753, Nov. 1959.

51. Krzywoblocki, M.Z., "Compressibility Effects in Circumferential Inlet Distortion in Axial Compressors," Ost. Ing-Arch: Pt. I: 13, 4, 214 (1959-1960); Pt. II., 14, 2, 79.

52. Dixon, S.L., "Rotating Stall in Compressor Blade Rows of Low Hub Tip Ratio," Ph.D. Thesis, Liverpool University, 1968.

53. Dunham, J., "Non-Axisymmetric Flows in Axial Compressors," Ph.D. Thesis, Cambridge Univ. Eng. Dept. 1962.

54. Dunham, J., "Non-Axisymmetric Flows in Axial Compressors," Mech. Eng. Sci., Monograph #3, 1965.

55. Dunham, J., "Observation of Stall Cells in a Single Stage Compressor," Aero Res. Council, London, CP 589, 1962.

56. Dunham, J., "Comment on an Acutator Disc Analysis of Inlet Distortion and Rotating Stall in Axial- Flow Turbomachines," Jnl. Aero. Sci., 29 362, 1962.

57. Greitzer, E.M., and Strand, T., "Asymmetric Swirling Flows in Turbomachine Annuli," ASME meeting, London, 1978.

58. Sears, W.R, "On Asymmetric Flow in an Axial Flow Compressor Stage," J. Appl. Mech., March 1953.

59. Hawthorne, W.R., McCune, J.E., Mitchell, N.A., and Tan, C.S., "Non-Axisymetric Flow Through an Annular Actuator Disc; Inlet Distortion

Problem," prepared for ASME meeting, London, April 1978.

60. Rizvi, S.A.H., "Inlet Maldistribution Effects in Axial-Compressor Rotors," Ph.D. Dissertation, Cambridge University, 1977.

61. Kantorovich, L.V., and V.I. Krylov, "Approximate Methods of Higher Analysis," Interscience Publishers, Inc., 1958.